

**AIAA 2021-2022 Undergraduate Team RFP
Responsive Aerial Fire Fighting Aircraft
Final Design Report**

Team Albatross – N513 "Firehawk"



Scott Brindise, Quang Do, Jason McIntyre, Roshan Patel, Andrew Strubhar,
Maryna Syb, Shrikanth Tandon, Yiyang Wang

Faculty Advisor: Dr. Jason Merret
University of Illinois at Urbana-Champaign
AE 443 - Aerospace Systems Design II
April 28, 2022







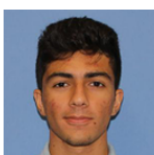





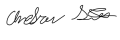

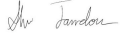

			
Scott Brindise Systems	Quang Do Propulsion	Jason McIntyre Stability and Control	Roshan Patel Performance
			
Andy Strubhar Team Lead	Maryna Syb Aerodynamics	Shri Tandon Structures	Yiyang Wang Mass Properties & Loads and Dynamics

Table 1 Team Albatross

Group Member	Primary Discipline	Secondary Discipline	AIAA Membership Number	Signature
Scott Brindise	Systems	Configuration & Drop/Refill	1357534	
Quang Do	Propulsion	Avionics	1357281	
Jason McIntyre	Stability and Control	Repair and Maintenance	1326237	
Roshan Patel	Performance	Landing Gear & Cost	1292764	
Andrew Strubhar	Team Lead	Certification	1253950	
Maryna Syb	Aerodynamics	Interior	1357414	
Shri Tandon	Structures		1325357	
Yiyang Wang	Mass Properties & Loads and Dynamics		1357037	

Faculty Advisor	Dr. Jason Merret	
-----------------	------------------	--

Contents

I	Compliance Checklist	vi
II	Introduction	1
II.A	Design Objectives	1
II.B	Design Philosophy	1
III	Concept of Operations	2
III.A	Overview	2
III.A.1	Requirements	2
III.B	Mission Profiles	3
III.B.1	Design Radius	3
III.B.2	Ferry Flight	4
III.C	OV-1 Diagram	5
IV	Sizing Analysis	6
IV.A	Similarity Analysis	6
IV.B	Initial Sizing	6
IV.C	Trade Study for Reference Area and Aspect Ratio	7
IV.D	Trade Study for Fuselage Dimensions	9
V	Configuration	10
V.A	General Configuration	10
V.B	Tail	12
V.C	Wing and Engines	12
V.D	Landing Gear	13
V.E	Flight Deck	13
VI	Propulsion	16
VI.A	Propulsion System Selection	16
VI.B	Engine Selection	16
VI.C	Safety Considerations	17
VI.D	Engine Performance	17
VI.E	Inlet, Nacelle, and Exhaust Design	19
VI.F	Systems	21
VII	Aerodynamics	22
VII.A	Airfoil Selection	22
VII.B	Wing Design	24
VII.C	High-Lift Devices	26
VII.D	Drag Build-Up	29
VII.E	Aircraft Analysis	31
VIII	Performance	33
VIII.A	Requirements and Approach	33
VIII.B	Flight Envelope	33
VIII.C	Flight Optimization	34
VIII.D	Fuel Burn and Drag	36
VIII.E	Field Length Analysis	37
VIII.F	Range performance	38
VIII.G	Future Work	39
IX	Stability and Control	40
IX.A	Tail Design	40

IX.B	Stabilizer Sizing	41
IX.C	Control Surface Design	44
IX.D	Trim Analysis	46
IX.E	Longitudinal Static Stability	48
IX.F	Lateral-Directional Static Stability	48
IX.G	Dynamic Stability	49
IX.H	Future Work	49
X	Structures and Loads	51
X.A	V-N diagram	51
X.B	Load paths	53
X.C	Loads	53
X.D	Sizing	55
X.E	Materials	57
X.F	Finite Element Methods	58
XI	Mass Properties	60
XI.A	Weight Estimation	60
XI.B	CG Estimation	62
XI.C	Trade Study on Retardant Tanks	67
XI.D	Future Work	67
XII	Systems	68
XII.A	Overall Layout	68
XII.B	Hydraulics	68
XII.C	Electrics	71
XII.D	Auxiliary Power Unit	72
XII.E	Engine Controls	72
XII.F	Fuel Systems	73
XII.G	Avionics	74
	XII.G.1 Mission Avionics	77
XII.H	Flight Controls	78
XII.I	Pneumatics	79
XII.J	Environmental Control and Oxygen	79
XII.K	Retardant Tanks and Handling Systems	80
XIII	Landing Gear	81
XIII.A	Configuration	81
XIII.B	Sizing	82
XIII.C	Braking System	84
XIV	Repair and Maintenance	85
XIV.A	Maintenance Approach	85
XIV.B	Repair Approach	85
XIV.C	Future Work	86
XV	Cost Analysis	87
XV.A	Business Case Analysis	87
XV.B	Production and Unit Cost	87
XV.C	Operational Cost	88
XV.D	Future Work	89
XVI	Conclusion	90

Nomenclature

$\frac{c'}{c}$	=	Slat Chord to Airfoil Chord
$\frac{c_f}{c}$	=	Flap Chord Percentage
\bar{C}_{d0}	=	Drag Coefficient
C_G	=	Center of Gravity
C_L	=	Lift Coefficient
C_{L_α}	=	Lift Curve Slope
$C_{L_{\delta e}}$	=	Lift Coefficient With Respect to Elevator Deflection
C_{l_β}	=	Roll Moment Coefficient With Respect to Sideslip Angle
$C_{l_{\delta a}}$	=	Roll Moment Coefficient With Respect to Aileron Deflection
C_{m0}	=	Pitching Moment Coefficient for Zero Lift Angle of Attack
C_{m_α}	=	Pitching Moment Coefficient With Respect to Angle of Attack
$C_{m_{\delta e}}$	=	Pitching Moment Coefficient With Respect to Elevator Deflection
C_{n_β}	=	Yaw Moment Coefficient With Respect to Sideslip Angle
$C_{n_{\delta a}}$	=	Yaw Moment Coefficient With Respect to Aileron Deflection
$C_{n_{\delta r}}$	=	Yaw Moment Coefficient With Respect to Rudder Deflection
ϵ_α	=	Downwash Gradient
$\frac{L}{D}$	=	Lift to Drag Ratio
S_W	=	Total Wing Area
S_{WF}	=	Affected Wing Area
V_A	=	design maneuvering speed
V_C	=	design cruising speed
V_D	=	design diving speed

Acronyms

AGL	=	Above Ground Level
AoA	=	Angle of Attack
APU	=	Auxiliary Power Unit
AR	=	Aspect Ratio
ATGS	=	Air Tactical Group Supervisor
BFL	=	Balanced Field Length
CAD	=	Computer Aided Design
CFD	=	Computational Fluid Dynamics
CFR	=	Code of Federal Regulations
CG	=	Center of Gravity
DISA	=	Defense Interchange Standards Association
EIS	=	Entry Into Service
FADEC	=	Full Authority Digital Engine Control
FS	=	Factor of Safety
GCAS	=	Ground Collision Avoidance System
IPPS	=	Integrated Powerplant System
LE MAC	=	Leading Edge Mean Aerodynamic Chord
LFL	=	Landing Field Length
MAC	=	Mean Aerodynamic Chord
MFD	=	Multi-Function Display
MLW	=	Maximum Landing Weight
MRW	=	Maximum Ramp Weight
MSL	=	Mean Sea Level
MTOW	=	Maximum Takeoff Weight
MZFW	=	Maximum Zero Fuel Weight
MOU	=	Memorandum of Understanding
NACA	=	National Advisory Committee for Aeronautics
NASA	=	National Aeronautics and Space Administration
OEI	=	One Engine Inoperative
OEW	=	Operating Empty Weight
RFP	=	Request For Proposal
SFC	=	Specific Fuel Consumption
TAWS	=	Terrain Avoidance and Warning System
TCAS	=	Traffic Collision and Avoidance System
TO	=	Takeoff
TOW	=	Takeoff Weight
USFS	=	United States Forest Service
VFR	=	Visual Flight Rules

I. Compliance Checklist

The 2021 - 2022 AIAA RFP, which calls for the design of a "Responsive Aerial Fire Fighting Aircraft", contains a total of 23 design requirements. Seven of those included requirements are extensions of other requirements, and are considered design objectives. Team Albatross' design, the N513 *Firehawk*, meets five of the seven design objectives and each design requirement. Table 2 lists these requirements, and for any of the objective requirements the true requirement can be found in the footnotes. The section in which that requirement is most discussed is also listed in the table. [1]

Table 2 AIAA RFP Requirements

Numerical Requirements				
Type	Description	RFP Value	N513 <i>Firehawk</i> Value	Sections
R	EIS Date	2030	2030	VI.B
R	Engine EIS	2028	2013	VI.B
O ^a	Fire Retardant Capacity	4,000 gal	8,000 gal	XII.K
R	Multi-Drop Capability	> 1 Drop & >2,000 gal per drop	At least 2 drops of 4,000 gallons	III.B.1
R	Fire Retardant Reload Speed	>= 500 gal/min	500 gal/min	XII.K
R	Retardant Density	<= 9 lb/gal	9 lb/gal	XII.K
O ^b	Drop Speed After Payload Drop	<= 125 kts	125 kts	VIII.D
R	Drop Altitude	<= 300 ft AGL	300 ft AGL	VIII.D
O ^c	Radius with full payload	400 nmi	805 nmi	VIII.D
O ^d	Design Ferry Range with no payload	3,000 nmi	3,051 nmi	VIII.D
R ^e	Dash Speed after drop	300 kts	380 knots	VIII.D
R	Balanced Field Length ^f	<= 8,000 ft	6,100 ft	VIII.D
General Requirements				
Type	Description	-	-	Sections
R	Capable of VFR and IFR flight with an autopilot	-	-	XII.G
R	Capable of flight in known icing conditions	-	-	XII.I
R	Certifiable by FAA 14 CFR § 25	-	-	III.C, V.E, XII.B, etc.
O	Systems and Avionics architecture for autonomous operations	-	-	XII.G

^aRequired fire retardant capacity is 4,000 gallons.

^bRequired Drop Speed is <= 150 knots.

^cRequired Design Radius with payload is 200 n mi.

^dRequired Design Ferry Range with no payload is 2,000 nmi.

^eObjective Dash Speed after drop is 400 knots.

^fAt 5,000 ft MSL elevation of a + 35 °F hot day.

II. Introduction

A. Design Objectives

Team Albatross is committed to producing a design that will satisfy all requirements in the AIAA RFP at as low of a cost to the consumer as possible. The designed aircraft will reach optional goals of a fire retardant capacity of 8,000 gallons, a drop speed of less than or equal to 125 kts, a design radius will full payload of at least 400 nmi, and a design ferry range of at least 3,000 nmi. The team chose to meet these design objectives in order to produce an aircraft that will be continually effective in fighting fires that have been growing in size for years. Giving *Firehawk* this extended range and retardant capacity will allow it fight large scale wildfires, and reach remote areas that other fire-fighters can not. Reaching these design goals will allow this design to be viewed favorably by larger customers, including the United States Forest Service and foreign equivalents, along with smaller state run conservation agencies. As wildfires continue to become larger and more devastation, larger groups such as the USFS or private contractors with large budgets will need to be called in to fight back. Team Albatross has designed this aircraft with groups like this in mind, who will be able to pay for aircraft designed directly for firefighting. Although certain design aspects with this consideration in mind may raise the, the benefits of an aircraft designed for a specific job will outweigh the small cost difference as wildfires continue to become more devastating. Including an extra 400 nmi of range will allow crews who previously may have had to refuel during a mission to travel further, execute mission objectives, and return to the point of takeoff in much less time than before. This is specifically significant for fire fighting aircraft, where response time is of the utmost importance. Airports with sufficient size to store fire fighting aircraft are often a sizable distance from new fires in the deep wilderness, also leading to increased response times due to the refuelling on the ground necessary for those flights. The team will also include fuel tanks that are large enough for the full ferry mission, and can be partially filled for a drop mission. This will add a level of compatibility to the aircraft, allowing it to be used for different mission categories with little to no retrofitting. Adding this capability will allow the aircraft to engage in aerial resource support, aerial detection, remote cargo delivery, and many other fire-fighting or general remote operation related tasks. This flexibility paired with the increased design range and easily increased ferry range will place this aircraft in a highly desirable market position.

B. Design Philosophy

Team Albatross follows a design philosophy which states: Aircraft design should be a highly iterative process based on the requirements of the RFP, data from existing aircraft, and any other specific design considerations related to the expected Concept of Operations of the aircraft. Thus, the first step the team took was to study similar, existing aircraft that perform similar fire fighting roles. Specifically, the Boeing 737-300 was used for first-iteration calculations. This was done by slowly changing the aircraft's parameters until all conditions in the RFP were met. These final design parameters were then used by the team as a starting point for their design. Throughout the first design period, this starting point was improved and refined using many methods, including equations from well respected aircraft design experts such as Raymer [2] and Roskam [3]. During the second period of the design process, the team focused on giving calculations and estimates more validity through further in-depth methods, such as the use of computational methods. The third design period was an extension of the second, with even further advanced computation tools.

III. Concept of Operations

A. Overview

1. Requirements

The RFP published by AIAA describes all of the mandatory requirements that the aircraft must meet [1]. Along with the required parameters, some items are listed as objectives that are optional to satisfy. Listed in Table 3 are the requirements that the aircraft will be designed to satisfy which comprise of a combination of some required and some objective requirements. The majority of the objective requirements that were selected were to improve the performance and capabilities of the aircraft.

Table 3 Design Requirements

General Requirements		
Category	Requirement Type	Description
Entry into service	Required	Year: 2030
	Required	Use existing engine(s) or one that is in development will be in service by 2028, or at least two years prior to the airplane EIS.
	Required	Assumptions on at least specific fuel consumption/efficiency, thrust/power and weight must be documented.
Fire Retardant Capacity	Objective	8,000 gal
	Required	Multi-drop capable; minimum 2,000 gal per drop
	Required	Fire retardant reload ≥ 500 gal / min
	Required	Retardant density of at least 9 lbs / gal
Payload Drop	Objective	Drop speed ≤ 125 kts
	Required	Drop altitude ≤ 300 ft AGL
Design Radius with Full Payload	Objective	400 nmi
Design Ferry Range (No Payload)	Objective	3,000 nmi
Dash Speed (After Payload Drop)	Objective	300 kts
Field Requirements	Required	Balanced field length $\leq 8,000$ ft @5,000 ft MSL elevation on a 35°F hot day
Certifications	Required	Capable of VFR and IFR flight with an autopilot
	Required	Capable of flight in known icing conditions
	Required	Meets applicable certification rules in FAA 14 CFR § 25
	Required	All missions below assume reserves and equipment required to meet applicable FARs

B. Mission Profiles

1. Design Radius

Per the requirements, the aircraft must be designed to combat fires with at least two retardant drops anywhere in a 400 nmi range. The mission profile shown in Figure 1 and described in Table 4 shows the expected maneuvers for each mission. There are two drops, one on the way out to the fire, and one on the return flight back to the base airfield. The worst case mission profile is highlighted in black, as this is the flight path that would consume the most amount of fuel. Climbing slightly between the two drops increases fuel efficiency. The aircraft has been designed to satisfy the mission in black, because the mission in orange is viable so long as the black one is. The portion of the mission profile that is in red is to account for a reserve or diverted flight.

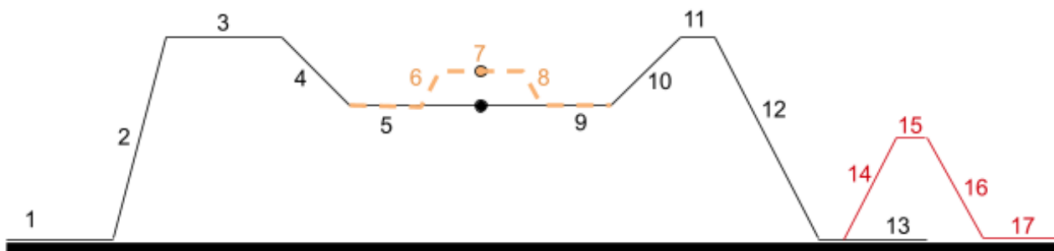


Fig. 1 Design Radius Mission Profile.

Table 4 Design Radius Flight with Two Drops

Segment Number	Description
1	Warm Up, Taxi and Take-Off
2,	Climb to Cruise
3	Fly to the designated drop site, with point
4	Descend to Drop Altitude
5,9	Designated Drop Altitudes
6	Ascend Back to Cruise Altitude
7	Point marking the 400-mile mark of the design radius
8	Descend slightly back to drop altitude
10	Climb back to cruise altitude
11	Cruise at Dash Speed of 300 kts
12	Landing
14	Go-Around Climb
15	Loiter/ Diversion
16	Landing
13,17	Taxi to stand
14	Go-around climb

2. Ferry Flight

The RFP also requires that the aircraft be able to complete a ferry flight of a much longer range, but with an empty payload. This flight will require a new mission profile which is shown in Figure 2 and described in Table 5. This flight will comprise of a step climb over the course of the ferry flight to optimize the fuel consumption. As with the Design Radius profile, the segments in red are to represent a reserve or diverted flight.

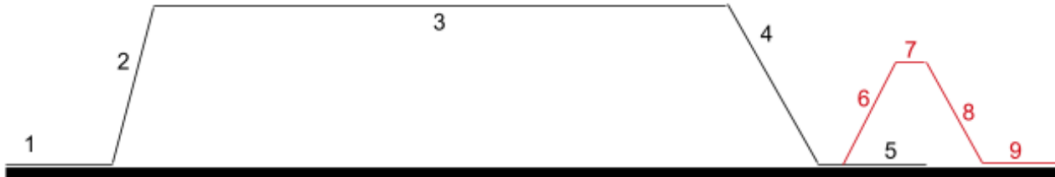


Fig. 2 Ferry Flight Mission Profile.

Table 5 Ferry Flight

Segment Number	Description
1	Warm Up, Taxi and Take-Off
2	Climb to Cruise Altitude
3	Level Cruise Flight
4	Landing
5	Taxi to Stand
6	Go-around climb
7	Loiter Altitude
8	Descend
9	Taxi to Stand

C. OV-1 Diagram

Firehawk will work in conjunction with at least two other aircraft at all times, along with boots-on-the-ground fire crews. The first of these other aircraft is called the Flight Path Leader, and is responsible for initial scouting of the affected area while also finding a safe flight path for *Firehawk* and any other large aircraft in the mission. The Air Tactical Group Supervisor (ATGS) is in-charge of the entire aerial operation, and is constant communication with each member of said operation. The ATGS is also responsible for visual reconnaissance, and makes the final call on where to drop the fire retardant. Figure 3 below shows an example mission for *Firehawk*, and real operations would follow the structure displayed.

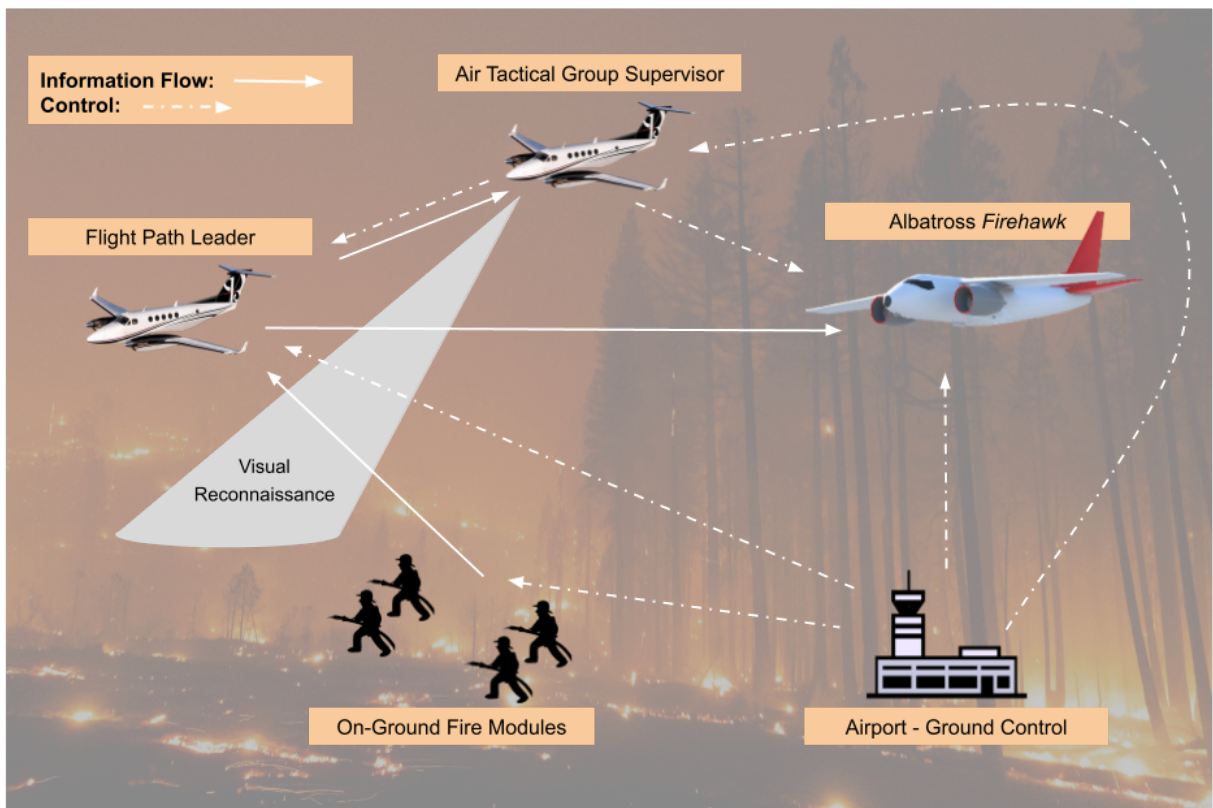


Fig. 3 N513 *Firehawk* OV-1 Diagram.

IV. Sizing Analysis

A. Similarity Analysis

The seed aircraft for this design is the Boeing 737-300. It was selected from a list of existing converted firefighting aircraft, all of which are capable of carrying payloads close to the required amount of 4,000 gallons. These aircraft include the 737-300, McDonnell Douglas MD-87, DC-10-30, and the Lockheed C-130H. Some information on these aircraft is shown in Figure 6.

Table 6 Reference Aircraft Parameters

Parameter	C-130H [4] [5]	B737-300 [6]	MD-87 [7]	DC-10-30 [8]
Range w Standard Load	1,208 nmi	2,255 nmi	2,900 nmi	4,000 nmi
Payload	3,000 gal	4,000 gal [9]	4,000 gal [10]	12,000 gal [11]
Engine Output (total)	18,364 hp	40,000 lb	43,400 lb [12]	151,200 lb [13]
MTOW	155,000 lb	138,500 lb	149,500 lb	555,000 lb

From these aircraft, the 737-300 was selected as the seed. The C-130 does not have enough payload capacity to meet the desired 4,000 gallon lower limit. The MD-87 and DC-10-30 have undesirable engine placement, as tail-mounted engines are generally more difficult to access for maintenance compared to under-wing units. The DC-10 is also over the 8,000 gallon upper limit for payload, which exceeding would drive up cost unnecessarily. The 737-300 has desirable engine placement and fits the payload bracket. It does not have the desired high wing configuration, but it was considered the best starting point.

The main data extracted from the similarity analysis for sizing included the dimensions of the 737-300's fuselage, engine parameters including nacelle dimensions and SFC, the maximum lift coefficient at landing conditions, and flight conditions including altitude, speed, and temperature variation.

B. Initial Sizing

The initial parameters of the aircraft were derived from the parameters of the 737-300, using a sizing process in which various parameters were changed to meet the requirements set in the RFP [1]. A wing area of 1,800 sq ft and an aspect ratio of 8 were selected, as this combination of wing area and aspect ratio minimized the stall speed and thrust required.

The airplane was sized around the drop and ferry missions, and it was found that the drop mission had a larger impact on driving the requirements for the airplane overall. The ferry mission had a higher fuel load requirement, however. As a result, the airplane was primarily designed around the drop mission, with the assumption that the aircraft would have additional internal tanks that would be fueled in order for it to reach the desired ferry range. Given that the aircraft will not be carrying a payload for a ferry flight, having it instead carry extra fuel for these flights would allow it to achieve the desired ferry range without requiring more powerful engines for the drop mission.

The team envisioned a larger airplane capable of carrying 8,000 gallons of retardant, as there are no purpose-built aircraft in this category. The only aircraft currently in service that fulfill this requirement are the DC-10, IL-76, and 747, all of which are converted passenger or cargo aircraft. A dedicated airplane capable of meeting this requirement would be better suited for aerial firefighting, as they would be purpose built for that mission while being able to employ newer technologies not included on current conversions. The other goals the team set were based on this ideology. The team determined that because a larger airplane should be capable of a longer range, a higher BFL would be an acceptable trade to keep costs down, as the airplane would have sufficient range to fly from airports with longer runways. With this in mind, the team also determined that the aircraft should be capable of the higher dash speed set in the RFP requirements so that it would be able to more quickly reach distant wildfires.

C. Trade Study for Reference Area and Aspect Ratio

The thrust required, structural weight, and aircraft performance heavily depended on the aircraft's wing aspect ratio and wing reference area, warranting an in depth trade study. Due to the aircraft being specifically designed to fight fires, the airplane performance at low speeds and thrust required are very high priority. Figure 4 shows visual evidence that increasing both the wing aspect ratio and wing area results in lower thrust required.

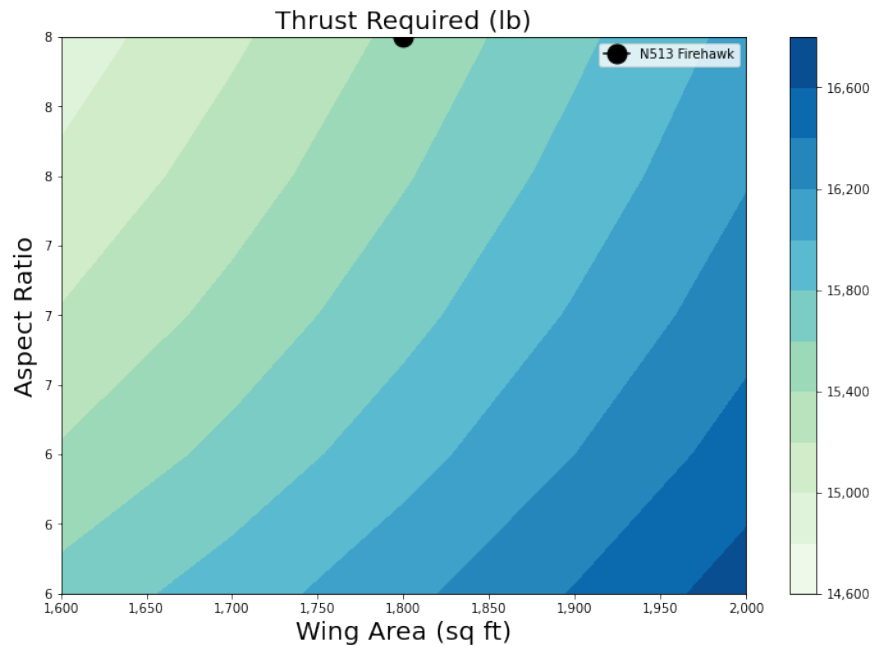


Fig. 4 Thrust Required as a Function of Aspect Ratio and Reference Area.

Figure 5 demonstrates that the stall speed is primarily a function of wing area with large wing reference areas resulting in the slowest drop speeds. Additionally, there are benefits to the maximum ferry range following the same trend as the thrust required as seen from Fig. 6.

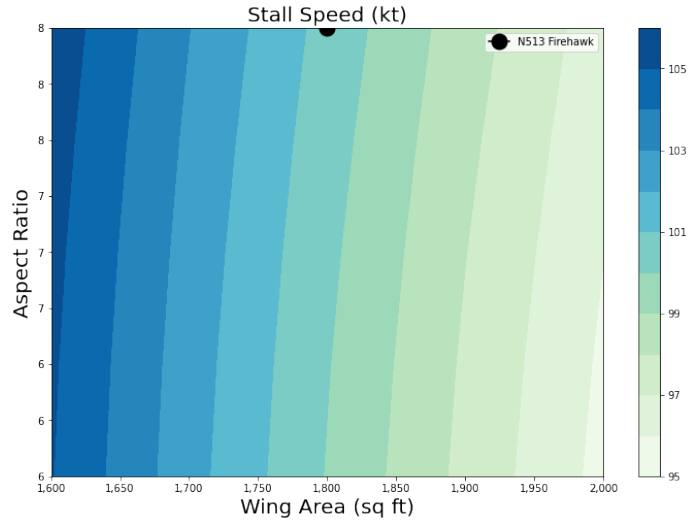


Fig. 5 Stall Speed as a Function of Aspect Ratio and Reference Area.

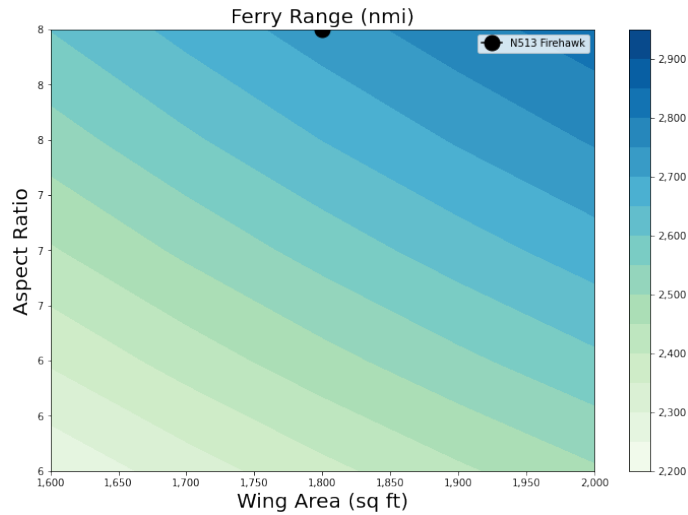


Fig. 6 Ferry Range as a Function of Aspect Ratio and Reference Area.

When completing the sizing for the aircraft, Team Albatross searched for good performance parameters while also minimizing the weight of the aircraft and leaving room for error. Minimizing the weight while reaching the desired performance and requirements results in the cheapest configuration. When comparing each factor, it was concluded that an aspect ratio of 8 and a wing reference area of 1,800 sq. ft. were acceptable.

D. Trade Study for Fuselage Dimensions

A trade study was performed for the aircraft's fuselage design, specifically for its diameter and length. The internal volume of the seed aircraft was calculated and compared to the volume required by an 8,000 gallon retardant tank, which showed that the fuselage was much larger than needed. Reducing the volume of the fuselage reduces surface area, which can reduce both weight and drag. This can be achieved by either shortening the fuselage, reducing the diameter, or both. Reducing the length would reduce structural stresses and allow more tail clearance on takeoff and landing, but it maintains the same frontal area as the seed aircraft which increases profile drag. This layout also offers a weight reduction by decreasing the surface area to volume ratio, but the shortening of the tail's control arm could very well offset these gains by requiring a larger, heavier tail that produces more drag. Reducing the diameter of the fuselage maintains the tail moment arm and reduces the profile drag, but does incur more demanding structural loads due to the long, thin structure which will require additional reinforcement and weight.

In order to understand this trade-off, a numeric comparison was done. Using the early 110" diameter fuselage as a baseline, a 153" diameter fuselage of the same volume was tested in the design spreadsheet, assuming a 25 percent increase in tail area to maintain controllability. It was found that even with this increase in tail area and weight, the resulting aircraft was about 9,000 lb lighter, required 2,000 lb of thrust less per engine, and could manage to drop payloads at 3 knots slower. In light of this, a diameter of 150" was selected for the aircraft.

Table 7 Comparison of various parameters for different fuselage designs.

Parameters	Seed Fuselage	Short Fuselage
Diameter (in)	110	153
Length (in)	1,300	940
Empty weight (lb)	87,596	78,950
Stall speed (kt)	100.2	97.7
Thrust required (lb)	21,987	19,857

V. Configuration

A. General Configuration

The aircraft has a circular cross-section fuselage, a conventional tail, high-mounted straight wings, and two turbofan engines on pylons under said wings. A CAD drawing 3-view and isometric view of the current configuration can be found on the next page.

Table 8 Wing & Tail Dimensions.

Parameters	Values	Units
Wing Area	1800	sq. ft
Wing Span	120	ft
Wing Root Chord	21.43	ft
Wing Tip Chord	8.57	ft
Wing AR	8	-
Wing Quarter Chord Sweep	0	deg
Wing Taper Ratio	0.4	-
Wing Anhedral Angle	2	deg
Wing Incidence Angle	2	deg
H-Tail Area	450	sq. ft
H-Tail Span	42.42	ft
H-Tail Root Chord	15.71	ft
H-Tail Tip Chord	5.5	ft
H-Tail Quarter Chord Sweep	15	deg
H-Tail Taper Ratio	0.35	-
H-Tail Dihedral Angle	5	deg
V-Tail Area	400	sq. ft
V-Tail Span	22.8	ft
V-Tail Root Chord	14.62	ft
V-Tail Tip Chord	2.92	ft
V-Tail Quarter Chord Sweep	25	deg
V-Tail Taper Ratio	0.2	-
Fuselage Diameter	150	in
Nose Length	175	in
Fuselage Tube Length	300	in
Tail Boom Length	450	in
Overall Length	976.5	in
Distance From Nose Gear to Main Gear	357.5	in
Main Gear Stance	174	in
Nose Gear Tire Diameter	33.35	in
Main Gear Tire Diameter	46.9	in
Tail Clearance Angle	16	deg

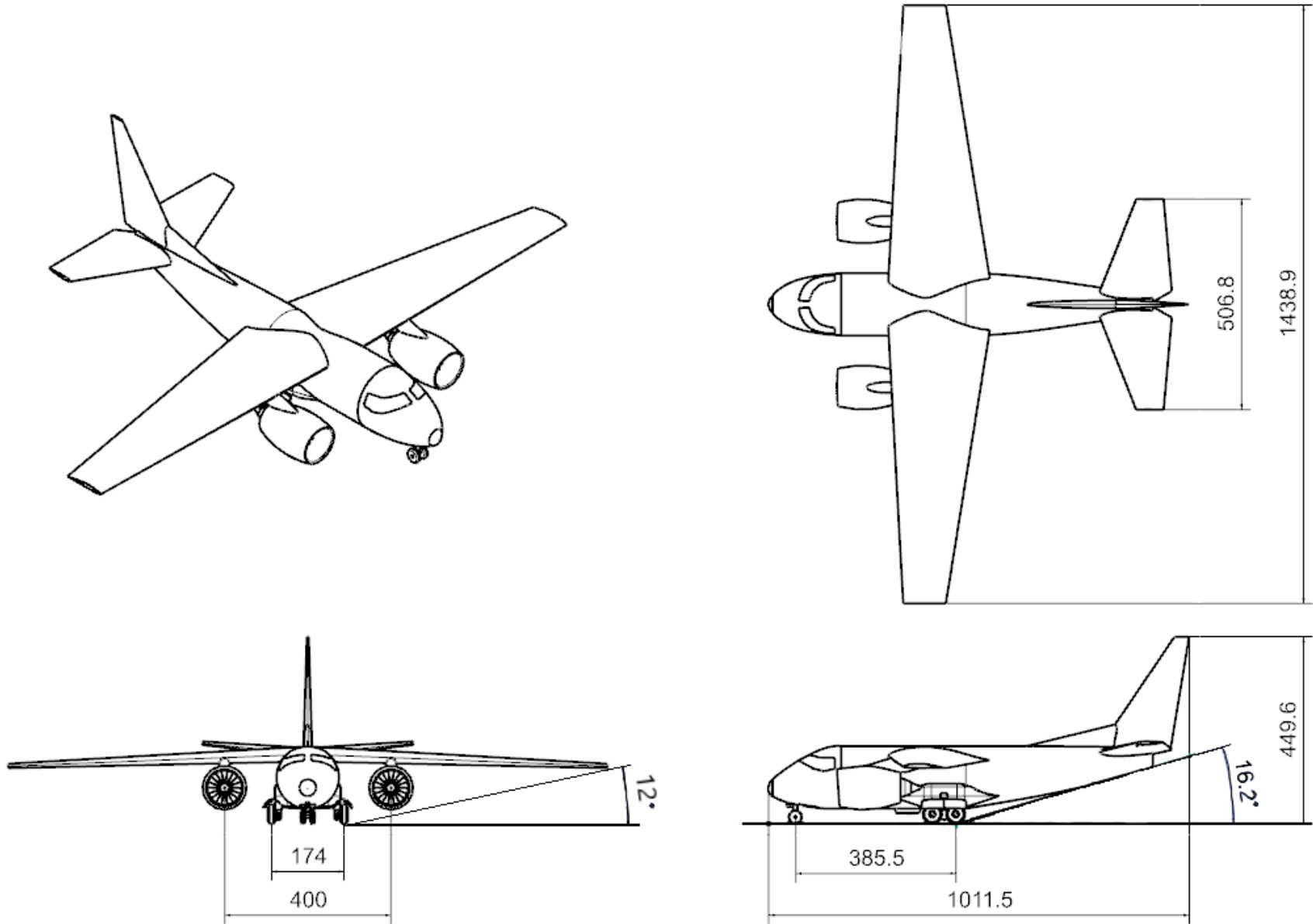


Fig. 7 N513 3-View.

B. Tail

A conventional tail was selected from a trade study of multiple tail configurations. A T-tail, twin boom tail and conventional tail were all considered.

T-tails allow for an overall smaller vertical tail due to the horizontal tail eliminating tip effects, and also allows for a smaller horizontal tail given the airflow is not disturbed by the main wings. However, T-tails demand a stronger and heavier structure in the vertical segment. T-tails are also susceptible to blanketing from the main wings at high AoA [14].

Twin boom tails allow for a shortened rear fuselage, which if done can reduce wetted area and fuselage weight. Twin boom tails don't suffer from blanketing of the vertical stabilizers by the fuselage at high AoA, and can provide sufficient vertical tail area when a single tail would be impractical. However, twin boom tails can increase the number of stabilizer tips (and the associated losses from tip effects), and require narrow and strong boom structures along with strengthening of the wings where they connect. The shorter fuselage would also reduce the usable volume in the aircraft for systems, payload and fuel [14].

A conventional tail offers relatively simple structure and light weight. Having the horizontal stabilizer below the vertical stabilizer can lead to rudder ineffectiveness due to blanketing in a spin, however this can be mitigated by careful relative placement/geometry of the two stabilizers [14]. Similar to the T-tail, a conventional tail preserves the rear fuselage and the space associated with it, a location often used for housing the APU. Although the horizontal stabilizers will be in the wake of the main wing, the subsonic operation of the aircraft means the placement of the horizontal tail at the same height as the wing is still viable [14].

C. Wing and Engines

A high wing with low-mounted engines was selected over other options for a number of reasons, namely maintenance, roll stability, and weight savings. Under-wing engines are commonly used on commercial aircraft, which allow for easy access to the engines for inspection, maintenance and replacement. Raising the wing allows for this engine configuration to be used with shorter landing gear, meaning both the fuselage and engines are low to the ground and easy to access. A high wing provides roll stability, and the lifted engines have thrust lines closer to the aircraft's center of gravity which reduces the pitching moment from the engines.

Two turbofans were selected for this aircraft. A larger number of engines usually increases the operational cost and complexity of an aircraft, meaning mounting fewer, stronger powerplants are desirable. Turbofan engines in the required thrust class are also used on many passenger aircraft today, so there are several options available. It was determined that two engines were sufficient to meet the requirements, as many passenger aircraft have similar thrust requirements.

D. Landing Gear

The aircraft has tricycle landing gear very similar to that of the C-130 and other moderately sized military cargo aircraft. The main gear is located in sponsons on the sides of the fuselage, retracting inwards into the belly. The nose gear is located in the nose, retracting rearward. The nature of this gear is further detailed in Landing Gear XIII.

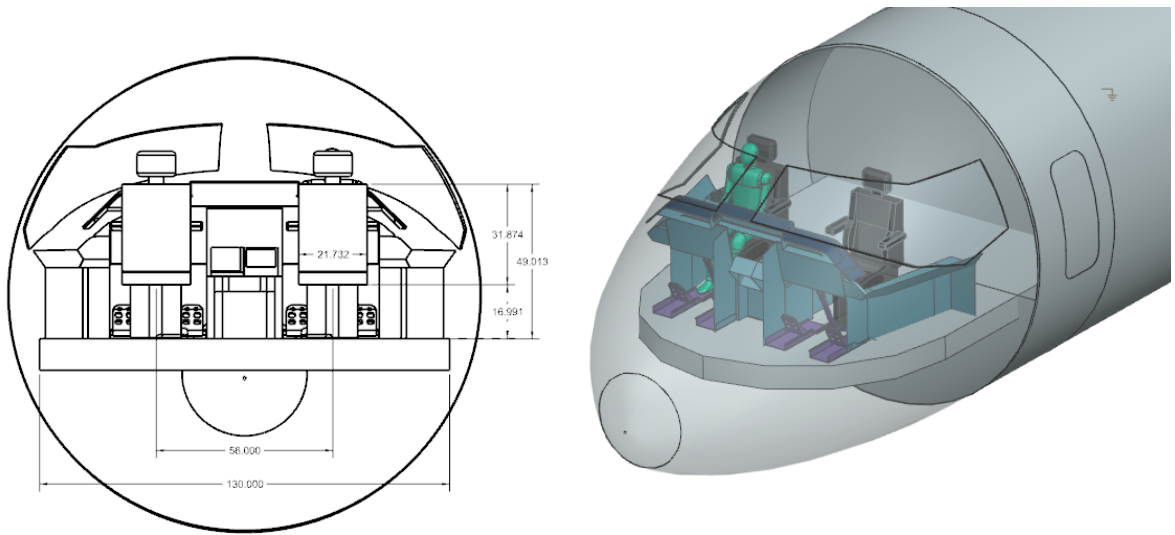
E. Flight Deck

In a human-piloted aircraft, the flight deck must be designed with respect to physical constraints. Techniques have been developed to measure and collect data from a representative sample of people who are to pilot the aircraft. The most comprehensive source of such data was found inside a three-volume edition, anthropometry and biomechanics study published by NASA [15]. In the United States, the FAA regulations currently require that transport category aircraft be designed for operating by crew members of physical height ranging from 5 ft 2 in. (157 cm) to 6 ft 3 in (190 cm) [16]. Furthermore, a universal population survey conducted in 2018 indicated an average increase in height over half a century to be 1.3 mm a year for males and 0.9 mm for females. The *Firehawk* pilot compartment design parameters were chosen to accommodate 95% male proportions of the population. The measurements and proportions of the human body were adjusted accordingly for the cockpit, seat, and cabin design. The flight deck was designed for a flight crew consisting of a pilot and co-pilot. Using the pilot's "design eye point" as a benchmark, the characteristic parameters and layout of the flight deck can be determined. Alignment using the eye's reference point enables the pilots to have an optimal field of view through the cockpit's windows to see what is around them outside the aircraft [17]. The seat, yoke-stick, and floor locations were determined according to the 50th percentile pilot's comfortable sitting posture, where the the leg position was assumed parallel with upper body [18].

Seat design aspects included the configuration of the seat pan and back structure, armrest, headrest, and a seat tilt of 75 degrees to align the pilots eye-level outside view [16]. Next, instead of a passenger entrance door, the 48 inch by 22 inch tall exit hatch located on the left side of the cockpit was adopted from the Boeing 757-200 (Package Freighter). For emergency processes, the small entrance crew door has both a rope and a set of inertial escape reels that provide a safe, controlled descent from the aircraft.

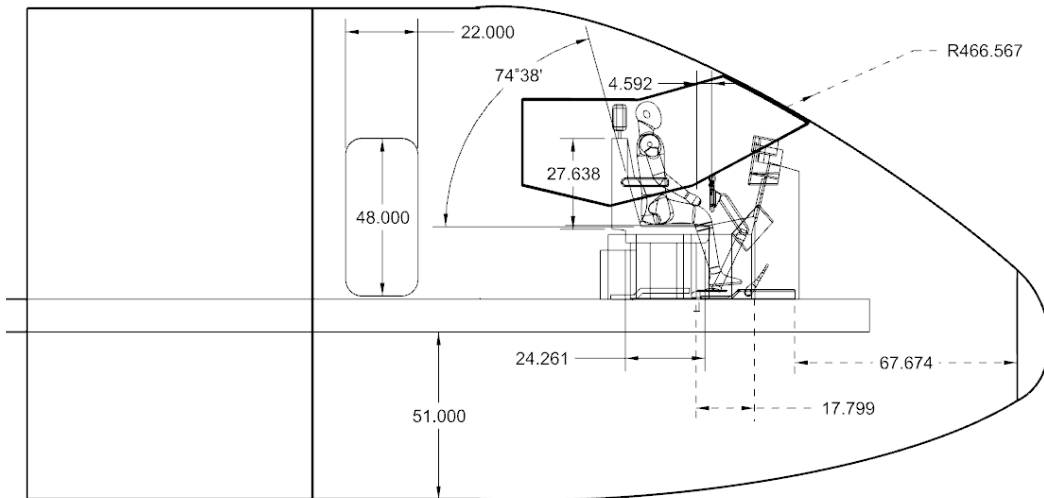
1. Pilot Viewing Angles

Outside the flight deck, the line of vision must guarantee adequate vision scope for all mission maneuvers [18]. The pilot compartment view regulations are outlined in the Advisory Circular 25.773-1, which clarifies 14 CFR § 25 [19]. The minimum vertical and horizontal field of vision requisites are summarized in Table 9, and are taken into account during the design process. The seat height and location were carefully adjusted to fall within the specified range, capable of passing the FAA viewing angle requirements.



(a) Pilot Compartment Back View Dimensional Drawing

(b) Pilot Compartment Isometric Shaded CAD Model View



(c) Pilot Compartment Front View Dimensional Drawing

Fig. 8 Flight Deck Configuration.

Table 9 14 CFR § 25.773 required and designed line of sight angles

Angles	Up-View	Down-View	Right of Center	Left of Center
Pilot View Required [deg]	25	17	20	20
Pilot View Designed [deg]	29	34	113	135

The unobstructed maximum vertical pilot viewing angle of 63 degrees, illustrated in Figure 9 satisfies the up-view and down-view from the pilots eye referencing the zero bearing horizon requirement. The horizontal field of view stretching 248 degrees has a window obstructing left of pilots center by 20 to 30 degrees, meaning the *Firehawk* is certifiable in terms of the compartment regulations.

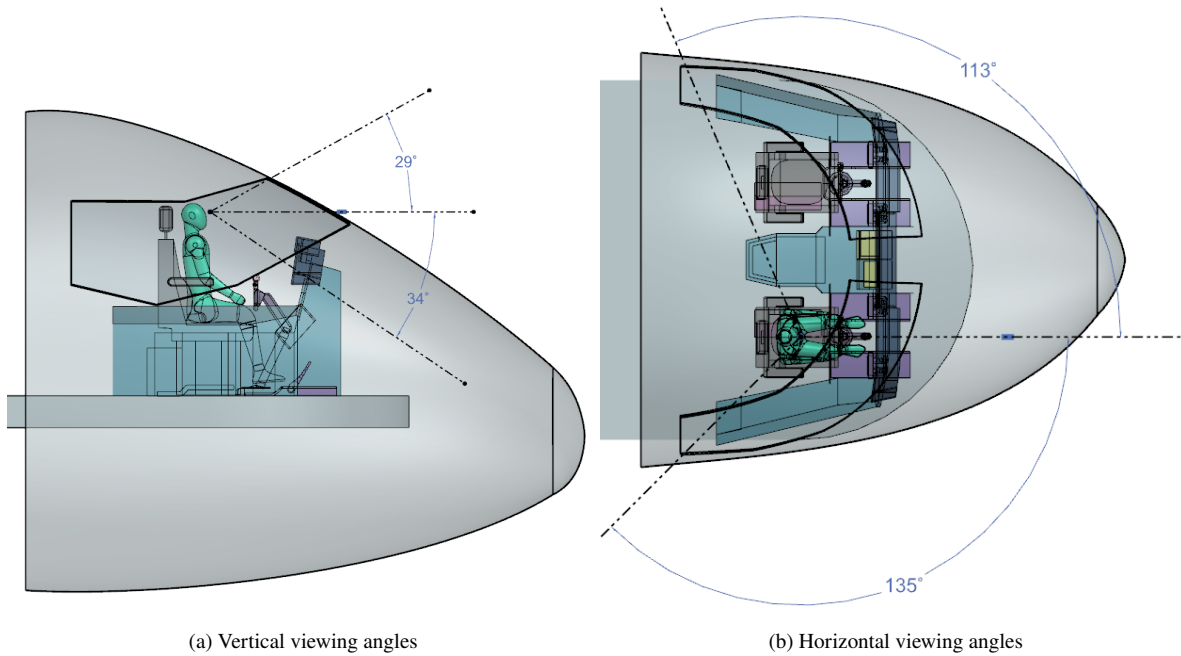


Fig. 9 Maximum Pilot Viewing Angles.

VI. Propulsion

A. Propulsion System Selection

The powerplant selection was determined through maximum thrust requirements found from the performance analysis of the mission profiles (detailed in Section VIII). The maximum thrust required is 41,000 lbf during takeoff at an altitude of 5,000 ft MSL and a speed of Mach 0.26, on a +35°F hot day. Due to thrust lapse from both altitude and lower air density as a result of ambient temperature, the total thrust required at standard sea level conditions is found to be 50,900 lb. The thrust required to meet payload capacity and BFL requirements rules out the possibility of using reciprocating engines as they lack sufficient power. Turbojet engines are unsuitable due to their poor efficiency at subsonic speeds compared to both turboprop and turbofan engines. In most commercial roles, including high capacity firefighting aircraft, they have been supplanted by turboprop and turbofan engines. Therefore, the team considered the usage of either turbofan or turboprop engines.

Turboprop engines were considered for the powerplant. However, assuming a propeller efficiency of 80% as stated in Raymer [2], the equivalent maximum power required would be about 34,700 hp. An airplane powered by the Europrop TP400-D6 (capable of 11,000 shp [20]), one of the most powerful turboprop engines currently in production, would require four engines for initial climb, while one using the more plentiful Allison T56 (capable of 4,591 shp [21]) would require eight engines. The power requirements of *Firehawk* means using turboprop engines is not viable, so turbofan engines were ultimately selected to power the airplane. In contrast to the number of turboprop engines needed to provide the required power, turbofan-powered aircraft with similar thrust requirements only require two engines.

As a purpose built high capacity firefighting aircraft designed to replace current aircraft (which are primarily conversions of passenger or cargo aircraft), it was important to prioritize both effectiveness and cost so operators would be able to justify purchasing this aircraft to replace existing firefighting aircraft.

B. Engine Selection

As stated in Section V, the airplane will be equipped with two engines. Therefore, the thrust required per engine is 25,450 lbf. Additionally, *Firehawk* will be operating in remote areas with high ambient air temperatures and air pollution like smoke, so additional thrust is desirable to account for thrust losses from operating in these conditions, including the possibility of OEI. More thrust also allows for increased design flexibility and future upgrades that may increase the weight of the airplane.

Many high capacity firefighting aircraft today are conversions of passenger aircraft, and *Firehawk* has similar thrust requirements to many modern passenger aircraft. Therefore, a trade study was conducted to select an engine in the required thrust class based on those currently being used by passenger aircraft today. The major factors that were considered when selecting the powerplant included takeoff thrust, SFC [22], reliability, and weight. Specifications for several engine options are tabulated in Table 10. Official SFC values were not available for the CFM LEAP-1A30 or

the PW1431GA-JM, so they were estimated based on company statements and comparisons with previous generation engines [23] [24].

Table 10 List of turbofan engines and important parameters

Engine	Takeoff Thrust [lb]	SFC [lb/lb-hr]	Weight [lb]	T/W Ratio
CFM56-5C3/F4 [25]	32,500	0.32	5,250	5.70
IAE V2530-A5 [25]	29,900	0.36	5,250	5.64
CFM LEAP-1A30 [26]	32,160	0.306 [23]	6,632	4.85
PW1431GA-JM [27]	31,572	0.315 [24]	6,300	5.01

The CFM LEAP-1A30 was selected as the powerplant of the airplane. It provides improved SFC compared to the CFM56-5C3/F4 and V2530-A5, while being superior in reliability to the PW1431GA-JM, with the Pratt & Whitney GTF series of engines having suffered from several in-flight failures [28] and excessive corrosion [29]. Although its thrust-to-weight ratio is lower than the PW1431GA-JM, it is not by a significant amount.

C. Safety Considerations

As detailed in Section VIII, in the event that one engine fails, the other engine will still provide enough power to allow *Firehawk* to successfully take off while satisfying the BFL requirement of 8,000 ft set in the RFP, as well as OEI requirements defined in 14 CFR § 25.121 [19], which require an airplane with one-engine-inoperative to climb at a minimum gradient of 2.4 percent during takeoff when the landing gear is fully retracted.

D. Engine Performance

Table 11 contains specifications for the selected engine. The weight of the integrated powerplant system is found using Raymer [2] and Roskam [3], as detailed in Section XI.

Table 11 CFM LEAP-1A30 Specifications

Parameter	Value
Takeoff thrust	32,160 lb
Static SFC (estimated)	0.306 lb/lb-hr
Dry weight	6,632 lb
Thrust-to-weight ratio (IPPS)	3.59
Length	131 in
Fan diameter	78 in
Max diameter (estimated)	84 in
Bypass ratio	11

Engine performance varies with many factors, including external conditions like altitude, speed, ambient temperature, as well as other variables like intake, nacelle, or nozzle geometry. The thrust available and SFC for the uninstalled engine was estimated using equations from Daidzic [30], who proposes a method to calculate both parameters for the

entire flight envelope. The installation losses are then calculated, as detailed in Section VI.E. The estimated thrust available and SFC for the installed engine at full throttle are plotted for altitudes from 0 to 36,000 ft and speeds from Mach 0 to Mach 0.8 on a hot day at +35°F in Figures 10 and 11. The plots are verified by static and cruise data for other high bypass turbofans as well as the plots in Raymer Appendix E [2].

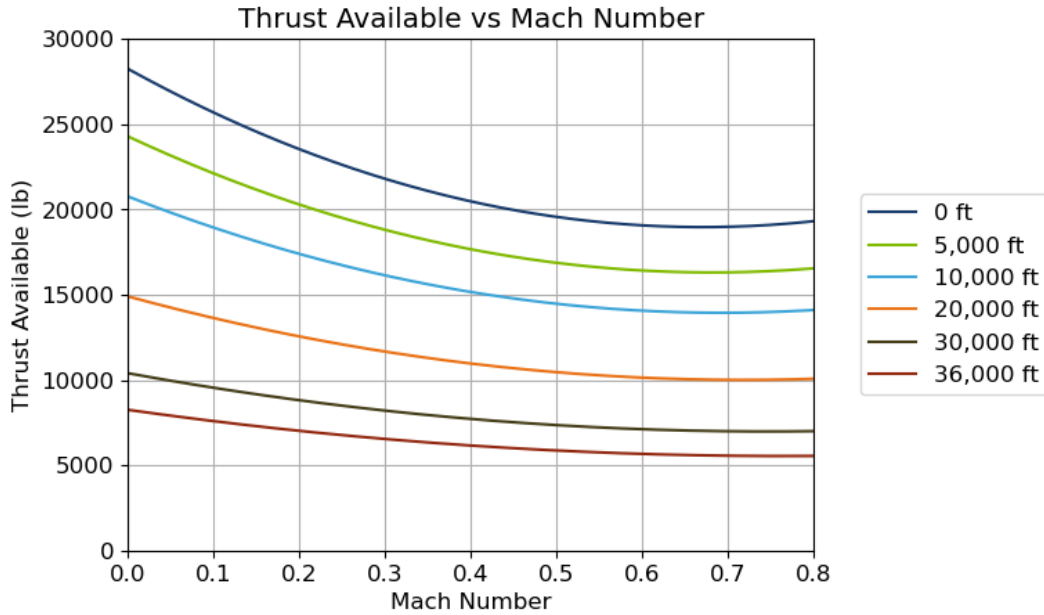


Fig. 10 Thrust available as a function of Mach number at different altitudes.

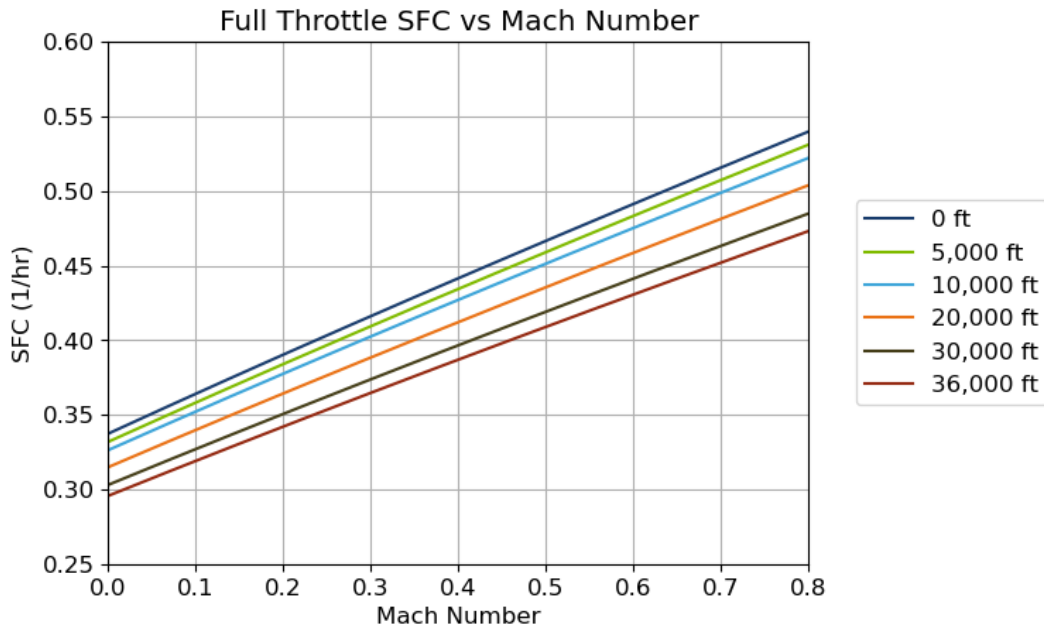


Fig. 11 Full throttle SFC as a function of Mach number at different altitudes.

SFC is also dependent on the throttle setting of the engine. Raymer Eqn 13.9 [2] provides a method to estimate the part-power SFC of the engine given the full throttle SFC and throttle setting. Part-power SFC of the installed engine is estimated at Mach 0.6, the cruise speed during the ferry mission, for throttle settings from 60% to 100%, and is shown in Figure 12. As can be seen, the SFC is minimized around 70% throttle.

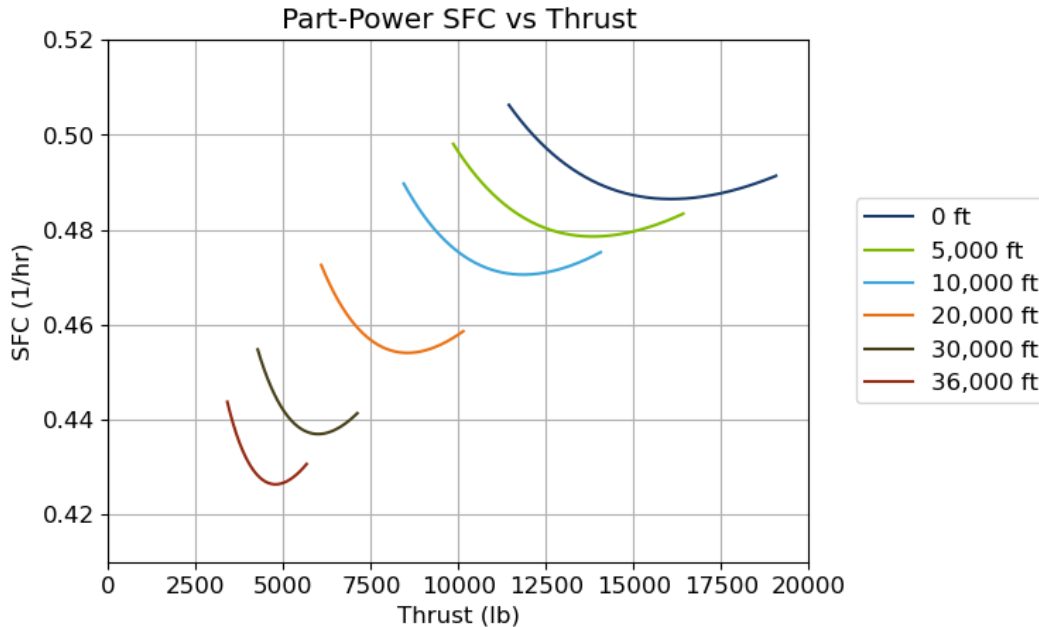


Fig. 12 SFC at 100% throttle vs. Mach number at different flight conditions.

E. Inlet, Nacelle, and Exhaust Design

The inlet front face is tilted 3.5 degrees down to account for the airplane angle of attack at low speeds, such as during takeoff and while dropping retardant. By angling the inlet as such, it will provide sufficient capture area for the engine at higher angles of attack. Especially at low speeds, where the airplane will be operating during drop missions, the angling of the inlet front face ensures that the engines do not experience a sudden decrease in thrust due to insufficient airflow. The inlet is also sized to be smaller than the engine fan face in order to decelerate incoming air, which would otherwise be too fast for the engine to operate efficiently. Isentropic flow relations are used between the inlet and fan areas to calculate an inlet area of about 93.7% of the fan area, or 36.0 ft². At a cruise speed of Mach 0.6, the inlet will decelerate incoming air to Mach 0.5, and is estimated to have a pressure recovery of about 99% according to Raymer [2]. Figure 13 shows the design of the engine inlet.

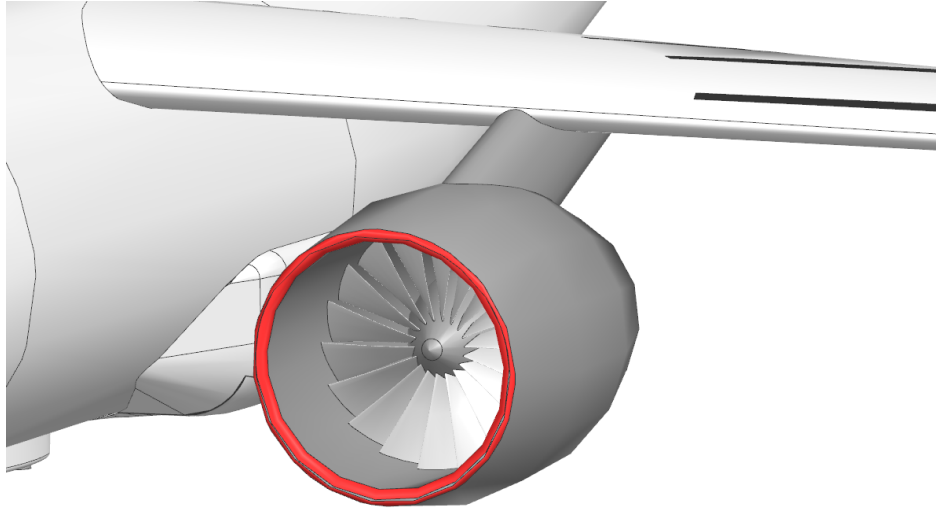


Fig. 13 Inlet design.

Raymer also specifies that for subsonic inlets, the inner and outer lip radius should be about 8% and 4% of the inlet front face radius respectively in order to minimize distortion and the effects of angle of attack during takeoff and landing [2]. Also, the design of the engine nacelle was based on that of the A320neo [31], while the manufacturer's nozzle was retained, as a nozzle specifically designed for other capabilities like thrust vectoring or stealth was unnecessary for the firefighting mission. Figure 14 shows the design of the engine nacelle and nozzle.

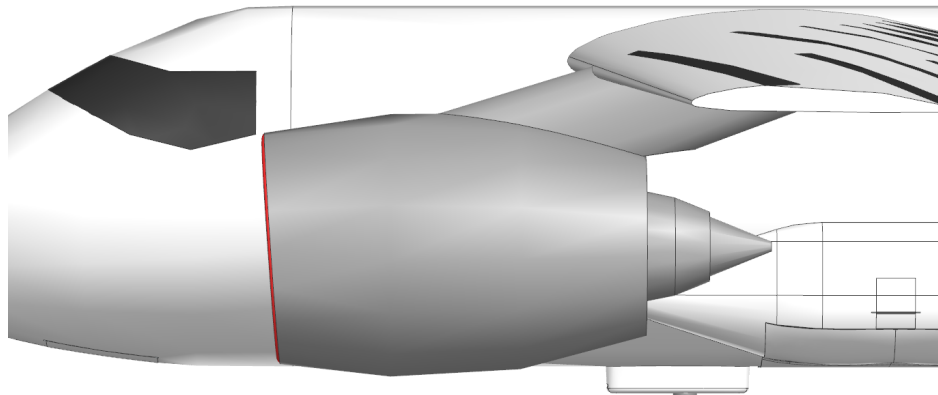


Fig. 14 Nacelle design.

It was determined that the engine had an thrust loss of about 6.3% when accounting for inlet pressure recovery, bleed

air extraction, and power extraction using Eqns 13.6 and 13.8 from Raymer [2]. The installed SFC is then calculated using the fuel mass flow rate and is found to increase by about 6.7%.

F. Systems

1. Engine System

The engines are controlled by a FADEC, which combines throttle inputs from the pilot with data from engine sensors to optimize performance. More information on the FADEC and engine architecture is detailed in Section **XII.E**.

2. Fuel System

The engines are fed fuel from three fuel tanks, two in the wing and one in the fuselage. The fuel system of *Firehawk* is further detailed in Section **XII.F**.

G. Future Work

The engine was selected based on a previous thrust requirement that is higher than the current maximum thrust requirement. As a result, the airplane has a significant amount of excess thrust even when accounting for installation, speed, and operational thrust losses during the firefighting mission. As a result, an engine with a lower maximum thrust may be more desirable to decrease costs and increase the average engine throttle setting to allow the airplane to cruise more efficiently during its ferry mission. The CFM LEAP is offered in many variants with similar weight and SFC, but different thrust ratings, allowing the powerplant to be sized to more appropriate thrust levels without significant changes to the airplane design.

Additionally, the team plans to further increase the fidelity of the engine performance data by using GasTurb to calculate the thrust available and SFC. GasTurb can also calculate thrust losses due to inlet design, bleed air offtakes, and shaft power offtakes. As more detailed numbers are provided for bleed air and power offtakes, installation losses can be calculated with higher accuracy.

Furthermore, the design of the engine inlet and nacelle should be further refined to account for the flight conditions that *Firehawk* will be flying at. The nacelle in particular is currently based on that of the A320neo, and further analysis and refinement should be performed to design a nacelle that is more aerodynamically efficient for the airplane's flight conditions.

VII. Aerodynamics

A. Airfoil Selection

The airfoil selection process for the design mission depends upon the ferry cruising speed of 0.6 Mach, therefore the first step in picking an airfoil was estimating the design lift coefficient for ferry cruise. This value was found to be 0.425. The correlation between relative thickness and the design Mach number for two-dimensional flow was determined by applying the unswept wing equation from Torenbeek [32]. Although a drag penalty is expected with thinner airfoils, a $t/c_{avg} = 0.12$ was desired. The idea behind this desire to have enough space for the fuel tanks and avoid leading edge stall of the low-aspect-ratio wing, while restricting wing weight. Next, aerodynamic analysis of NACA four, five, and six-digit airfoils was performed using the vortex-lattice software XFLR5 and integral method described by Eppler via JavaFoil [33] [34]. The computational results were comparable to experimental wind tunnel data obtained from “Theory of Wing Sections” for only the lower Reynolds numbers [35]. Since the software is unable to accurately analyze airfoils in the transonic regime, a combination of Airfoil Tools [36] and SOLIDWORKS flow simulation was adopted to obtain aerodynamic data related to isolated airfoils [37]. The analysis was performed at the highest mission Reynolds number of 41.5×10^6 corresponding to the critical dash mission segment after the drop when aircraft climbs back to the cruising altitude of 20,000 feet above sea level. Candidate airfoils were compared in Table 12 below. For the trade study, desired aerodynamic characteristics were ranked in order of importance: maximum lift coefficient to minimize V_{stall} , angle of stall, drag coefficient at maximum lift coefficient, pitching moment coefficient, and the lift and drag coefficient at zero geometric angle of attack.

Table 12 Airfoil Section

Airfoil	Cl_{max} at $Re = 41.5 \times 10^6$	α_{stall} (deg)	$Cd(Cl_{max})$	C_{mo}	Cl_0	Cd_0
4412	1.5	13	0.0148	-0.090	0.4	0.0060
4417	1.4	14	0.0152	-0.043	0.3	0.0065
23012	1.5	12	0.0124	-0.013	0.3	0.0060
63A412	1.55	15	0.0120	-0.004	0.4	0.0039
64A414	1.76	16	0.0122	-0.004	0.4	0.0044
63A015	1.8	14	0.0128	0.000	0.0	0.0052
64A410	1.65	13	0.0116	-0.042	0.4	0.0040

It was found that the five-digit airfoils have poor stall characteristics compared to the four-digit. Moreover, the six-series demonstrated the highest maximum lift coefficient which out-weighs the disadvantage of a sharper stall quality. During cruise in the transonic regime, air flow on top of the airfoil will become supersonic and generate shock waves. Hence, supercritical airfoils were found more advantageous for the *Firehawk*, since they are designed with a flatter upper surface to provide a smoother deceleration of the supersonic flow region. Figure 15 shows the aerodynamic performance of two such high cambered airfoils (NACA 64-414 and 64-410) corresponding to ferry cruise condition of

$M = 0.6$, $Re = 22.6 \times 10^6$, and a smooth surface condition $a = 0.6$.

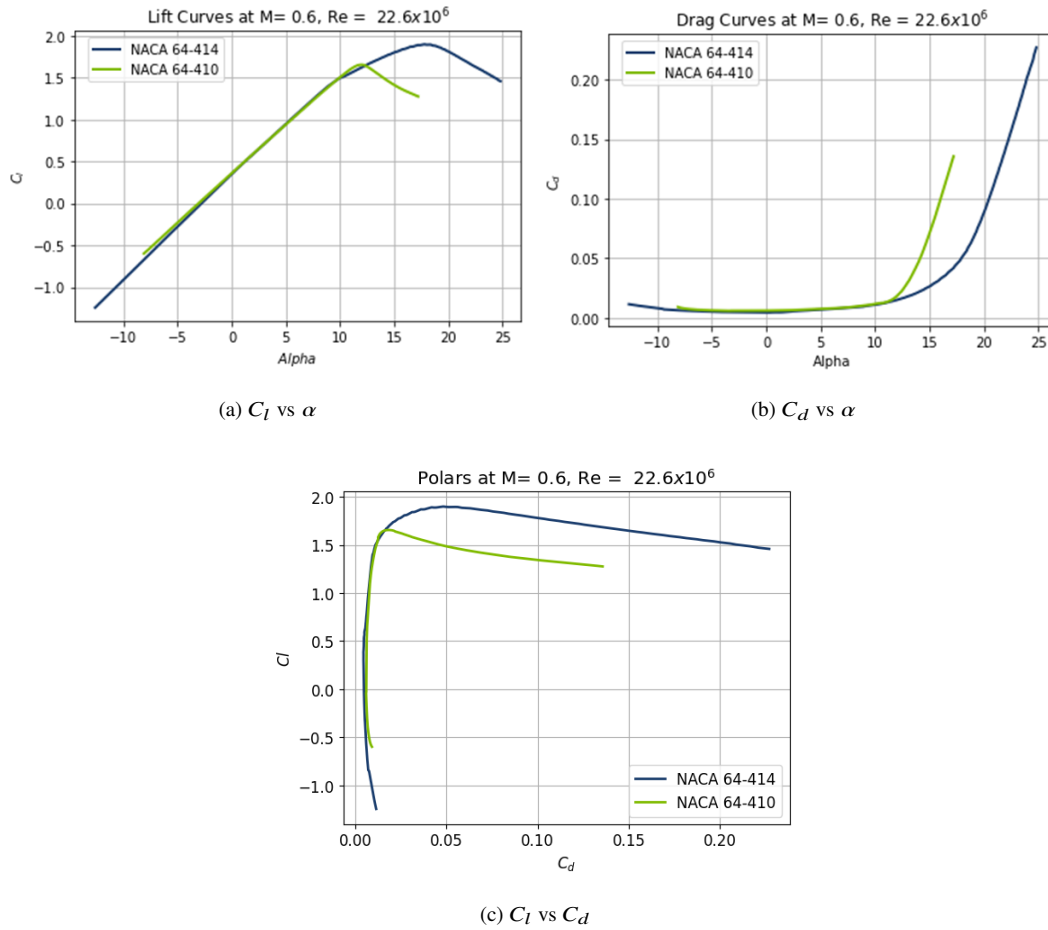
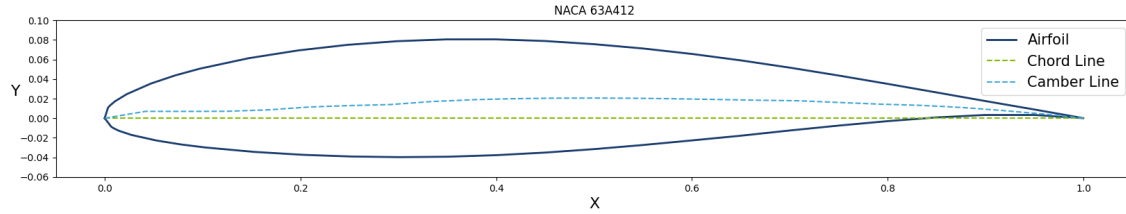
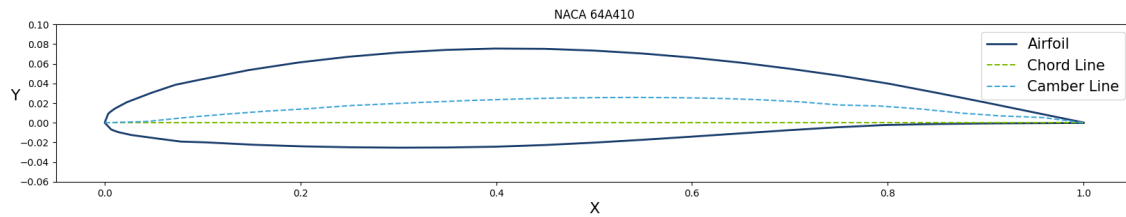


Fig. 15 Cruise Aerodynamic Results using XFLR5.

According to the mission profile, it can be observed that the selected airfoils are capable of bearing the highest speed condition of Mach 0.6. The root chord airfoil was chosen to be NACA 64-414 with the thinner NACA 64-410 tip chord airfoil geometry shown in Figure 16. The $C_{l_{max}}$ at the ferry cruising altitude was determined to be 1.86 and 1.56 for the chord and tip respectively. The lift-over-drag ratio at the same condition is 14.45, which is in accordance with the derived requirements by performance. These airfoils were found suitable because small decreases in drag caused large increases in lift to drag ratios. From the drag polar plots in Fig. 15, it can be seen that both airfoils have minimum drag near zero angle of attack when C_l is equal to the design lift coefficient.



(a) NACA 63A412



(b) NACA 64A410

Fig. 16 Final Airfoil Design.

B. Wing Design

The wing configuration was inspired by the seed aircraft, the Boeing 737-300. According to the mission profile in Section VIII, the operating cruise velocity for the design ferry range reaches a maximum of Mach 0.6. Furthermore, after the payload drop, the dash segment reaches the required calibrated airspeed of 300 knots at Mach 0.58. Since critical flight conditions of operation are below the critical Mach speed for a straight wing aircraft [2], the main challenge in designing the wing was accounting for the low stall speed and high Reynolds numbers.

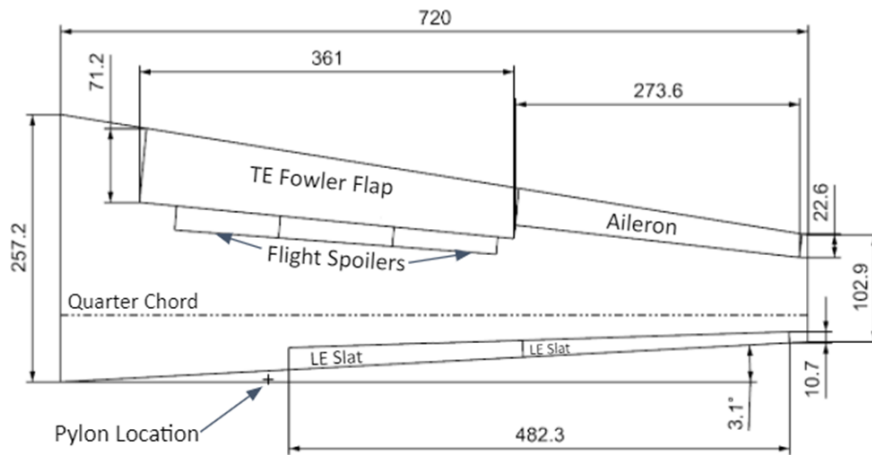


Fig. 17 Top Drawing of Major Wing Dimensions with Control Surfaces Layout (inches).

As a consequence, a straight wing was employed meaning the quarter chord sweep was set to zero degrees as shown in Figure 17. This was in order to prevent the wing from reaching its critical Mach number in high cruising speed

conditions. Thus it was concluded that reducing the wing leading edge sweep to 3.12 degrees would lower the structural weight of the wing and be a more optimal for the mission.

Table 13 Wing Geometry

Parameter	Firehawk
Wing Area	1,800 ft ²
Span	120 ft
AR	8
Wing Loading	87.33 psf
Taper Ratio	0.4
Root Chord	21.43 ft
Tip Chord	8.57 ft
Mean Aerodynamic Center	15.92 ft
LE Sweep	3.1 deg
Dihedral Angle	-2 deg
Incidence Angle	2 deg

Next, a trade study was conducted to determine the optimal aspect and taper ratio combination. The aspect ratios ranged from five to ten in increments of one, while the taper ratio was varies by 0.05 from 0.25 to 0.45. According to numerical analysis results, the minimum induced drag coefficient and maximum Oswald efficiency factor values were obtained at the taper ratio of 0.4. At zero geometric angle of attack, the highest lift coefficient and lowest empty weight was achieved at an aspect ratio of eight. When the weight reduction from increasing the taper is taken into account, a taper ratio of about of 0.4 was chosen, yielding a nearly elliptical lift distribution, most ideal for the unswept wings as shown in Figure 18. Using the MTOW of 159,675 lbs, the wing area was determined to be 1800 ft² with a wing loading of 87.7 psf.

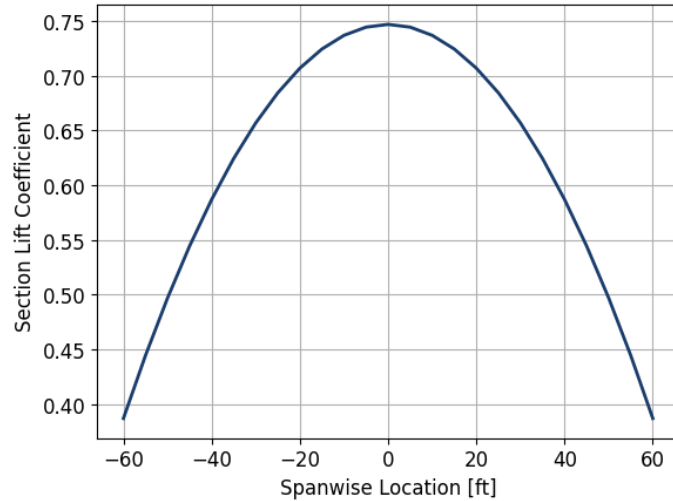


Fig. 18 Lift distribution along the Wingspan.

The spanwise lift distribution was analyzed at zero angle of attack for the cruise configuration by normalizing the sectional lift coefficient by the total lift coefficient. The wing root incidence was set to 2 degrees because it yields a positive angle of attack during take-off and decreases drag in cruise flight. The anhedral was set to be -2 deg based on roll stability calculations in Section IX as well as to pass the engine ground clearance standard set by 14 CFR § 23.933 [38]. The chosen parameters were comparable to historical data and similar weight class fire-fighting aircraft, with the final wingspan dimension equal to 120 ft and a mean aerodynamic chord of 16 ft.

C. High-Lift Devices

The design of high lift devices was driven by the landing and takeoff distance requirements. Determined in Section VIII.E, the required coefficient of lift 0.709 is essential to taking off in less than 8,000 feet at an altitude of 5,000 ft $\text{DISA} \pm 35^\circ\text{F}$. After evaluating the control surfaces of similar aircraft, four different high lift devices were considered for the trailing edge design: split flaps, hinged flaps, zap flaps, and Fowler flaps. For the leading edge, Krueger flaps, variable camber flaps, and slats were considered for the trade study. Since Fowler flaps are the most widely-used flap design in the commercial industry, the trailing-edge high lift system was sized by choosing an initial flap to wing area ratio similar to the Boeing 737 arrangement [39]. Next, a parametric trade study was conducted to optimize the high lift sizing by iterating until the desired landing and takeoff change in lift coefficients, δC_{Lmax} , were achieved. Analysis considered a variation of flap chord percentages $\frac{c_f}{c}$ with the section lift effectiveness, $\alpha \delta f$, plotted against a range of deflection angles in Figure 19.

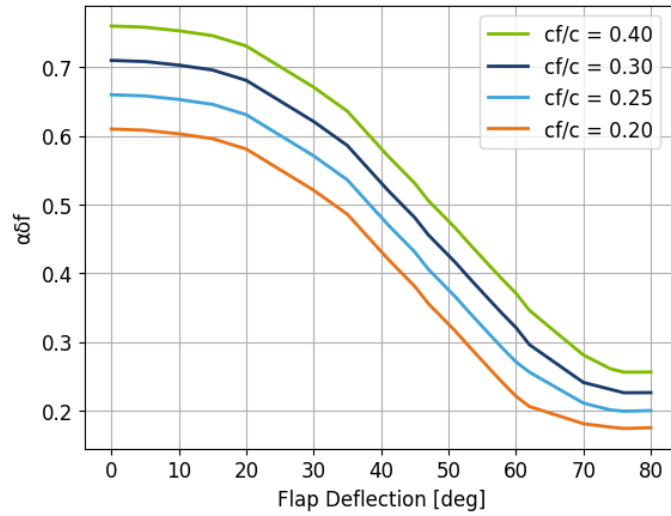


Fig. 19 Section lift effectiveness of single-slotted Fowler flaps.

Extending the Fowler flaps between 30 to 40 degrees increased projected area thus shifting the lift curve to the right. The leading-edge slat was crucial for delaying flow separation and allowing more lift generation without reducing the stall angle of attack. The fully deflected tip airfoil combination of trailing edge Fowler flap and leading edge slat in Fig. 21 was determined as a highly efficient lift-increasing arrangement for the *Firehawk*.

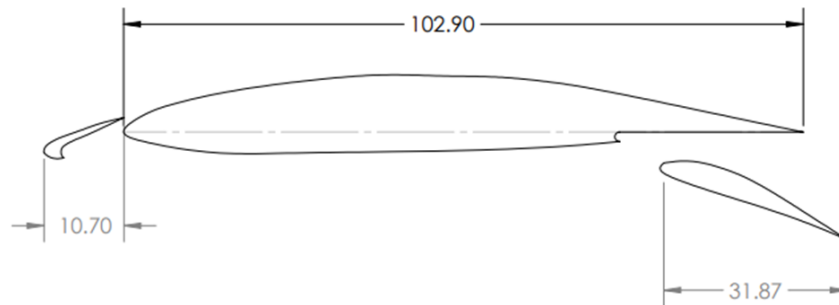


Fig. 20 NACA 64-410 high lift devices drawing (inches).

Parameter	Value
Fowler area [ft ²]	771.5
Slat area [ft ²]	1,170
Fowler extension ratio (c'/c)	1.3
Slat extension ratio (c'/c)	1.04
Fowler $\frac{S_{WF}}{S_w}$	0.55
Fowler $\frac{S_{WF}}{S_w}$	0.65
Flap extension ratio (cf/c)	0.3
Fowler Hinge angle (deg)	9.2
Slat Hinge angle (deg)	3

Table 14 High-Lift Devices Dimensions

To begin analysis, the 2D lift curve slope, $C_{l\alpha}$ and maximum coefficient of lift of the wing in clean configuration were estimated in AVL to be 6.89 per radian and 1.76 respectively [40]. Then using Eq. 12.6 in Raymer the 3D lift curve slope of the wing were calculated, resulting in $C_{L\alpha} = 4.22$ per radian (0.074 deg^{-1}). Lift contributions from the rest of the aircraft components were accounted for by adding an additional 8% to the wing slope. The resulting lift curve slope was determined to be 4.56 per radian (0.079 deg^{-1}), with a clean configuration lift coefficient at zero angle of attack equal to $C_{L0} = 0.44$. Maximum lift for the take-off and landing configurations were estimated by adjusting the zero lift angle of attack in accordance to the trend effects of the chosen trailing edge deflections as demonstrated in Figure 21.

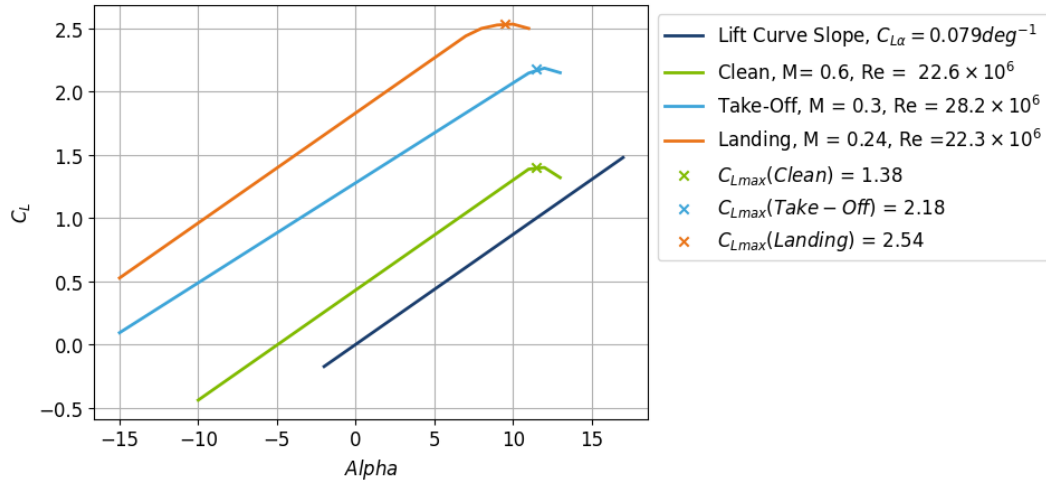


Fig. 21 Low Speed Lift Curves of single-slotted Fowler flaps.

For the chosen angles of deflection and the effects of leading edge slats, the takeoff and landing configurations results were calculated using Nicolai [41] in Table 15. Since high-lift system performance is dominated by viscous effects for multi-element airfoils, results inconsistencies of the two-dimensional Navier Stokes simulations were nullified by using a high-fidelity software.

Flight Condition	LE Slat Deflection	Slat ΔC_{Lmax}	TE Fowler Flap Deflection	Fowler ΔC_{Lmax}	C_{Lmax}
Takeoff	15 deg	0.38	30 deg	0.81	2.57
Landing	35 deg	0.43	45 deg	1.16	2.96

Table 15 Impact of HLD on C_{Lmax}

D. Drag Build-Up

Total drag is made up of induced, parasitic, and compressibility drag. Since the airplane will be operating at high Reynolds numbers, the flow along the components' surfaces are assumed to be entirely turbulent when calculating skin friction coefficients. Parasite drag was computed using Raymer's component buildup method, where Eq. 7.12 was used to determine the ratio between wetted area and reference area to be $\frac{S_{wet}}{S_{ref}} = 4.84$ [2]. Further wetted surface area estimations of the aircraft's components were found using the equations in Chapter 9 of Nicolai [41]. Interference effects on component drag were estimated with the interference factor values adopted from Raymer [2] and the drag count for the cruise condition summarized in Table 16.

Table 16 Parasitic Drag Build-Up at Cruise [Count]

Component	Cruise	Contribution (%)
Wing	71.7	42
Fuselage	30.1	18
Horizontal Stabilizer	24.8	15
Vertical Stabilizer	20.9	12
Nacelle	11.06	7
Landing Gear	7.32	4
Pylons	2.5	1
Flap Hinges	1.6	1
Total	169.0	100

After the wing, vertical tail, horizontal tail, fuselage, engine nacelles and flaps were modeled in OpenVSP [42]. The OpenVSP PARASITE drag tool generated corresponding results for each element to the Raymer's component buildup and equivalent skin friction methods. The verified component contributions to the cruising parasitic drag are shown in the pie chart below.

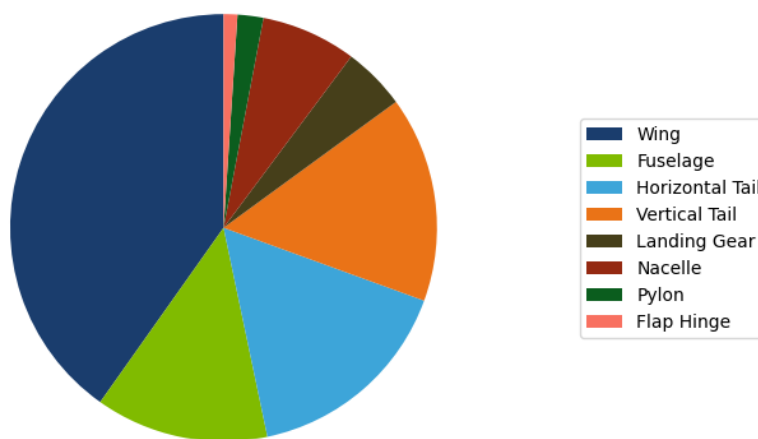


Fig. 22 Parasite Drag Build-Up at Cruise.

Induced drag or drag due to lift was calculated to be 0.0714 using the Oswald efficiency factor of 0.81 and Eq. (12.2) in Raymer [2]. Trim drag was set to 10 % of induced drag based on Nicolai's assumption [41]. Next, the drag experienced during transonic flight due to presence of shock waves called wave drag was found in OpenVSP using

the area-ruling technique by Richard Whitcomb of NACA in 1952 [43]. The aircraft will experience 19.27 counts of wave drag at Mach 0.6. Lastly, flap induced drag and numerically estimated using a combination of equation from the DATCOM method 1978 [44] and Roskam [3]. Contribution of pressure drag caused by large flap deflection angles were found from the SOLIDWORKS Flow simulations, confirming that our take off and landing drag was accurately estimated in Table 17.

Table 17 Takeoff and Landing Drag Build-Up

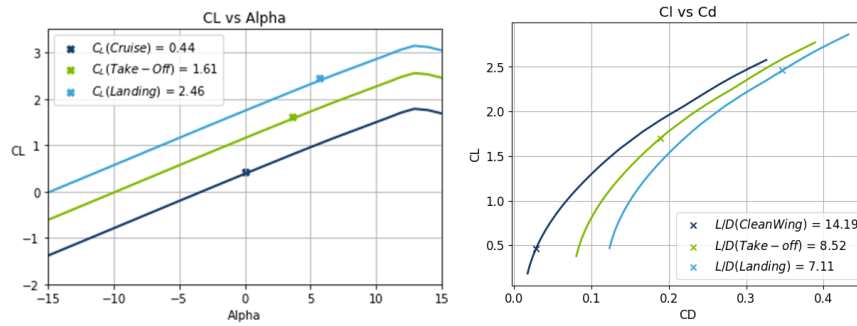
Drag Type	Takeoff	Landing
C_{D0}	0.0814	0.1191
C_{Di}	0.05452	0.07138
C_{Dtrim}	0.00545	0.00716
C_{Dwave}	0.001727	0.001964
C_{Dflap}	0.0534	0.1436
C_{Dexcr}	0.000617	0.00077
C_{Dtotal}	0.189	0.346

E. Aircraft Analysis

With the defined geometry and airfoils selected, the next step was to confirm the aerodynamic capability of the current aircraft design in OpenVSPAERO, a fast vortex lattice solver for critical mission conditions [42]. Table 18 summarizes the Mach and Reynolds numbers at the key flight segments of the mission. The same deflections angles were set for the dash and drop segments as for the take-off and landing conditions.

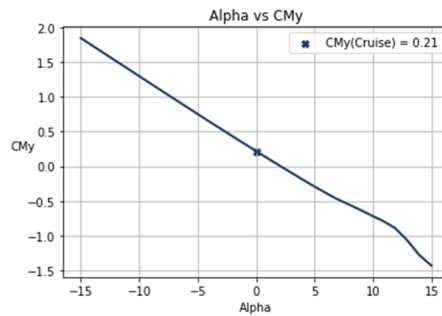
Table 18 Full Wing Analysis for Key Mission Conditions

Flight Condition	Reynolds Number	Mach	AOA	CL_{max}
Take-Off	28.2×10^6	0.30	15	2.53
Ferry Cruise	22.6×10^6	0.60	16	1.89
Drop Descent	29.6×10^6	0.38	15	2.85
Dash	41.5×10^6	0.58	14.5	2.65
Landing	22.3×10^6	0.24	15	2.94



(a) C_L vs α

(b) C_L vs C_d



(c) CM_y vs α

Fig. 23 VSPAERO Analysis for aircraft takeoff and landing lift curve slope and drag polars.

The aircraft's cruise, takeoff, and landing lift curves and drag polars are plotted in Figure 23 and are consistent with the flight operation limits calculated in Section VIII.

Table 19 Key Aircraft Information

Parameter	Cruise	Takeoff	Landing
α [deg]	0.52	3.6	5.7
C_L	0.44	1.61	2.46
C_{Dtot}	0.031	0.189	0.346
$\frac{L}{D}$	14.19	8.52	7.11

VIII. Performance

A. Requirements and Approach

From the RFP [1] and derived requirements, it was determined that the aircraft must be able to carry an 8,000 lb payload on a drop mission that has a radius of at least 400 nmi from the departure airfield, as well as fly for a minimum of 3,000 nmi on an empty payload. The aircraft must also be capable of operating at an airfield with a BFL of at most 8,000 ft at 5,000 ft MSL on a +35°F hot day.

To further reiterate on the discussion in Section III.B, the aircraft will perform a multi-drop capable mission in which the aircraft will descend to a minimum of 300 ft MSL and drop retardant ahead of the fire's path twice. To satisfy the 400 nmi design radius requirement, the aircraft will perform its first drop prior to the 400 nmi mark, on its way away from the departure airport, and then drop the remainder of the retardant after turning around and coming back to the airport.

B. Flight Envelope

The flight envelope representing the operable regime of the design aircraft is shown in Figure 24. The graph is composed of multiple lines, V_{min} and V_{max} of which when within, the aircraft can technically operate, despite having only a single pound of fuel in the tanks.

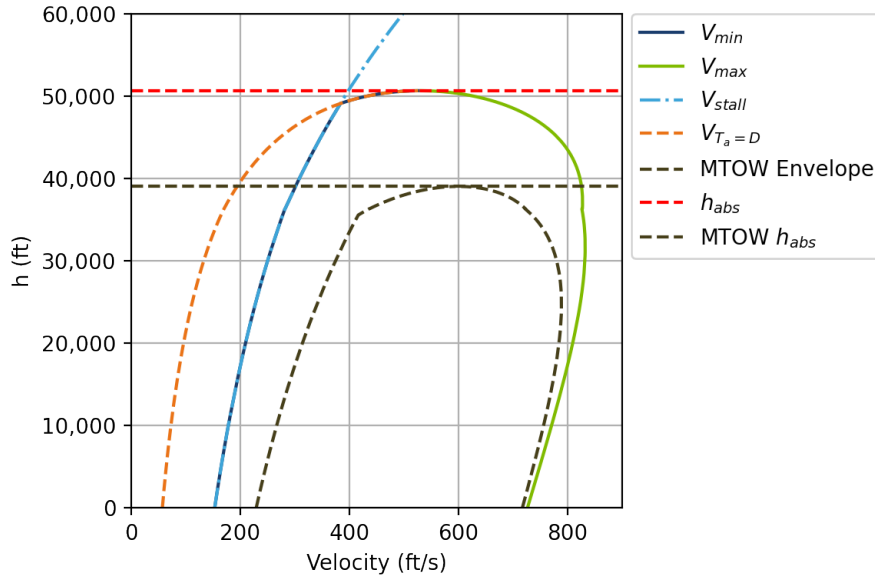


Fig. 24 Flight Envelope.

This envelope indicates the airplane has an absolute ceiling of 50,500 ft. However, as indicated by the dark gray lines, if the aircraft was to cruise at its MTOW, the operating envelope is significantly smaller.

C. Flight Optimization

As the ferry mission is very different to the drop mission, it would seem trivial that the aircraft operates at different speeds and altitudes based on its mission. The drop mission has many different flight conditions in and of itself, implying that each major segment of the flight should be optimized. The optimal flight speed and altitude of each flight segment was determined by maximizing the $\frac{L}{D}$ coefficient that was most relevant to the goal of the segment. For example, as the goal of the ferry mission is to achieve a long range, the aircraft has been designed such that cruise is at the condition where $\frac{L^{1/2}}{D}$ is maximized, because that is the condition that maximizes the Breguet range equation.

For each flight segment many different requirements and considerations need to be made, that include any combination, of weight, speed and altitude. For example, when the aircraft is preparing to make its first drop, it is flying with a full payload. If a second drop is to be made, the airplane would perform differently than it did for the first drop if it was flying at the same conditions, because this time it has half of the payload. Calculations to this level of specificity were not completed at this stage in the design, but has been considered for future work and is further discussed in Section VIII.G. The reason for this is because the aircraft at this point in the design is designed to fly along the solid black line in figure 1. The dashed yellow line signifies an ideal profile that is satisfied so long as the mission in black is. At this stage in the design, there were a total of seven different flight conditions that needed to be considered and are tabulated in Table 20. These conditions were decided based off a basic calculation that involved finding the maximum $\frac{L}{D}$, $\frac{L^{1/2}}{D}$, $\frac{L^{3/2}}{D}$ at each Mach number and altitude. They are shown in Figures 25-27.

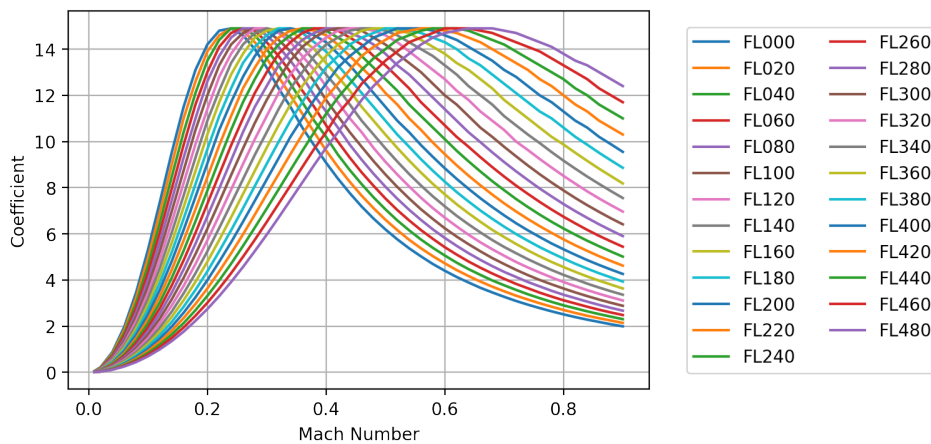


Fig. 25 Curves of Maximum $\frac{L}{D}$ as a Function of Mach and Altitude.

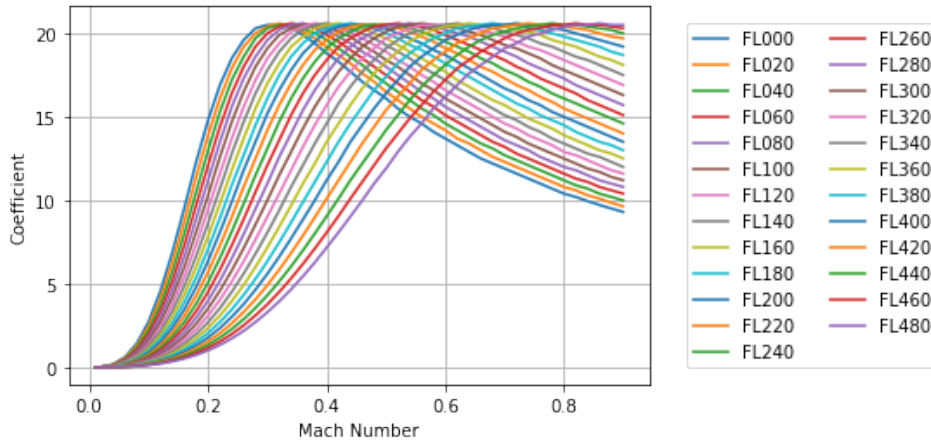


Fig. 26 Curves of Maximum $\frac{L^{1/2}}{D}$ as a Function of Mach and Altitude.

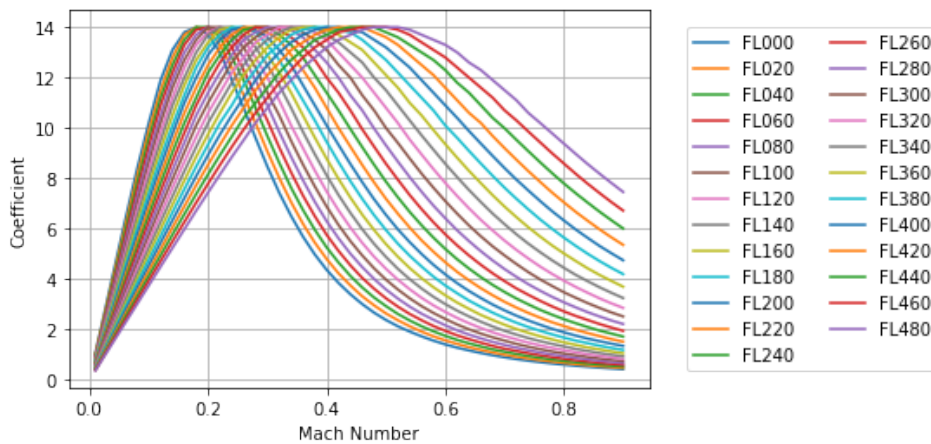


Fig. 27 Curves of Maximum $\frac{L^{3/2}}{D}$ as a Function of Mach and Altitude.

Based on certain requirements and flight conditions, a particular maximum was selected. For example, the goal of the ferry flight was to maximize the range of the aircraft. A ferry cruise was selected to be flown at M 0.6 because this was the Reynolds Number that was acceptable by aerodynamics of the wing as well as was acceptable according to the flight envelope shown in Figure 24. At M 0.6 it can be seen that in Figure 26, the $\frac{L^{1/2}}{D}$ is maximized at FL320. The coefficients that are relevant at FL320 are shown in Figure 28. Thus that is flight condition that is used in a time step integration to determine the precise performance characteristics of the airplane.

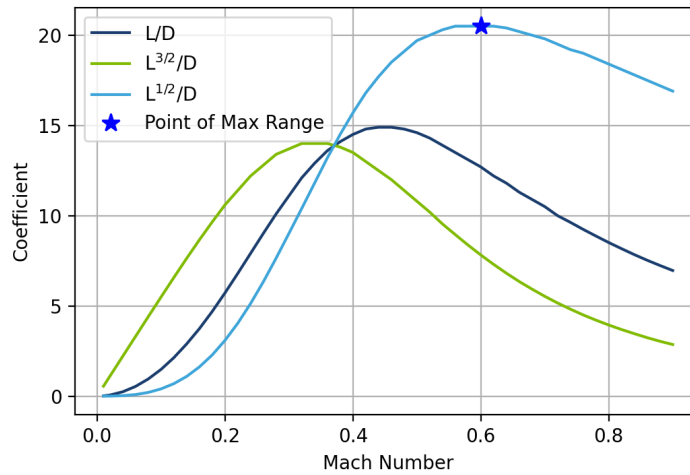


Fig. 28 $\frac{L}{D}$ coefficients at FL320.

This process was repeated for each of the other six flight conditions and is tabulated in Table 20.

Table 20 Designed Flight Conditions

Flight Condition	Operating Mach Number	Operating Altitude	Factors in Selection
Ferry Cruise	M 0.60	FL320	Speed and Altitude, $\frac{L^{1/2}}{D}$ Maximized
Pre-Drop Cruise	M 0.38	FL100	Weight, Minimize Fuel Burn, $\frac{L}{D}$ Maximized
During Drop Cruise	M 0.32	FL030	Speed (Must Satisfy ≤ 125 kts), $\frac{L^{3/2}}{D}$ Maximized
Dash (Post Drop) Cruise	M 0.58	FL200	Speed (Must Satisfy 400kts), $\frac{L}{D}$ Maximized
Loiter Condition (No Payload, Design Mission)	M 0.29	FL060	Minimum Thrust Required, $\frac{L^{3/2}}{D}$ Maximized
Loiter Condition (Full Payload, Design Mission)	M 0.29	FL060	Minimum Thrust Required, $\frac{L^{3/2}}{D}$ Maximized
Loiter Condition (Ferry Mission)	M 0.29	FL060	Minimum Thrust Required, $\frac{L^{3/2}}{D}$ Maximized

D. Fuel Burn and Drag

To accurately calculate the fuel burn and the range of the aircraft, a time step integration was developed and implemented. The goal is to create a solver that is more accurate to the Breguet Range Equation and that can accommodate different operating conditions to yield different results. Two outputs of the time step solver when the flight conditions listed in Table 20 are incorporated are the average drag and the total fuel burn for each segment. The values are listed in Table 21. While the solver is intended to a significantly more accurate estimation than the Breguet

Range equation, the actual performance of the aircraft's average drag and fuel burn should be within 1% of the number quoted in Table 21.

Table 21 Key Flight Statistics

Flight	Segment	Average Drag (lb)	Horizontal Distance Covered (nmi)	Fuel Burned (lb)	Time of Segment (min)
Ferry Flight	Climb	6,619	27.1	907	7
	Cruise	6,615	3050	22,532	496
	Descent	4746	27.1	464	6.5
	Diversion Climb	5782	14.2	162	4.2
	Loiter/Diversion	4695	200	2549	48
	Descent	4682	14.2	482	4.2
Total			3,246.6	31,116	526.4
Design Flight	Climb	10024	6.38	702	2
	Cruise	8,937	240	4,357	40
	Drop Descent	10,432	5.0	327	2
	Drop Loiter	13,014	240	3196	77
	Climb	8,811	3.95	425	1
	Cruise	8,937	240	4,145	40
	Descent	9,937	7.12	361	2
	Diversion Climb	8,964	5.2	597	2
	Loiter/Diversion	8,820	58.6	948	12
	Descent	7,986	7	238	2
Total			813.25	19,421.49	180

E. Field Length Analysis

The balanced Field Length was calculated using equations in both Raymer [2] and Rosakam [3]. Using a carbon ceramic braking coefficient of $\mu = 0.48$ as opposed to $\mu = 0.40$ for standard steel brakes the aircraft is capable of achieving a BFL of 6,200 ft at an altitude of 5000 ft DISA \pm 35°F on dry asphalt with a rolling coefficient of 0.03. Even on a wet asphalt surface with a rolling friction coefficient of 0.05, the *Firehawk* is capable of operating on a BFL of 7,750 feet. This data is validated because a trade study conducted with aircraft of similar weight class such as the Airbus A319, showed similar BFL metrics.

F. Range performance

The range performance of the aircraft is calculated when the $\frac{L^{1/2}}{D}$ is maximized as shown in Figures 25 - 27. As for the ferry mission, the range will be maximized when flying at M 0.60 at FL320. The graph shown in Figure 29 shows the range of the aircraft for any given payload when operating at these conditions. Some notable points are tabulated in Table 22. The range of an empty payload may seem large, however the calculation used to produce the plot assumed all fuel is used during cruise, where in reality, a large portion of the fuel is used during climb thus reducing the range of an actual mission. Also, the ferry mission includes fuel for a reserve mission where the payload-range plot assumes one straight flight.

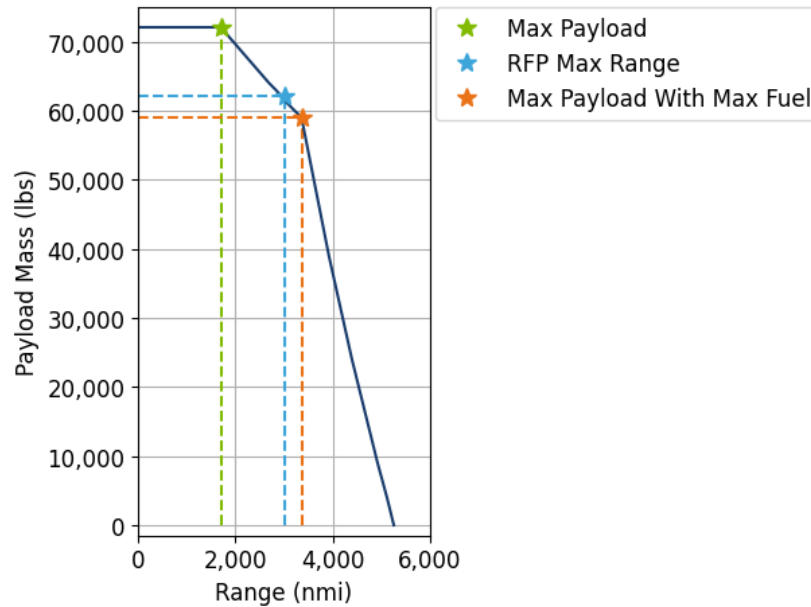


Fig. 29 Payload Range Diagram.

Mission	Payload (lbs)	Fuel (lbs)	Range (nmi)
Max Payload	72,000	15,300	1,705
3,000 nmi	62,200	25,100	3,000
Max Fuel and Payload	59,000	28,300	3,360
Max Range	0	28,300	5,250

Table 22 Payload Range Data

The RFP requirement of a 3,000 nmi radius is quite clearly satisfied and as can be seen by the green star in Figure 29, the 3,000 nmi range is satisfied when carrying 62,200 lbs of payload, albeit not accounting for fuel used for any other portion of the flight except for cruise.

G. Future Work

Future work will involve finding a much more detailed analysis of the takeoff field length to ensure that the aircraft can perform and satisfy the RFP requirement of taking off. Further research could include more detailed analysis into the braking capabilities of the carbon ceramic brakes. Using a time step integration for the take off ground run and stopping distance could provide a more accurate estimation of the balanced field length. Additional work will include calculating the $\frac{L}{D}$ coefficients of the portions of the flight indicated in yellow in Figure 1. This will provide a better understanding of the fuel consumption during ideal flight profiles. Other work would also be finding optimal rate of climb and incorporating a step-climb into the ferry cruise.

IX. Stability and Control

A. Tail Design

The horizontal and vertical stabilizer for the aircraft is in a conventional tail design. The reasoning behind the conventional tail design is discussed in the configuration section.

Table 23 Horizontal and Vertical Stabilizer Airfoil Trade Study

Airfoil	C_{D_0} Horizontal Tail	C_{D_0} Vertical Tail	$C_{l_{max}}$
NACA 0009	0.00414	0.00244	1.25
NACA 0012	0.00444	0.00261	1.40
NACA 0015	0.00479	0.00282	1.45

For the tail design, a symmetric airfoil was chosen because symmetric airfoils exhibit equal effects in orientations at a fixed positive or negative angle of attack. Symmetric airfoils are easier to analyze and are more predictable in flight when considering that the airfoil camber will affect the control surface effectiveness. Additionally, because the aircraft is symmetric, the vertical stabilizer should be symmetric with a zero angle of incidence as there is no rotational flow that would be caused from a propeller. The trade study in Table 23 justifies the NACA 0012 airfoil for both the aircraft's horizontal and vertical stabilizer. The airfoil drag data is taken from the aerodynamic drag buildup and maximum lift coefficient from Airfoil Tools. [36] The NACA 0012 is the middle ground between the NACA 0009 and NACA 0015 when comparing the resulting drag penalty for both the horizontal and vertical stabilizer. Because the aircraft is not designed to fly at transonic speeds, the drag of the NACA 0012 is less important of a consideration. The resulting decisions were primarily based on the structural integrity of the stabilizers and the restoring moments that would be produced. The $C_{l_{max}}$ of the NACA 0012 is roughly the same as the NACA 0015 without sacrificing the added drag and weight of a thicker airfoil, while also having a considerably higher $C_{l_{max}}$ than that of the NACA 0009. In summary, the NACA 0012 airfoil was chosen as it is likely to have the greatest restoring moment without adding unnecessary drag or weight.

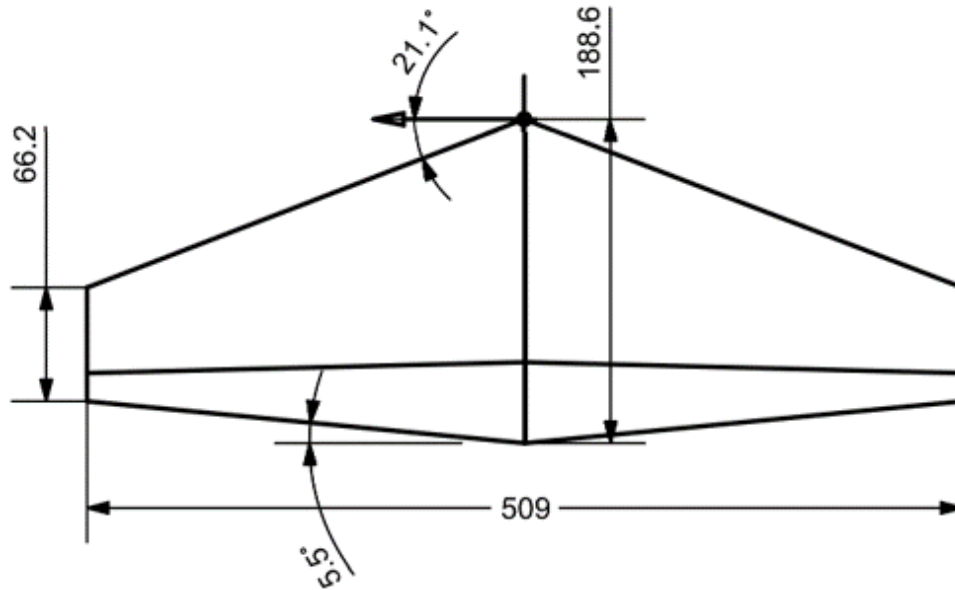


Fig. 30 Horizontal Stabilizer Measured in Inches.

B. Stabilizer Sizing

When comparing horizontal tail sizes, the primary consideration was the static margin and forward rotation limit of the aircraft. According to Raymer [2], the static margin for a transport aircraft is typically between 5-10 percent. Performing a trade study on the horizontal tail size in Table 24, the resulting static margins and area ratios are listed with maximum forward rotation versus most forward cg listed as the forward rotation safety margin. The scissor plot in Fig. 31 gives a visual representation of the impact of area ratio of the horizontal tail to the stability margin and forward rotation limits of the aircraft. The most forward and most aft cg limits are considered during a system failure when one side of the retardant tanks fails to deploy. When analyzing in detail, Table 24 demonstrates that 400 sq. ft. is the minimum tail size that would work with the aircraft. However, the aircraft was chosen to have a 450 sq. ft. horizontal stabilizer as it provides more flexibility when considering adding spare equipment further aft of the retardant tanks, while allowing for more lift to rotate the aircraft on takeoff. Increasing the horizontal stabilizer area beyond 450 sq. ft. was decided to be unnecessary as the tail size increase would only add extra weight to the aircraft with increased structural complexity.

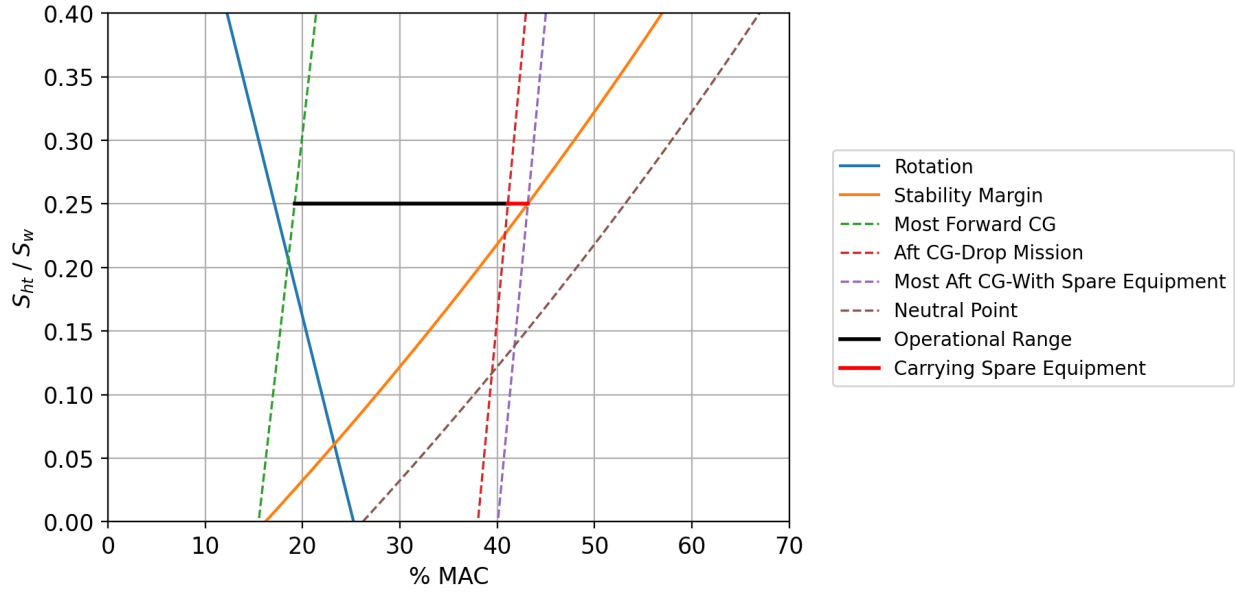


Fig. 31 Scissor Diagram for Horizontal Stabilizer Sizing.

Table 24 Horizontal Tail Sizing Trade Study

Horizontal Tail Size	Aft-most Static Margin	Forward Rotation Safety Margin	S_h/S_w
350 sq. ft.	7.21%	-0.55%	0.194
400 sq. ft.	9.66%	0.76%	0.222
450 sq. ft.	12.0%	2.06%	0.25
500 sq. ft.	14.4%	3.36%	0.277
550 sq. ft.	16.7%	4.72%	0.305

Table 25 Tail Sizing Parameters

Parameters	Horizontal Stabilizer	Vertical Stabilizer	Units
Root Chord	188.6	175.4	in.
Tip Chord	66.2	35.1	in.
Leading Edge Sweep	21.1	31	deg.
Quarter Chord Sweep	15	25	deg.
Area	450	400	sq. ft.
Span	509	273.6	in.
Leading Edge Location	831.6	834.9	in.
Incidence Angle	-2	0	deg.
Taper Ratio	0.35	0.2	-
Tail Volume Coefficient	0.700	0.0825	-

The vertical tail sizing was primarily based off of the constraining condition of takeoff with one engine inoperable as it requires the largest yawing moment to be produced for the aircraft. Because the vertical stabilizer is used to create a yawing moment, the yawing moment coefficients for the aircraft were added for OEI conditions with the thrust and drag of the two engines being represented in coefficient form. Using the vertical stabilizer size of 400 sq. ft. allowed the aircraft to fly straight when considering the thrust from one engine and drag from the other.

Given the horizontal and vertical stabilizer areas, other stabilizer parameters were found and are shown in Table 25. Side view sketches for the horizontal and vertical stabilizer can be found in Fig. 30 and 32, respectively.

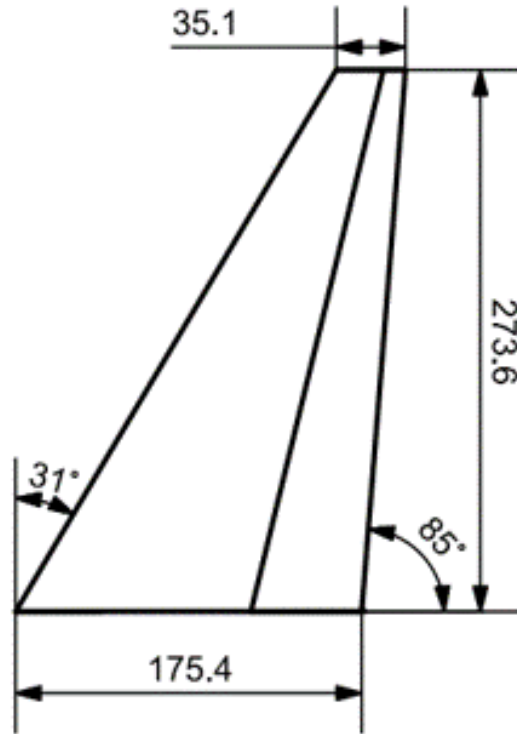


Fig. 32 Vertical Stabilizer Measured in Inches.

C. Control Surface Design

The sizing was initially determined from ratios listed in Raymer [2] of historical values, then compared to the aircraft's requirements. The flap and aileron dimensions can be found in Fig. 17. The rudder and elevator dimensions can be found in Fig. 32 and 30, respectively. The control surface chord ratio, span ratio, and deflection ranges are all listed in Table 26.

In order to check the chord and span ratios for the ailerons, the roll rate was determined for -30 to 30 degrees bank angle. The time it takes for the aircraft to roll from -30 to 30 is 4.6 seconds which is sufficient for FAA regulations and pilot comfort level. For the rudder, the chord and span ratio was checked during OEI, with a maximum rudder deflection angle of 20.5 degrees at stall speed for takeoff. The rudder is therefore sized large enough as it has enough deflection to counter the OEI takeoff requirements. The elevator sizing was taken into account for takeoff rotation with maximum deflection and is also sized adequately as the aircraft can easily rotate when reaching the stall speed, which is designed for additional safety.

Table 26 Control Surface Sizing

Parameter	Aileron	Elevator	Rudder	TE Slotted Fowler Flaps
Chord Ratio	22%	25%	32%	30%
Span Ratio	38%	100%	100%	50%
Deflection Range	20 deg.	20 deg.	26 deg.	40 deg.

The restrictions on the deflection range are determined based off of the Boeing 737's maximum deflection ranges in addition to linear control restrictions. Once the control surface deflection reaches above around 25 degrees the control surface undergoes nonlinear effects that need to be taken into account when evaluating the maximum deflection needed. When analyzing the deflection range and control surface size, the maximum hinge moments were taken into account as well. The hinge moments for each control surface are listed in Table 27. The method for finding the hinge moments is from Etkin and Reid.[45] The elevator and rudder hinge moments are on the same order of magnitude as the surface areas are nearly the same, and the ailerons require much less torque from the actuators as the surface area and chord ratio for each aileron is much smaller than the elevator and rudder. The flaps will require a very large amount of torque meaning that there will be a lead screw connected to an actuator to control the flaps.

Table 27 Control Surface Hinge Moments

	Aileron	Elevator	Rudder	TE Slotted Fowler Flaps
Maximum Hinge Moment	90 lb ft.	230 lb ft.	185 lb ft.	3,700 lb ft.

D. Trim Analysis

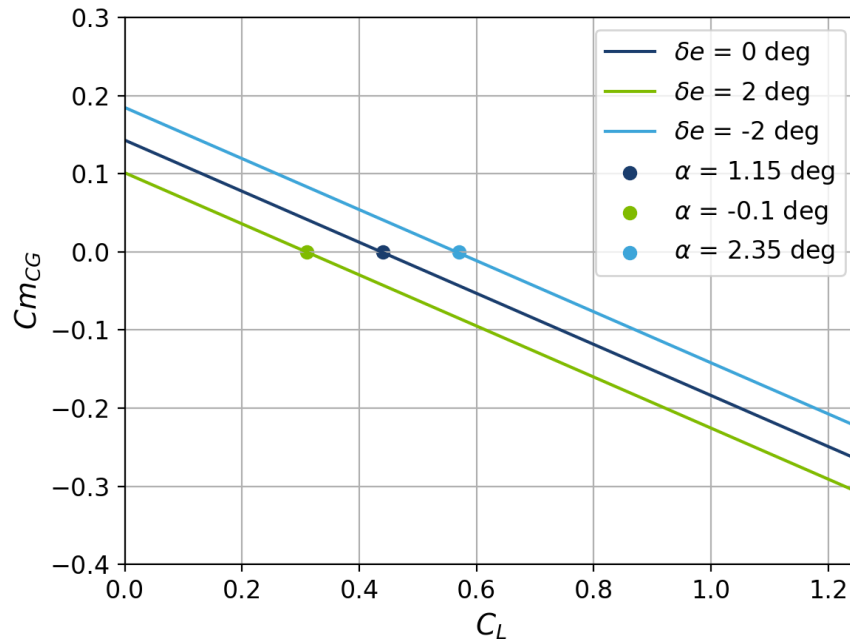


Fig. 33 Cruise Trim Diagram with Flap Deflection of 0 deg.

The trim diagram is shown for cruise, takeoff, and landing using elevator deflections of 0, -2, and 2 degrees shown in Fig. 33, 34, and 35. The trim diagram implies that the aircraft is longitudinally stable as the pitching moment decreases with increased angle of attack which is proportional to the lift coefficient. One thing to note is that at the cruise condition, the aircraft holds the average cruise lift coefficient of about 0.45 with zero elevator deflection. The wing incidence and horizontal tail incidence angles were set for minimizing drag during the ferry cruise mission as well as allowing for the aircraft to fly a low speed drop mission. The wing incidence angle is set to 2 degrees as the aircraft can fly at around 1 degree angle of attack for the cruise flight and 5 degrees angle of attack for the drop mission. The calculation follows an equation found in Roskam [3] that relates the cruise lift coefficient with the lift curve slope of the aircraft. Increasing the wing angle of incidence too much would lead to a negative cruise angle of attack which would be unconventional and be affected by negative lift generated by the fuselage. Additionally, a smaller angle of incidence for the wing would require the aircraft to fly at a higher angle of attack for the drop mission which would decrease visibility for the pilots. After setting the wing incidence angle to 2 degrees pitch up, it was determined that the horizontal tail incidence angle should be set to 2 degrees pitch down to trim for a zero elevator deflection in the cruise mission to decrease drag and maximize the range of the aircraft.

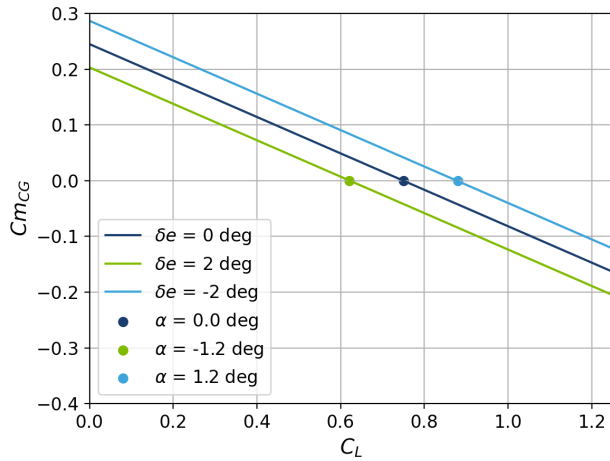


Fig. 34 Takeoff Trim Diagram with Flap Deflection of 30 deg.

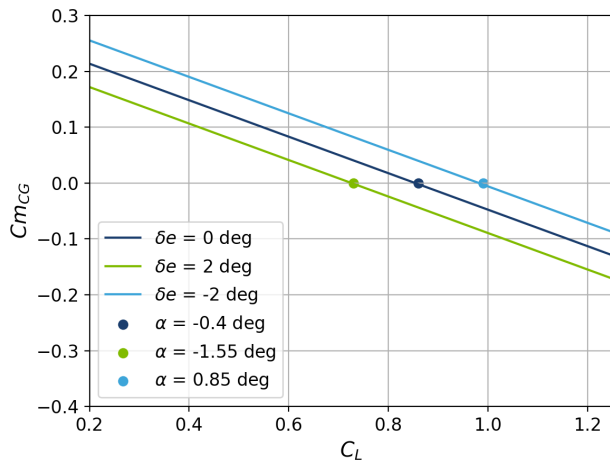


Fig. 35 Landing Trim Diagram with Flap Deflection of 40 deg.

When comparing the takeoff and landing trim diagrams with the cruise trim diagram, it is noticeable that the lift coefficients are much higher due to the flap deflection and the angle of attack values change for the same elevator deflections. Because the aircraft exceeds the range requirements and the elevators are capable of maneuvering the aircraft, a variable incidence tail was not considered as it would increase the weight and complexity of the aircraft, which would impact the cost.

E. Longitudinal Static Stability

Table 28 Longitudinal Stability and Control Derivatives

$C_{L\alpha}$	$C_{m\alpha}$	ϵ_α	$C_{m\delta e}$	$C_{L\delta e}$
6.04	-1.52	0.406	-1.20	0.44

Table 28 shows the lift and pitching moment variations with respect to changes in angle of attack. It is important to have a negative $C_{m\alpha}$ value as a negative value will act as a restoring moment to bring the aircraft to the desired position in steady level flight. The values for $C_{L\alpha}$ and $C_{m\alpha}$ were calculated using the methods listed in Raymer [2]. The $C_{L\alpha}$ calculation primarily involved the cruise speed of the aircraft while the $C_{m\alpha}$ calculation involved the center of gravity, wing and tail aerodynamic centers, area ratios, ϵ_α and $C_{L\alpha}$. The ϵ_α calculation was found from Roskam which involved tail distance, tail height, wing aspect ratio, and fuselage parameters [3]. The calculation for $C_{m\delta e}$ was found from elevator effectiveness and effectiveness of the horizontal stabilizer. [16]

The static margin range was calculated based off of the CG range in percent mean aerodynamic chord found from Mass Properties. Recalculating the $C_{m\alpha}$ values at the endpoints of the CG range and dividing by the $C_{L\alpha}$ of the aircraft results in a direct relation with the static margin. Raymer states that a typical range for the static margin of a transport aircraft is roughly 5 to 10 percent [2]. As long as the static margin for the aircraft is positive, the aircraft has longitudinal static stability. The minimum static margin for the aircraft is 12% MAC which means that there is longitudinal static stability. The calculations for the cg range, static margin, and the aircraft neutral point are all tabulated in Table 29.

Table 29 Longitudinal Static Stability Parameters

CG Range (% MAC)	Static Margin Range (% MAC)	Neutral Point (% MAC)
19.1%–41.0%	12.0%–33.9%	53.0%

F. Lateral-Directional Static Stability

For lateral and directional static stability, the rolling moment and the yawing moment should return the aircraft to a state of zero bank angle and zero side-slip angle. This means that the coefficient for rolling moment ($C_{l\beta}$) needs to be negative while the coefficient for the yawing moment ($C_{n\beta}$) needs to be positive. The values for these coefficients are calculated using equations in Raymer and Roskam. [2][46] From Table 30, the values for $C_{l\beta}$ and $C_{n\beta}$ indicate that the aircraft has both lateral and directional static stability.

Table 30 Lateral-Directional Stability and Control Derivatives

$C_{l\beta}$	$C_{n\beta}$	$C_{l\delta a}$	$C_{n\delta a}$	$C_{n\delta r}$
-0.12	0.15	0.32	-0.02	-0.07

G. Dynamic Stability**Table 31 Longitudinal Dynamic Stability**

Mode	Natural Frequency (rad/s)	Period (s)	Damping Ratio (nd)
Short Period	2.44	2.56	0.0456
Phugoid	0.0517	121	0.345

For the longitudinal dynamic stability of the aircraft, the natural frequency, period, and damping ratio are listed for the short period and phugoid in Table 31. The values listed are for cruise during the ferry mission. The short period response is on the order of seconds with a 2.56 second period for high frequency disturbances while the phugoid has a much longer period of 121 seconds. The short period response and phugoid are found from Roskam Part I as approximations. [46]

Table 32 Lateral-Directional Dynamic Stability

Dutch Roll Natural Frequency	1.41 rad/s
Dutch Roll Damping Ratio	0.102
Time to Half for Roll	0.842 s
Doubling Time for Spiral Mode	18.9 s

The lateral-directional dynamic stability has been approximated for the dutch roll natural frequency and damping ratio, the time to half for roll, and doubling time for spiral mode in Table 32. The dutch roll, spiral mode and roll parameters are also found from Roskam. [3] The dutch roll natural frequency should be on the same order as the short period which is the case for this aircraft. Because the aircraft is not spirally stable, the aircraft will need to be corrected with rudder and aileron inputs.

H. Future Work

In the future, the horizontal and vertical tail sizing will need to be verified using more in depth analysis to track the center of gravity of the aircraft. The final size for the horizontal stabilizer is likely to stay very similar to the current

design with more emphasis placed on the sweep angle and taper ratios for drag and control surface effectiveness. The aircraft will need to have additional CFD verification and wind tunnel testing to cross check the static and dynamic stability of the aircraft. The additional testing would allow for the refinement of the horizontal and vertical stabilizers and be used to verify the airfoil selection as well.

X. Structures and Loads

A. V-N diagram

Because *Firehawk's* maximum takeoff weight is over 12,500 pounds, it falls in the transport aircraft category and is regulated by Title 14 of CFR § 25 [19]. Therefore the positive limit load factor has to be greater than or equal to 2.5. The team decided to keep n_{lim} at 2.5 because when a minimum factor of safety of 1.5 is applied, ultimate load factor becomes 3.75. 3.75 is the same as other transport category aircraft including the B-737-200, the MD-80, and the DC-10.

Pos. Limit load	2.5
Neg. Limit load	-1
Pos. Ultimate Load	3.75
Neg. Ultimate Load	-1.5

According to Roskam Part V, Section 4.2, Equation 4.4-4.23, two V-N diagrams have been derived [3]. One diagram is for the drop mission, and the other for the ferry mission. The flying airspeed for the two missions are different due to the fact that the aircraft is flying at different altitude and different weight.

For the ferry mission V-N diagram, the design cruising speed is higher than the calculated minimum requirement, thus the V_C is taken from Section VIII. V_D is 1.25 times V_C , therefore it also increased.

Parameters	Drop (KEAS)	Ferry (KEAS)
Positive 1-g stall speed	133	106
Negative stall speed	165	131
V_A	210	167
V_C	277	347
V_D	347	434

Gust load factor lines are developed for the drop mission considering this mission is required to bear more load. The method used is generated from Roskam Part V Equations 4.4-4.23 [3].

Table 33 Gust Line Functions

Gust Load Factor Line	Function
$n_{lim, Gust, V_B}$	$1 \pm 0.009014V$
$n_{lim, Gust, V_C}$	$1 \pm 0.006829V$
$n_{lim, Gust, V_D}$	$1 \pm 0.003414V$

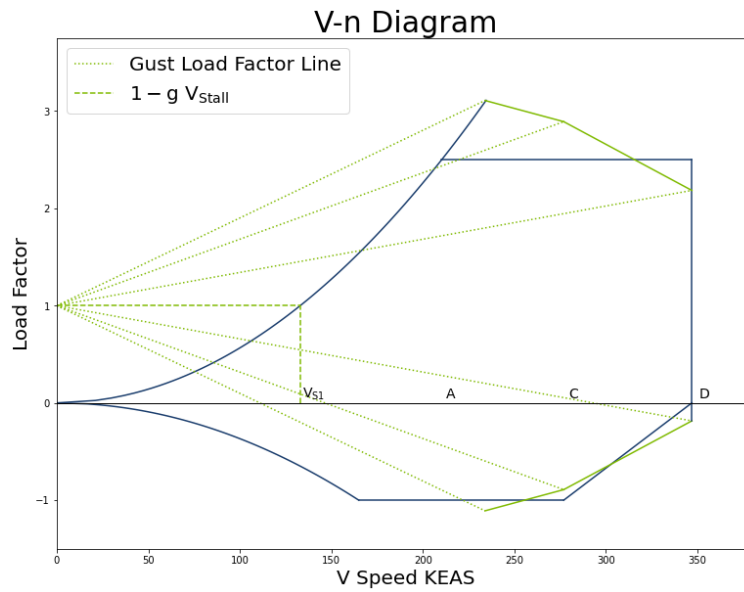


Fig. 36 V-N diagram with gust loads (Drop Mission).

As Fig. 36 shows, the effect of gust load is mainly from maneuvering speed to cruising speed.

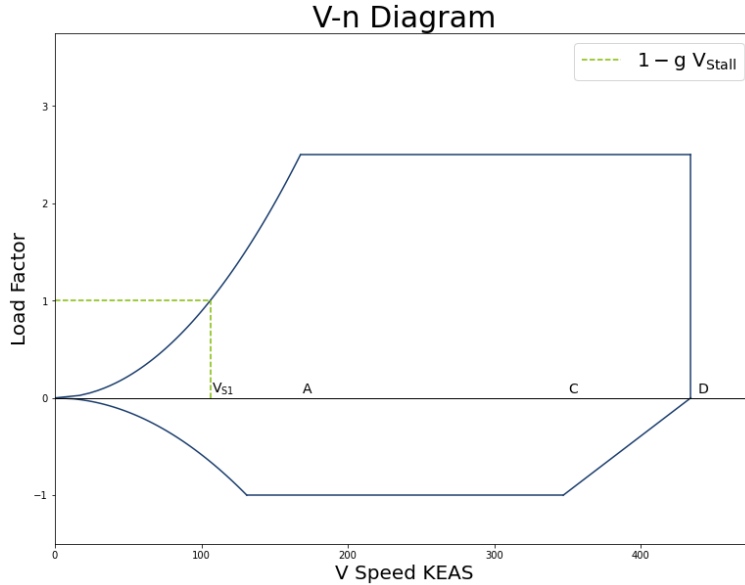


Fig. 37 V-N diagram (Ferry Mission).

For the regular drop mission, when the aircraft is cruising at FL100, the max diving speed V_D is Mach 0.54. For the regular ferry mission, when it is cruising at FL320, the max diving speed V_D is Mach 0.75.

B. Load paths

Three load cases are analyzed during the structural development process, the landing gear, engine, and the wing. These 3 load cases are chosen because they experience the majority of the operation load of the aircraft. When the landing gears hit the ground, they transfer load from the wheels to the main strut, then to a mounted reinforcement plate on the fuselage. The engines transfer both shear and bending load to the pylon, then the pylons transfer load to the main spars of the wings. The wing transfers load to the top of the fuselage. All the loads are analyzed for structural safety of the aircraft.

C. Loads

The wing loading was estimated using OpenVSP lift distribution simulation data [42]. The max loading scenario considered was at MTOW and at max diving speed. The limit load factor of 2.5 was considered during the analysis. The weight of engine and wing itself is also taken into consideration. The engine mount was taken as a point load on the wing, and the thickness of the wing was considered uniform across the span. The weight of fuel was assumed to be only in wing tanks. The shear stress and bending moment across one side of the wing span are plotted below in Fig. 38 and Fig. 39.

As shown in Fig. 38, the max shear force experienced is at the root of the wing, which is 245,200 lbs. The max moment is also at the root of the wing, which is 6,223,000 ft-lbs. When FS of 1.5 is applied, the ultimate shear is

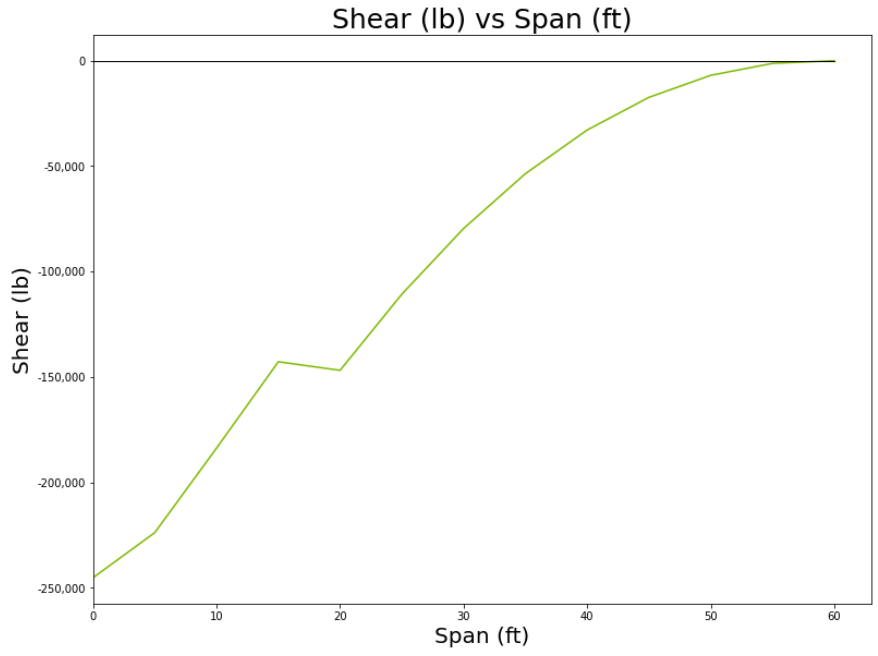


Fig. 38 Wing Shear.

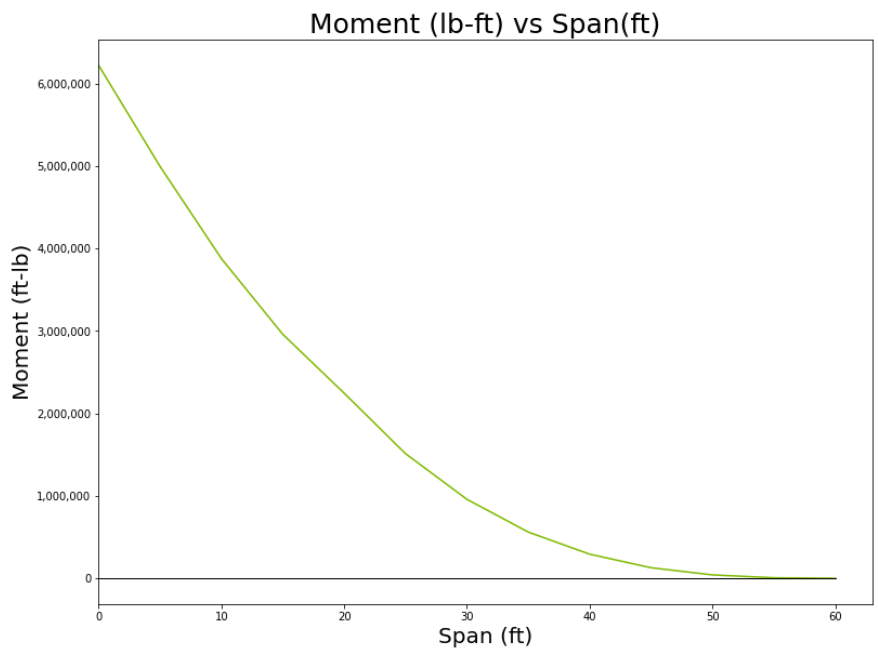


Fig. 39 Wing Bending Moment.

367,700 lbs, and the ultimate moment is 9,334,500 ft-lbs.

For the Engine loads, the FS applied is also 1.5. The distance from engine center to wing is 6.25 ft. The loads on each engine are listed in the table below. The vertical load have also accounted for the 3.75 ultimate load factor.

Vertical Load (lb)	33,600
Shear Load (lb)	48,200
Torque (lb-ft)	201,000
Ultimate Torque (lb-ft)	301,500

For the Landing gear, the MLW is 133,900 lb, calculated based on Commercial Airplane Design Principles Equation 4.6 [47]. More details can be found in Section XIII.

D. Sizing

Through various trade studies and supporting research, a number of structural considerations could be made. The first was with respect to spars. The likely unstable atmospheric conditions that the aircraft will fly in during a drop mission warrants a need for a wing that has the ability to handle turbulence well. Turbulence can affect aspects such as the center of gravity (sloshing fire retardant), and while tanks can be designed to limit sloshing, having an aircraft that can navigate those bumps smoothly prevents exacerbation of that issue, as well as making the aircraft easier for the pilots to fly. As such, a two-spar configuration was chosen, with two long spars running the length of the wing, and additional internal support from the walls of the wet wing fuel tank as well as any other transverse internal structural components. Overall design theory and approach was taken from the methods outlined by Niu [48]. As per considerations also taken from seed aircraft as well as other aircraft with similar wing configurations, the leading spar is placed at approximately 8% of the chord length and the trailing spar is approximately 61% of the chord length from aileron to tip. A flat metal plate for ease of engine mounting was added at 200 inches from the root chord. This was done to increase support for the weight of the engine attached at the end of those spars) and provide a stiffer frame in the area where the fuel tank would be placed. The ribs were placed at 30 inch intervals throughout the wing. Final dimensions result in 0.5 inch thick ribs with 8 circular holes cut from them in order to reduce weight and maintain the bulk of its stiffness. The spars had a number of considerations taken to ensure both strength as well minimize weight. The balance in design found that best accomplishes this goal is an I beam spar with variable sizing. The I beam at the root consists of a 1.5 inch thick web with a 0.75 inch thick top and bottom flange. The height is eight inches between the exterior surfaces of the flanges and the width of the flanges are six inches. The beam at the tip consists of an I shape with a 0.75 inch thick web and 0.5 inch thick flanges. The distance between exterior flange faces at the tip is six inches and the width of each flange is three inches. These can be visualized in the wing views below.

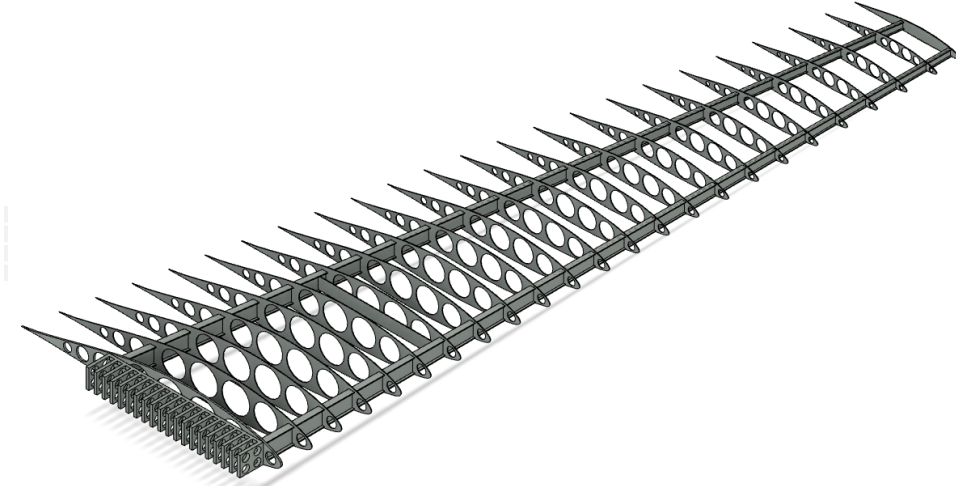


Fig. 40 Orthographic Spars/Ribs View.

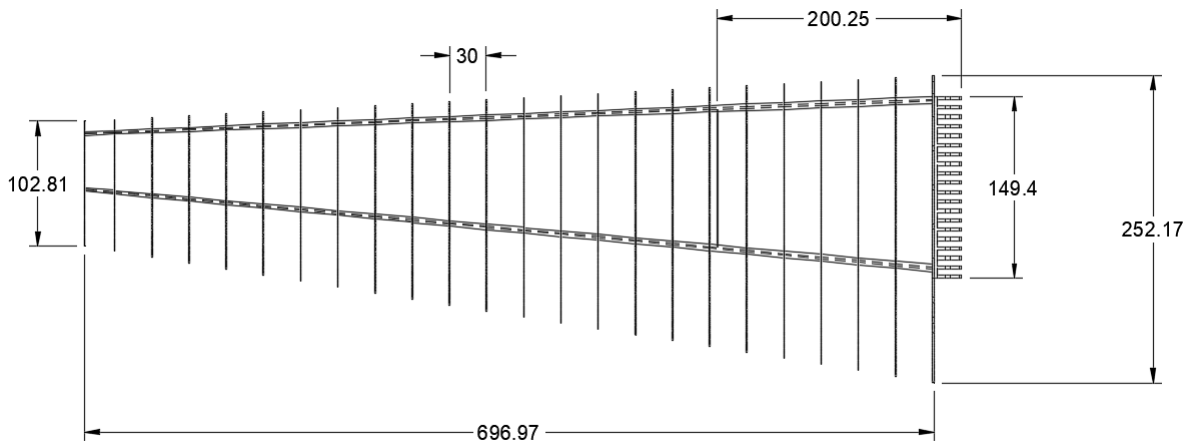


Fig. 41 Dimensional View.

The fuselage utilizes 0.5 inch thick frames with a maximum interior diameter of 71 inches and an exterior diameter of 75 inches (four inch wide web). The material used is Aluminum 7075-T6. The ribs experience a spacing of 17 inches and have four one inch diameter aluminum pipes running through the ribs to add stiffness to the structure. There will also be one inch Z-Stringers throughout the entire fuselage to complete the body. The main fuselage structure is shown in Fig. 42.

The skin thickness was determined by methods taken from Abbott Aerospace and the NASA-TM-X-73306 Structures Manual Volume II. This models the fuselage as a thin metallic cylindrical shell under a given load. The equation solved for the maximum pressure the cylinder can handle as a function of the radius of the shell and the thickness. Using expected flight maximum dynamic pressure, the equation was flipped to solve for required thickness, found to be 0.03

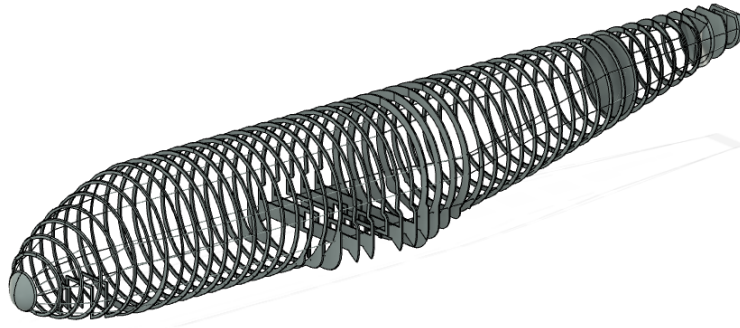


Fig. 42 Orthographic Fuselage View.

inches. This is consistent with other resources that analyze skin thickness of existing aircraft. [49]

E. Materials

One aspect that also needed to be considered was the materials chosen for structural applications. The most common material used in aircraft construction has been aluminum alloy, however, with advances in technology, composites have become a viable manufacturing option as well. Through looking at structural/material trade studies, traditional manufacturing still enables an aluminum construction to be the most cost-effective, so it was determined that aluminum alloys would make the bulk of the aircraft structural components. An analysis of the MIL-HDBK-5J handbook of materials selections demonstrated that aluminum 7075-T6 would be the best choice for load bearing components due to its high yield strength, meaning it would be able to repeatedly bear the flight loads. The material properties as found through Vartabedian are listed below [50]. For aircraft skin, both the wing and the fuselage will be made out of Aluminum 2024 due to its flexibility.

Variable	Value
Density (lb/in ³)	0.101
Young's Modulus - Tensile (psi)	10,400,000
Young's Modulus - Compressive (psi)	10,700,000
Poisson's Ratio	0.330
Scatter Factor	4.00
Compressive Yield Stress (psi)	71,000
Compressive Ultimate Stress (psi)	81,000
Tensile Yield Stress (psi)	71,000
Tensile Compressive Stress (psi)	81,000

F. Finite Element Methods

The load path follows the determined lift distribution. In setting up structural analysis to determine the wings ability to handle loads, the Autodesk Fusion 360 software was used to achieve a finite element analysis. The setup utilized a stepped lift distribution with lb-force magnitudes that reflected the calculated lift distribution that the aircraft would need to bear. The weight of the engine was also taken into consideration with a 70/30 bias towards the front due to its positioning. Fig. 43 demonstrates the areas utilized in simulating forces.

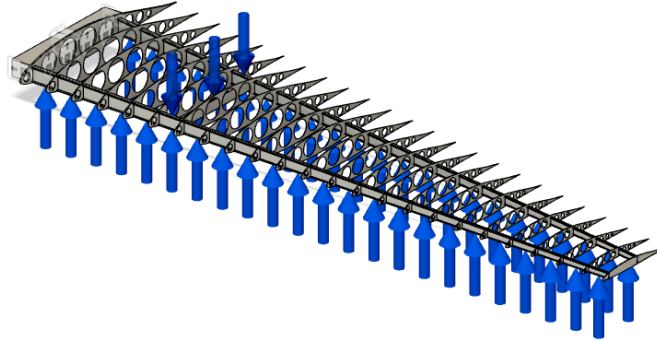


Fig. 43 Load path of the wing.

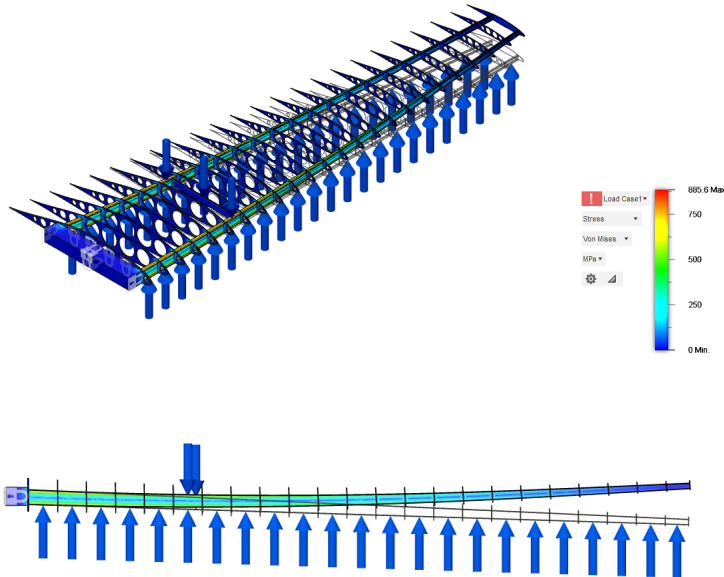


Fig. 44 Stress distribution of the wing.

As seen in Figure X.F, the wing is safely able to bear the loads sustained during flight as well as having a margin

for safety. A Von Mises stress distribution is displayed. Fusion 360 listed a 3.54 load factor upon completion of the simulation; however, the ultimate load factor is higher given that the stepped lift distribution resulted in a simulation of loads that were an overestimate of flight conditions at MTOW. As a result, an ultimate load factor of around 3.7 – 3.75 can be expected for this wing. The wing tip experiences a max deformation of 39 inches in each direction before failure.

XI. Mass Properties

A. Weight Estimation

At the preliminary design phase, the initial weight estimation was made based on the seed aircraft. Two methods were used, a bottom-up method from Raymer Table 15.5 [2]. The other method was a top-down method, the Roskam Class I method [3]. In addition, 2 aircraft were compared to our initial sizing, the DC-10-30 and MD-80 aircraft.

The DC-10-30 and MD-80 were chosen for a number of reasons. First, because they are under the jet transport group in Roskam. Second, they are later versions of jet transports among the 8 provided by Roskam. Third, MD-80 series have similar gross weight (78,950 lb & 76,130 lb) and similar wing reference areas (1,270 ft^2 & 1,800 ft^2). The DC-10-30 can carry 98,726 lb of payload, which is slightly higher than the team's designed payload capacity. [3]

After the aircraft geometry was determined, a more detailed weight estimation method had to be used. The Raymer cargo/transport statistical method was selected, because the *Firehawk* is a transport class aircraft [2] (Equations 15.25-15.45). *Firehawk* is designed mainly for carrying heavy retardant and can only fly at subsonic regime, which is very similar to other transport category aircraft. Thus this statistical method can be trusted.

Multiple assumptions have been made. The system electrical rating was assumed to be 50 kW. The avionics system is assumed to be 1,400 lb, based the large size of the aircraft. The thickness to chord ratio is not constant, thus the average was used. The total control surface area is calculated based on the proportion to wing area. The uninstalled APU weight is taken from the Boeing 737-600 and the A320-200 since the MTOW of *Firehawk* is between these two airplanes.

After estimating using the methods above, a CAD model analysis was also performed. The material assumed was Al 7075 for all load bearing structures and Al 2024 for skin. All skin thickness was assumed to be 0.03 in thick.

After all the methods were performed, the final weight estimation combined the estimated weight with different factors. The CAD model had the highest factor of 0.6 since it is closest to the actual design, the Raymer transport method had a factor of 0.2 since it is a detailed statistical method, and the other methods had factor of 0.2 combined. The systems weight is different than other components, because only statistical methods can be used. Engine Dry weight is taken from the actual engine selected, the CFM LEAP-1A30. The final empty weight buildup is shown below in Table 34.

Table 34 Approximate Empty Weight Build Up

Item	Weight (lb)	Location (in)
Wing	16,323	350
Fuselage	12,491	410
Nacelle	2,929	249
Nose Landing Gear	617	92
Main Landing Gear	4,684	423
H. Tail	1767	910
V. Tail	1,368	910
Engine	12,500	249
Exhaust and Thrust Reverser	1,720	249
Fuel System	783	249
Avionics & Instruments	3,120	72
Surface Controls	1,754	620
Hydraulic Systems	386	422
Pneumatic System	280	470
Electrical System	990	325
APU	646	670
Oxygen System	142	250
Air Cond. System	525	250
Anti-icing System	337	312
Furnishing	5,543	325
Operating Items	2105	350
Fuel Tank	215	388
Retardant Tank	2,031	350
Total Empty	72,275	361

The CG location of each component is relative to the datum, which is the nose tip of the aircraft. Most location are determined by the CAD model. For more detailed configuration see Section V. The other weights include the Fuel, Payload (fire retardant), and crew. The aircraft is designed to carry a maximum payload of 72,000 lb. 15,300 lb of fuel is required for the drop mission and 28,300 lb of fuel for the ferry mission. Crew members are assumed to weigh no more than 200 lbs from Roskam Part I Page 58 [3]. The MLW is from General Aviation Aircraft Design Fig. 4.7 [51]. The MRW is based on adding taxi and run-up fuel to MTOW.

Table 35 Other Relevant Weights

Weight Parameter	Weight (lb)
Total Empty	72,300
Crew	400
OEW	72,700
MTOW	160,000
Ferry TO	101,000
MRW	160,500
MLW	133,900
MZFW	144,700

B. CG Estimation

After applying the location of each weight to the calculation, the CG of aircraft was determined. The LE MAC data is gathered from the CAD model, which is 302.2 in from the nose tip. MAC is 15.92 ft. The CG was also analyzed for the most extreme cases, for example when 2 retardant tanks on one side are fully empty and all the fuel is sloshed to the opposite side. For detailed retardant and fuel tank configuration, see Section XII.

Table 36 Longitudinal Center of Gravity

Scenarios	CG (% MAC)
OEW	30.71
MTOW	30.16
Ferry TO	34.68
MZFW	27.87
Extreme Forward	19.27
Extreme Aft	40.92
Forward Limit	17.10
Aft Limit	43.14

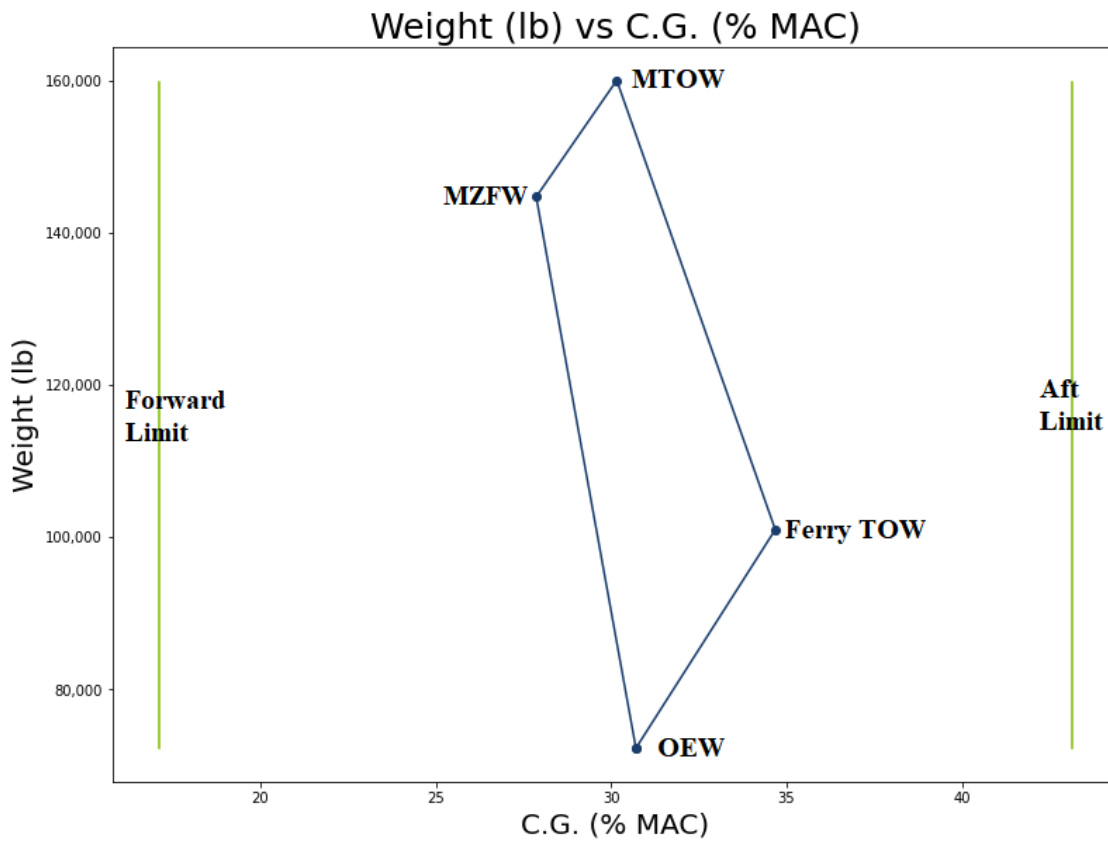


Fig. 45 CG Envelope.

The forward limit and aft limit are determined from the scissor diagram. As shown by Table 36, the aircraft can withstand even the most extreme cases. A CG travel graph was developed for showing CG shift during normal flight conditions. The flight angle in climb and descent are 12% and -12% respectively, and the liquid level is taken into consideration. This Plot is shown in Fig. 46.

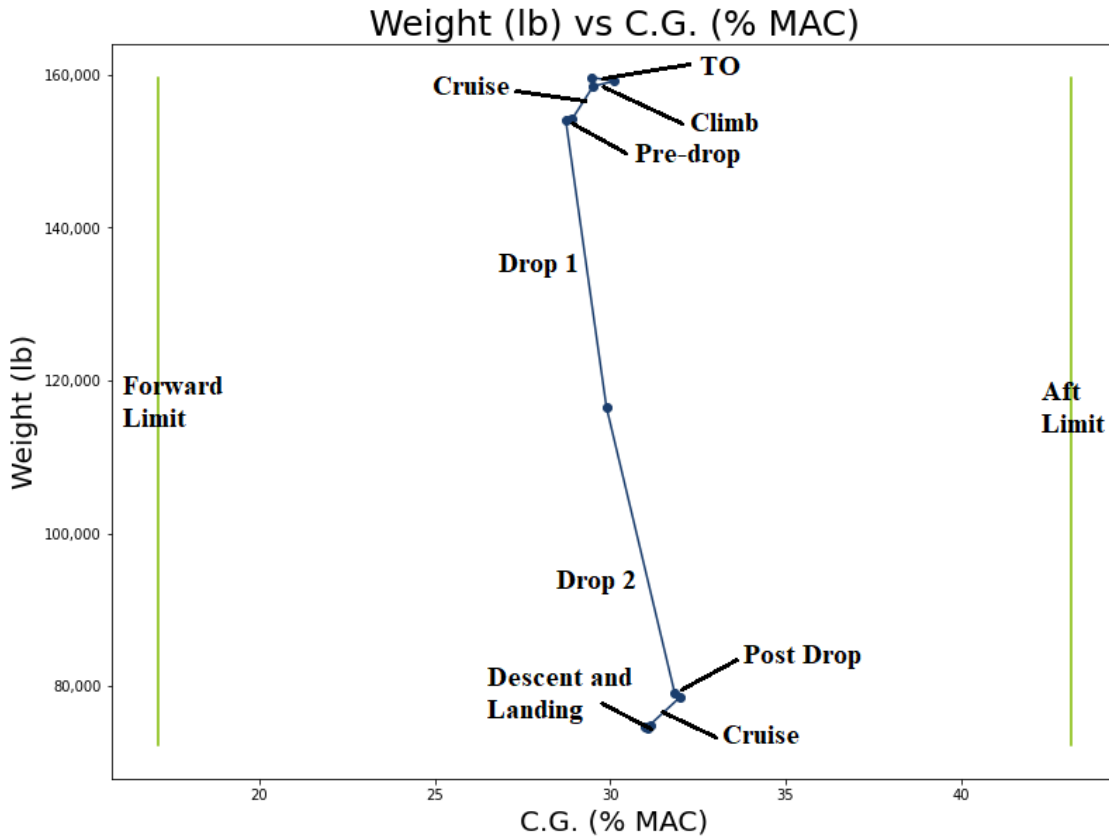


Fig. 46 CG Travel.

During a designed max-loaded mission, the aircraft first burns fuel during taxiing and takeoff. Then the airplane climb to a cruising altitude of 10,000 ft. Next, the aircraft burns fuel to fly toward the fire location, and the aircraft has to dive down and drop fire retardant. The airplane first drops the retardant in the forward-most and aft-most tanks. Then, the aircraft will drop all of its fire retardant in the middle two tanks, and climb to 20,000 ft altitude. Finally, it dashes to return to the airport, and descends to prepare for landing. The final stage will be landing at the airport.

For the most extreme cases, the forward-most CG is at 19.27% MAC and the aft-most CG is at 40.92% MAC. These are still within the forward and aft limit. The limits and extreme cases are shown in Fig. 47, and this range is shown on *Firehawk* in Fig. 48.

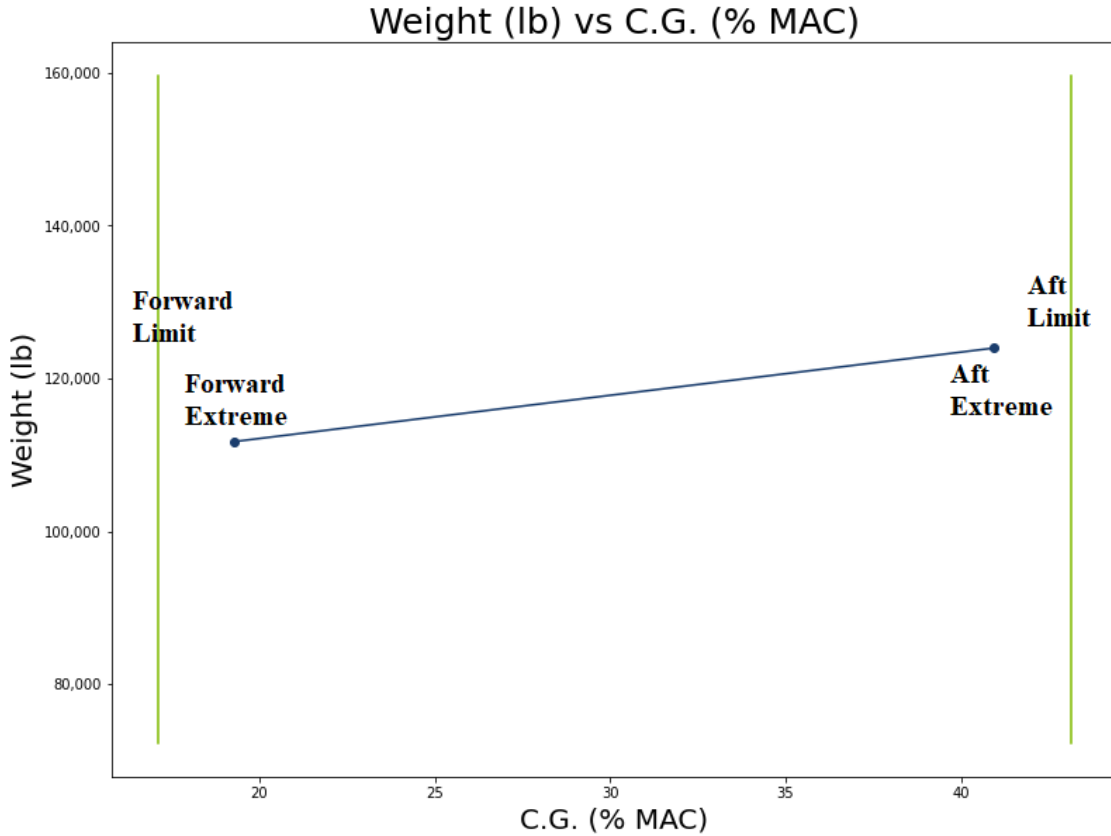


Fig. 47 CG Extreme Cases.

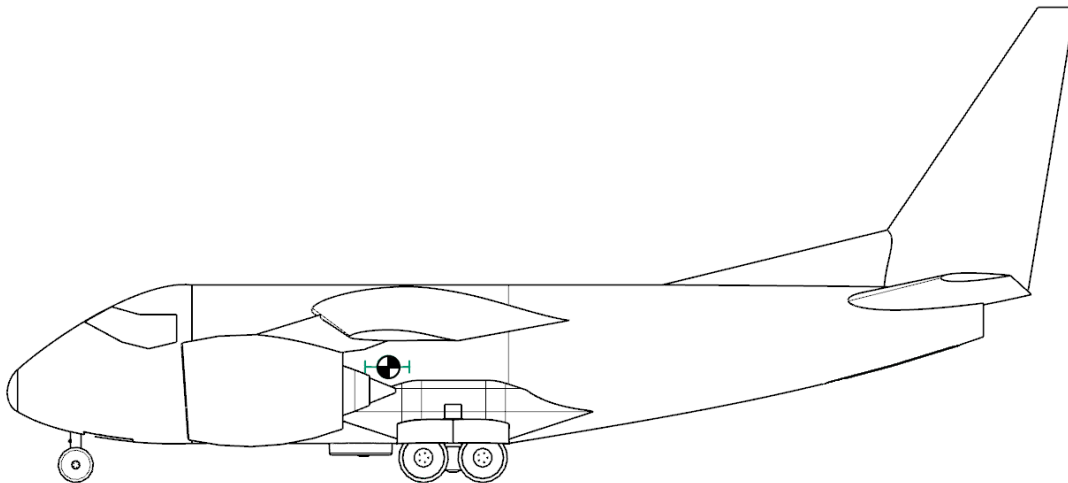


Fig. 48 Side CG Range.

The vertical CG was also analyzed, with the datum point at the ground level when wheels are down. The relative distance between CG and the datum under each scenario is shown in the table and graph below.

Table 37 Vertical Center of Gravity

Scenarios	CG (in)
OEW	110.0
MTOW	103.5
Ferry TO	124.0
MZFW	97.5

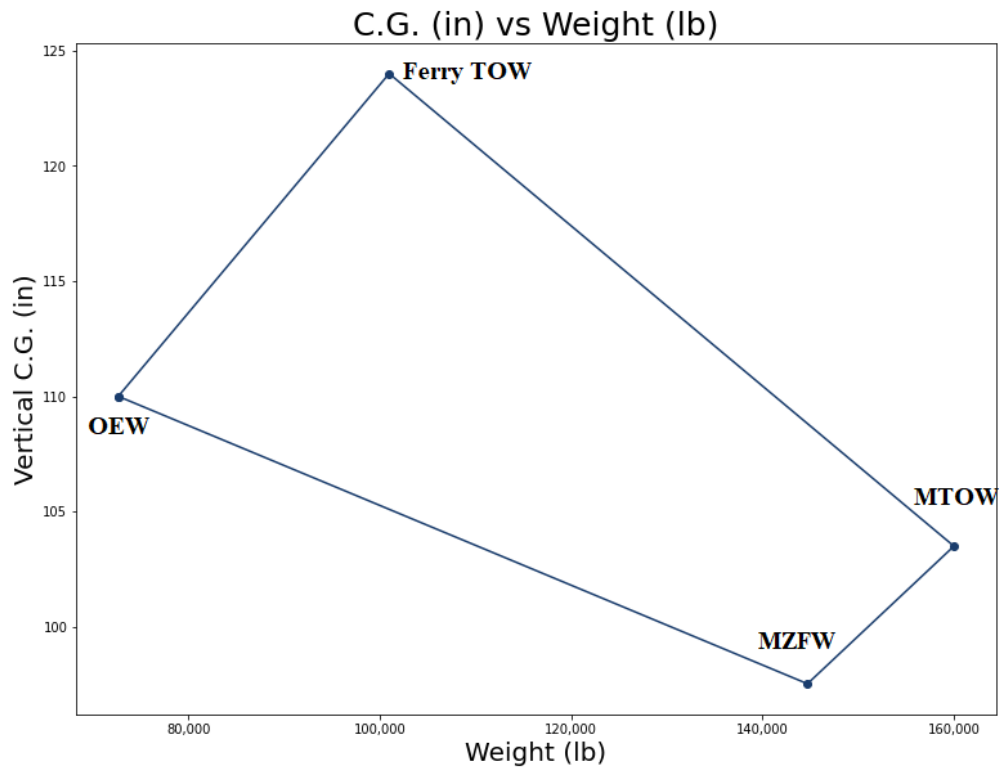


Fig. 49 Vertical CG Envelope.

The extreme case for Lateral C.G. was determined when half of retardant filled the one side of the tank, and wing fuel tank on the other side totally leaked, leaving half of total MTOW fuel. The max shift of lateral C.G. is 18.03 in. The airplane is stable even in extreme conditions. This is due to the fact that the wing tanks are close to the center.

C. Trade Study on Retardant Tanks

A trade study was done on the retardant tanks in the design process. The two options of retardant tanks taken into consideration were built-in fixed tanks or removable tanks. After calculations, the team found that there would not be sufficient room for the center fuel tank and main landing gear if a removable tank was integrated. If the retardant tank was lengthened, the CG range would be larger than the limit. Furthermore, the empty weight would need to increase and the systems would not have sufficient room to be placed. For those reasons, the built-in tank design was chosen. The down-side is the aircraft does not have the capability of carrying large cargo, as the tanks fill that area. The *Firehawk* traded this cargo feature for lower empty weight and a more stable CG.

D. Future Work

The weight of the dry engine was an outdated value, thus for the future it would be better to test and weigh with the real engine data. The systems weights are still based on a statistical method due to the fact they are not determined yet. The weight might change when the systems are decided and tested by hand. The location of each component is likely to slightly adjust once testing is done. More detailed CG will be calculated after testing for safety of the aircraft.

XII. Systems

A. Overall Layout

The system positions in the aircraft are laid out in the following diagram. Other than the fuel tanks and retardant tank, system sizing is approximate.

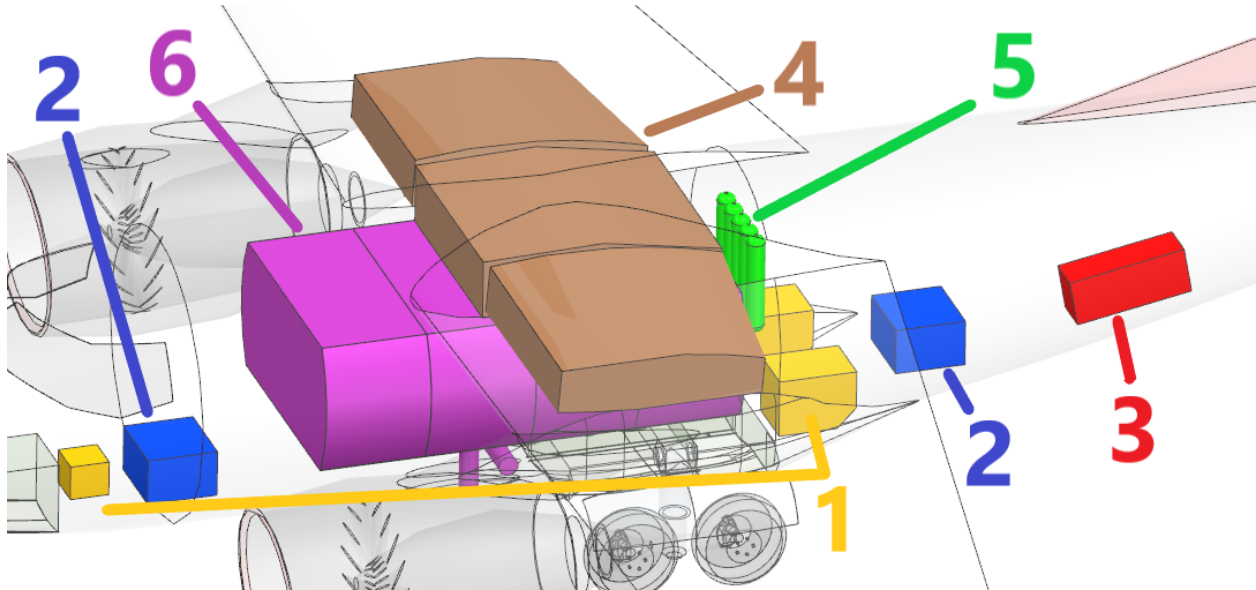


Fig. 50 Overall System Layout.

Table 38 Component Locations

Item	Number
Hydraulics	1
Electrics	2
APU	3
Fuel Tanks	4
Pneumatic Tanks	5
Payload Tanks	6

B. Hydraulics

The aircraft is currently designed to use hydraulics consisting of two primary systems with a backup secondary system, similar to the seed aircraft [52]. Each system will have its own reservoir, pump and accumulator. The aircraft's engines have mechanical hydraulic pumps which are connected to the two primary hydraulic systems, with the port system linked to the port engine and vice versa. Both primaries will have direct connections to the tail control surfaces, ailerons, and landing gear, while most other actuators would be driven by only one system. Hydraulics will be used to control all control surfaces, landing gear steering and deployment, and thrust reversers. In the case of both engines

failing, hydraulic pumps can be driven by electric power supplied by the APU and/or the ram air turbine. The connections and subsystem allocations are shown in full in Figure 52. The two primary hydraulic systems are centered just aft of the main landing gear wells and the secondary is centered just aft of the nose gear well 51.

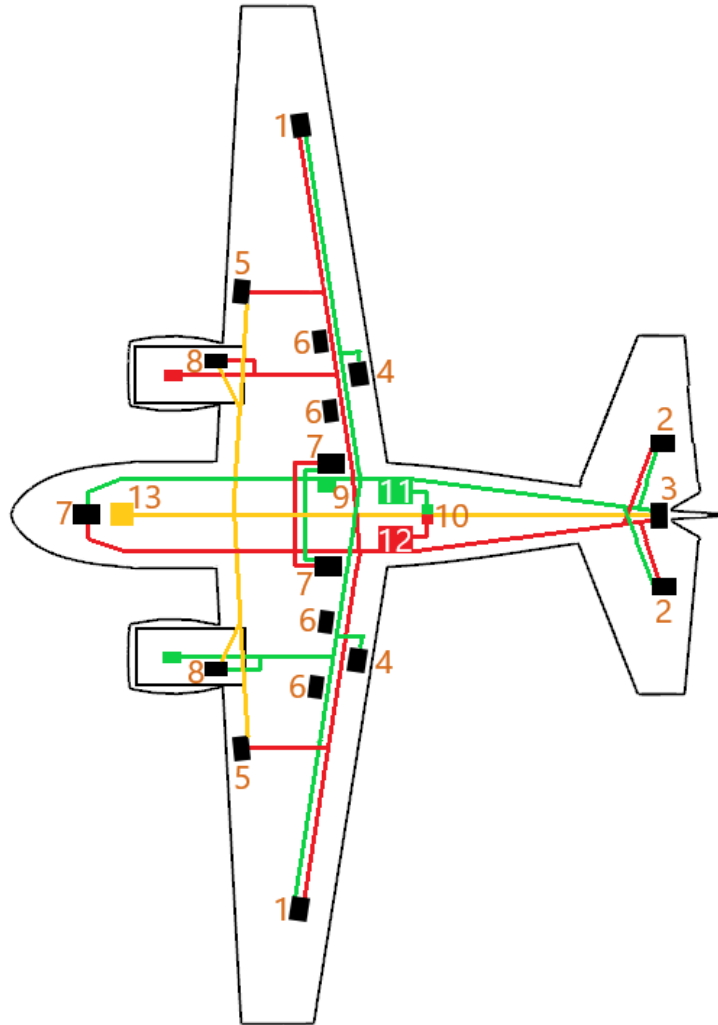


Fig. 51 Hydraulics System Layout.

Table 39 Component Locations

Item	Number
Aileron Actuators	1
Elevator Actuators	2
Rudder Actuators	3
Trailing Edge Flap Actuators	4
Leading Edge Slat Actuators	5
Spoiler Actuators	6
Landing Gear Actuators	7
Thrust Reverser Actuators	8
Landing Gear Transfer Unit	9
Power Transfer Unit	10
Hydraulic Reservoir 2	11
Hydraulic Reservoir 1	12
Hydraulic Reservoir 3	13

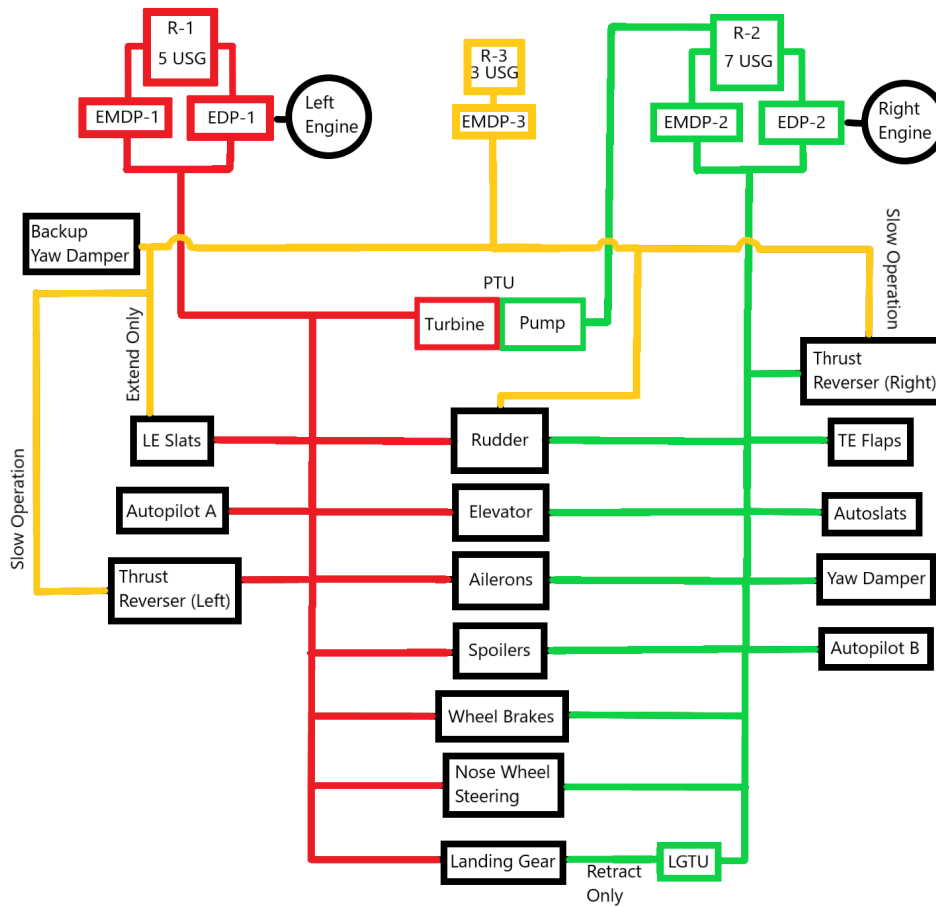


Fig. 52 Hydraulics System Connection Diagram.

In the case of a fan burst, the aircraft's hydraulic systems have lines spaced out for the section of the fuselage between the engines. The lines are distributed as shown in Figure 53.

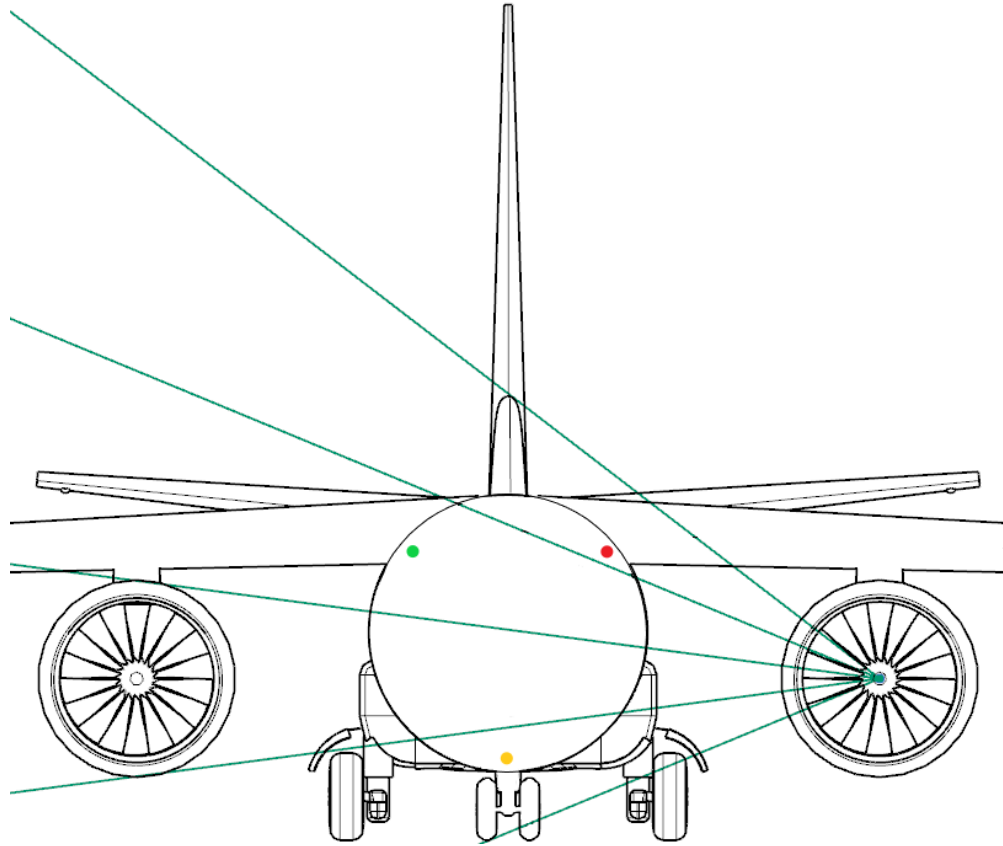


Fig. 53 Hydraulic Line Locations with 15 Degree Fan Burst Lines.

C. Electrics

The aircraft will be powered primarily from generators mounted to the main engines. For start-up, batteries can start the APU, which then provides the power necessary to run needed systems on the ground. The electrics system will supply power for avionics, environmental control, hydraulic pumps, fuel pumps, and lighting. If both engines and APU are non-functional in flight, the ram air turbine can be used to provide electrical power, as it is directly connected to a generator.

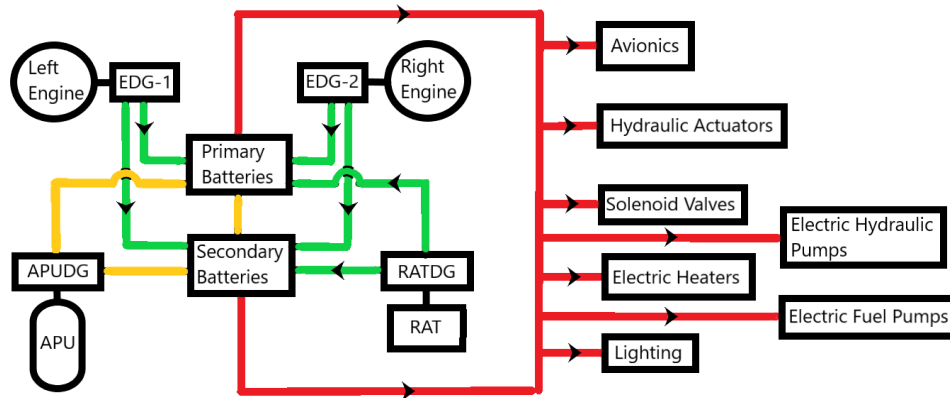


Fig. 54 Electrics System Connection Diagram.

D. Auxiliary Power Unit

A number of APUs used on variants of the seed aircraft have been compiled in Table 40, as the power, bleed air and other requirements for the APU are considered to be similar to the seed aircraft. [52]

Table 40 List of Possible APUs

APU	Application
Honeywell 131-9[B]	B737-MAX
Sundstrand APS 2000	B737-3/4/500
Garrett 36-280	B737-3/4/500
Allied Signal 131-9(B)	B737-NG / MAX

The APU is positioned in the tail boom of the aircraft. A door in the tail boom will be used to provide intake air to the unit, and the exhaust produced can be vented via the flat end of the tail boom. Although there are non-air breathing APU technologies in development, it is unlikely they would be available or cost-effective due to low availability compared to existing air-breathing APUs. Additionally, using an existing APU would allow for the same fuel to be used for both itself and the main engines.

E. Engine Controls

The main engines on the aircraft are managed by a Full Authority Digital Engine Control (FADEC) system. This system interprets the throttle lever positions using air data from the aircraft's instruments and engine sensors in order to produce control inputs for the engines. This reduces engine thrust changes while the throttles are stationary, which reduces the work load on the pilots. The FADEC provides inputs for the Fuel Management Units, mechanical devices responsible for regulating fuel feed and bleed air take-offs. A layout of the FADEC is shown in Figure 55.

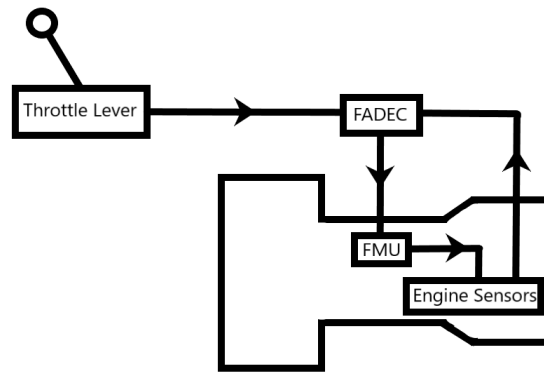


Fig. 55 FADEC Diagram.

F. Fuel Systems

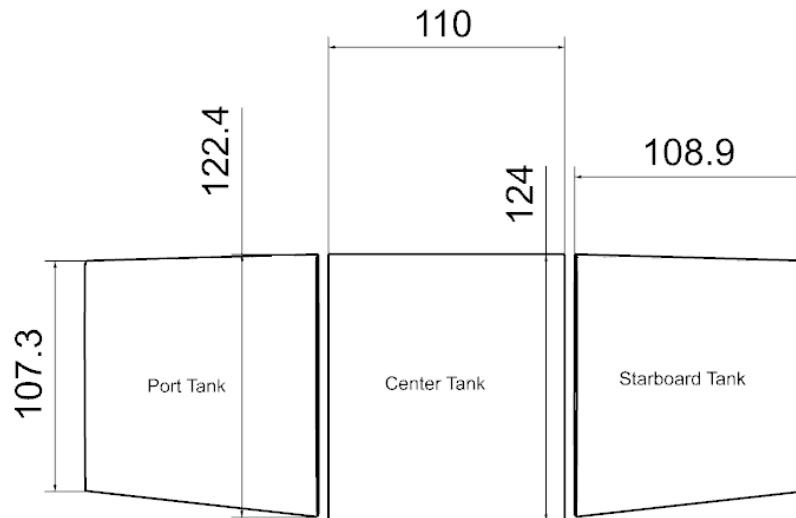


Fig. 56 Fuel Tank Dimensions in Inches.

The fuel tanks on this aircraft are located within the wing structure, situated between the main spars and divided by specific ribs. The tank overall tank layout is shown in Figure 56. The outer skin of the wings will constitute the top and bottom of the wing tanks, while the centerline tank has more independent structure due to the lack of lower wing skin in the fuselage. Each engine has its own fuel pump, and additional electric pumps are installed in the wing to allow for moving fuel from one tank to another. In the case of an engine pump failing, both engine pumps are capable of supplying fuel to the other engine via cross-feed lines. Electric 'boost' pumps connected to the wing tanks can also provide fuel pressure if the engine driven pumps are incapable/insufficient due to failure or damage. Similarly, the APU can feed itself fuel by use of the APU-driven pump (or can be fed by another electric boost pump) connected to the

centerline tank. The fuel system’s connection layout and tank capacities are detailed in Figure 57.

All lines leading to the engines or APU from a fuel tank have filters fitted to help insure impurities do not cause engine damage. Each tank has a set of fuel level sensors with associated displays in the cockpit. The wing tanks are fitted with emergency fuel dump valves, allowing for more than half of the aircraft’s fuel tankage to be emptied even if transfer pumps and valves fail.

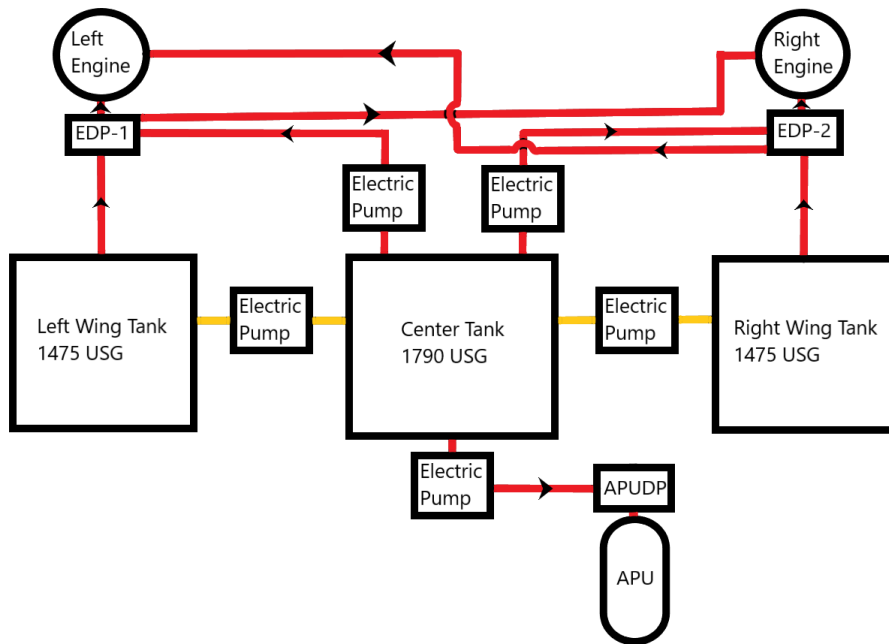


Fig. 57 Fuel System Connection Diagram.

G. Avionics

1. Autonomous Operations

Although autonomous operations would reduce the hazard for crews and cut costs by eliminating the costs of paying and training crews, technology for autonomous operations is not sufficiently developed for aircraft of this size. Current fully autonomous aircraft are limited to small general aviation aircraft, such as the experimental Reliable Robotics conversion of the Cessna 208, and are not currently certified for routine operations as of January 2022 [53]. The cost of certification and technology development for autonomous technologies would significantly outweigh any cost savings from eliminating the crew. Furthermore, autonomous technologies are far from being sufficiently developed for usage in the aerial firefighting mission. As a result, *Firehawk* will not provide architecture to support autonomous operations, and will be designed without this capability in mind.

2. *Flight Avionics*

The main avionics for the airplane were selected to satisfy the requirements listed in 14 CFR § 25 to comply with FAA regulations, which require instruments and indicators for flight control, navigation, communication, and the powerplant, among other requirements. Diversity in avionics is favorable to increase safety and redundancy; the chance of a critical failure is greatly reduced, and any problems can be located more quickly. For example, the Airbus A320 uses communications equipment from several companies including Cobham SATCOM, Collins Aerospace, HR Smith (Technical Developments) Ltd, and Panasonic Avionics Corporation [54]. Additionally, choosing individual systems and packages allows the avionics selection to be tailored specifically to the mission profiles that *Firehawk* will fly.

Due to overall similarities and requirements, many of the essential components selected were based on those used in modern commercial transport aircraft like the 787 [55], the A320neo [54], and the 737 [56]. It is assumed that the proposed airplane will be built in the United States as well, so American companies are preferred where possible to ease logistics. Many of the models selected are packages that come with a variety of individual instruments; for example, the Collins Aerospace ISS-2100 is a configurable system that includes a weather radar, TCAS, TAWS, and a surveillance system. These systems and components are listed in Table 41, and represent some of the newest avionics systems in use today.

Table 41 List of Selected Avionics

Category	System	Model
Communications	Flight deck audio system	AvtechTyee Flight deck digital control audio system
Communications	Communications Antennas	Cobham SATCOM HGA-7001 high gain antenna
Communications	Antenna Systems	HR Smith Antennas
Communications	Airborne Communication Systems	Avionica satLINK Iridium communications gateway
Communications	Radio Communications Equipment	Collins Aerospace communications system (VHF-2100, SAT-2100, HFS 900D, flight system digital control audio system)
Flight Management Systems	Common core system and airborne flight recorder	GE Aviation Systems flight management systems
Flight Management Systems	Autopilot	Honeywell Aerospace Primus 1000
Indicators and Instruments	Flight deck display system	Collins Aerospace LCD displays and HUDs
Indicators and Instruments	Fuel indicators	Collins Aerospace fuel quantity indicating systems
Indicators and Instruments	Flight instruments	Thales AVS France electronic flight instrument systems
Indicators and Instruments	Backup flight instruments	Thales AVS France Integrated Electronic Standby Instrument
Indicators and Instruments	Flight indicators	Collins Aerospace radar/radio altimeters, angle of attack indicators
Indicators and Instruments	Pressure gauges	QED/Inc. pressure indicators
Navigation	Multi-mode receivers	Collins Aerospace multi-mode receivers
Navigation	Automatic direction finder	Collins Aerospace ADF-900
Navigation	Distance measuring equipment	Collins Aerospace DME-900
Navigation	Inertial components and systems	Honeywell Aerospace navigation package with inertial reference system, air data system, multi-mode receivers
Warning Systems	Integrated Surveillance System	Collins Aerospace ISS-2100 with weather radar, traffic alert, collision avoidance, terrain awareness and warning systems
Warning Systems	Ground proximity warning system	Honeywell Aerospace EGPWS

1. Mission Avionics

In addition to the selected avionics, the firefighting mission introduces several unique challenges that require specialized systems to address. Currently, fixed-wing firefighting operations in the US are only performed during daytime under VFR conditions due to restrictions placed by the USDA Forest Service [57]. As a result, the avionics for the drop mission are primarily selected with the goal of enhancing situational awareness and improving safety.

Firehawk features several external cameras. The main camera system is a combined visual-infrared unit mounted on a gimbal in front of the nose gear, as shown in Figure 58. These cameras can be used to improve situational awareness by offering extra viewing angles, spot distant fires, and observe the success of a retardant drop. The display from either of these cameras can be projected onto any MFD in the flight deck, and duplicated camera controls allow either crew member to view and control the camera unit.

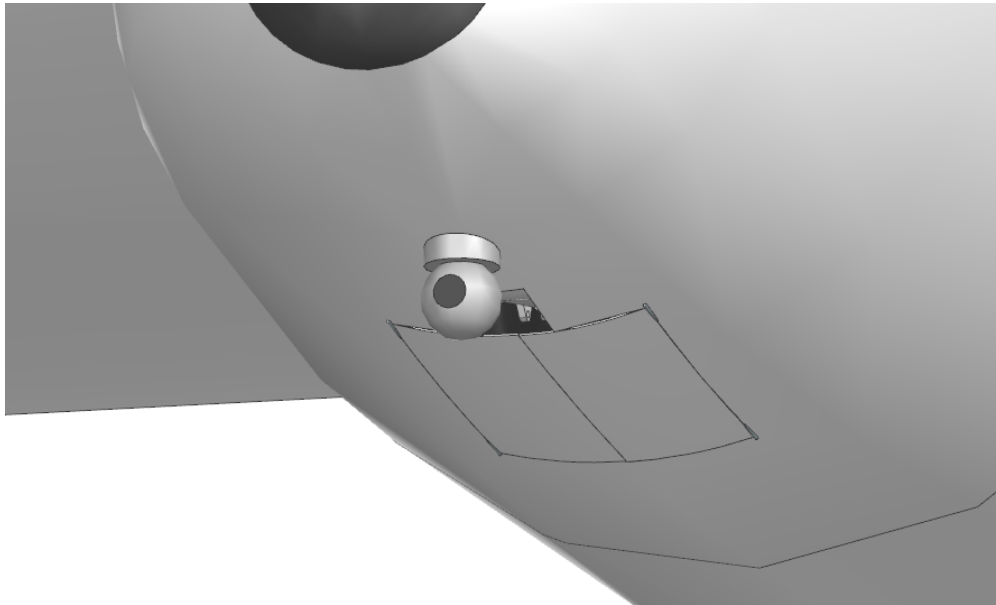


Fig. 58 Visual-infrared camera unit as mounted on the *Firehawk*.

A drop computer based on the Air Tractor Fire Response Dispersal System is also installed in the airplane, designed to simplify the drop process for the crew in order to reduce their workload and allow them to focus on controlling the airplane while it is at low altitude. Crews can set the amount of retardant dropped and the coverage level, then the computer will compute the flowrate of the retardant based on dynamic factors like *Firehawk*'s airspeed, attitude, and acceleration. Alternatively, the retardant drop can be controlled manually, with the crew having full control over the amount of retardant dropped, the selected retardant tanks, and the retardant flowrate. A mockup of the drop computer interface is seen in Figure 59. [58]

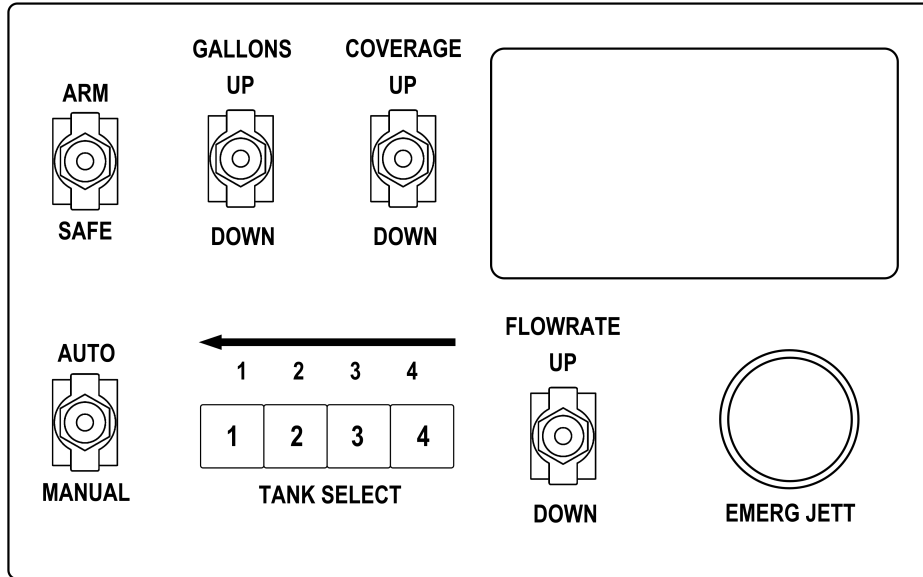


Fig. 59 Drop computer interface mockup for use on *Firehawk*.

Advances in drop systems and retardants, such as the HyDrop system, which uses liquid pellets to allow the airplane to drop from higher altitude without the retardant dispersing [59], have led to the possibility of fixed-wing aircraft being cleared for usage in night aerial firefighting missions. Although *Firehawk* is primarily designed around the current VFR restrictions set by the USFS, considerations have been made to allow for the installation of additional systems as they become available or necessary, like if *Firehawk* is cleared for night-time operations. For example, an automatic GCAS system would help reduce the likelihood of controlled flight into terrain, which is a larger consideration at night where visibility is limited. Additionally, a proposed system by Canaan Avionics, the Multi-Link Drop Computer [60], would allow multiple aircraft to interface to send navigation data like drop points or flight paths between a lead airplane and a drop airplane, enhancing situational awareness and precision of retardant drops.

H. Flight Controls

The flight controls on the aircraft will utilize a number of other systems in their functioning. Hydraulic power is provided to drive control surface actuators, which are controlled by electric signals from the aircraft's fly-by-wire software integrated into the avionics package.

I. Pneumatics

The pneumatic systems on the aircraft are divided in two. One system is centered around five air tanks which serve to pressurize the retardant tank and to drive an emergency gear release. The details of these tanks are shown in Table 42. [61] The other system is fed by bleed air from the main engines and APU, which feed air to the environmental control unit and to the anti-icing ducts in the wings. All controls for pneumatic actuators and valves are purely electrical. Air pressure is provided for the air tanks by ground support equipment before take-off, as the retardant tank is expected to have a fixed number of uses in flight, and adding a compressor would increase weight.

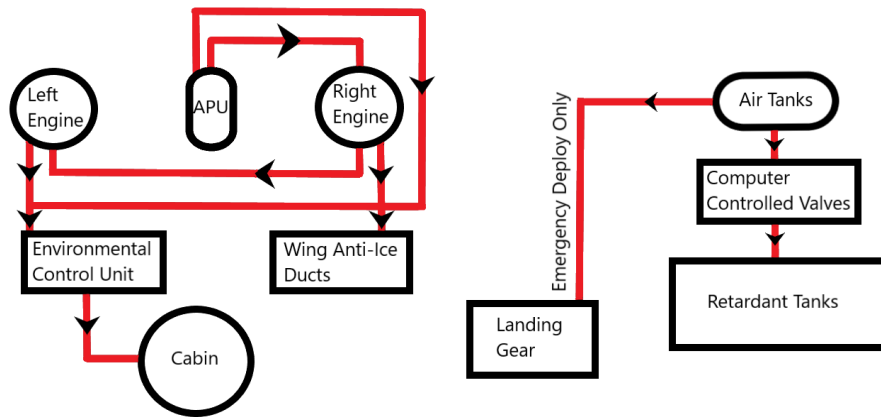


Fig. 60 Pneumatic System Connection Diagram.

Table 42 Nitrogen Tank Parameters

Number of Tanks	5
Length (in)	52.8
Diameter (in)	9.8
Max Pressure (PSIG)	2216
Total Nitrogen Capacity (lbm)	87

J. Environmental Control and Oxygen

The environmental control systems and oxygen are located near the cockpit. Air for standard operation will be drawn off of the main engines. In the case of both engines failing, bleed air from the APU can be used for maintaining cabin pressure. If the APU also fails or there is otherwise a loss of cabin pressure, masks for the pilots will be supplied with oxygen by pressurized bottles in the cabin. The cabin is pressurized to 8,000 ft equivalent.

K. Retardant Tanks and Handling Systems

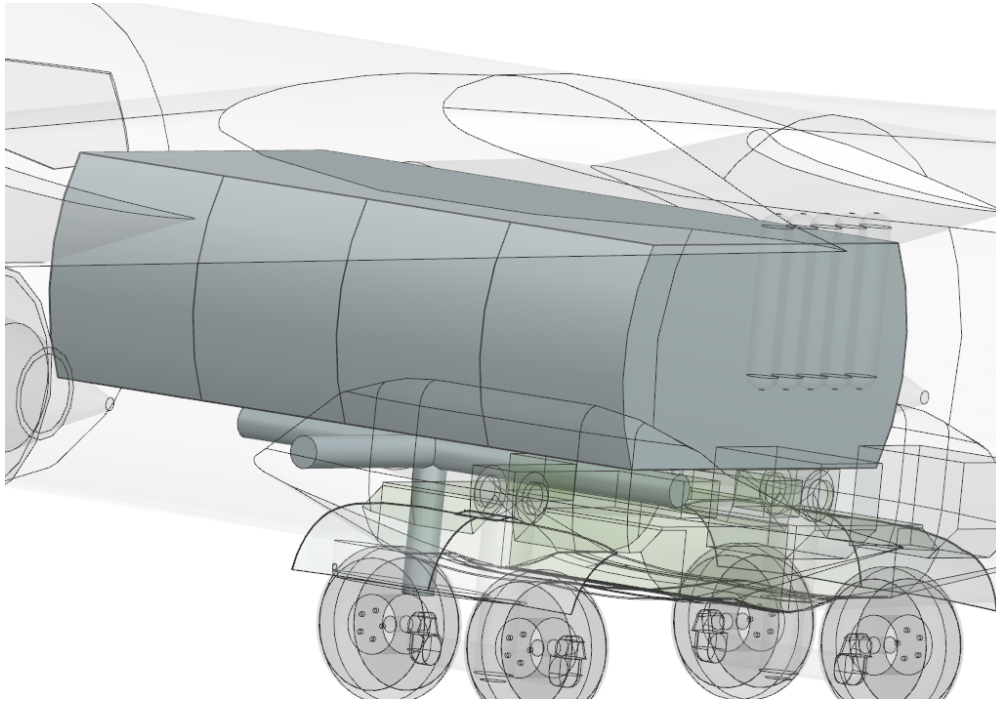


Fig. 61 Payload Tanks Seen From Slightly Aft.

The retardant tanks on this aircraft are designed to hold 8,000 gallons of a pre-mixed fire retardant of 9 lb/gal, and are situated in the center of the fuselage. The tanks are to have one single outer shell, split into four separate volumes by divider walls. When dropping retardant, the fore and aft-most chambers can be emptied at the same time, and the inner two can be emptied for a second drop. This configuration and drop method were chosen in order to minimize shifting of CG when in flight, although CG limit calculations assume worst-case valve failures in this setup. The tank drop order can be controlled directly by the drop controller interface shown in Figure 59. Splitting the tanks with vertical walls along the length of the aircraft prevents liquid from sloshing forward and back by any significant degree. Retardant will be loaded via a hose hookup near the main gear on the left sponson just forward of the main gear, with a pipe going from this connection to a main pipe connected to the bottom of each tank. This requires a ground-based pump to push the liquid up by about 70 inches. Retardant will be dropped by use of pressurized air injected into the retardant tanks. Regulation of retardant drop rate will be accomplished by controlling the pressure in the tanks, as the nozzle for ejecting retardant will have a fixed diameter. The air used to pressurize the retardant tanks will be stored in a set of five tanks positioned just aft of the rear wall of the retardant tank cluster.

Table 43 Payload Tank Parameters

Number of Tanks	4
Overall Length (in)	218
Outer Diameter (in)	138
Height (in)	68
Wall Thickness (in)	0.25
Max Pressure (PSIG)	30
Total Usable Capacity (lbm)	72,000

XIII. Landing Gear

A. Configuration

A high wing aircraft has many advantages at the landing gear level. The wing-mounted engines are much higher when compared to engines mounted on the wings of low wing configurations, meaning the landing gear can be much shorter. This allows for more interior payload volume because the wheel wells can be much smaller. Many different configurations can be applied to aircraft, but there are only a few that can be applicable to a plane of this size. For example, a taildragger configuration is primarily used on general aviation aircraft, and outriggers would not be advisable because the gear would need to be very tall due to the high wing configuration. Of the high wing aircraft that are currently in production, there is a common trend in the configuration of landing gear for aircraft that are roughly the same size as the Boeing 737. From a brief visual similarity analysis of the C-130 Hercules, the ATR-72, and Kawasaki C-1, all three employed a tricycle configuration with the nose and main gear retracting into the fuselage. While they all varied in terms of the number of tires that were on the main gear trucks, the nose gear is a simple two-wheel bogey. Considering these visual commonalities, it makes sense that the design aircraft will follow suit, by employing a tricycle configuration. This configuration will allow for a maximized tip-back angle for rotation on takeoff, as well as flare during touchdown. A tricycle configuration has many advantages on the ground such as good pilot visibility and kinematic stability.

Several trade studies we're conducted in order to determine the final configuration of the landing gear. Many high wing aircraft were observed, however the only airplane that matched the weight class of the design aircraft was the Lockheed Martin C-130 Hercules. That aircraft employs a tricycle landing gear configuration with fuselage mounted blisters for the main gear. When considering the retraction system, the many different configurations were considered, however to allow for maximum capacity within the fuselage, the wheels will collapse entirely into the blisters by folding inwards toward the center of the fuselage, rather than folding translationally along the length of the fuselage as they do on the C-130. Gear-tilt has not been included but has not yet been ruled out at this point in the design. The final configuration can be seen in Figure 62.

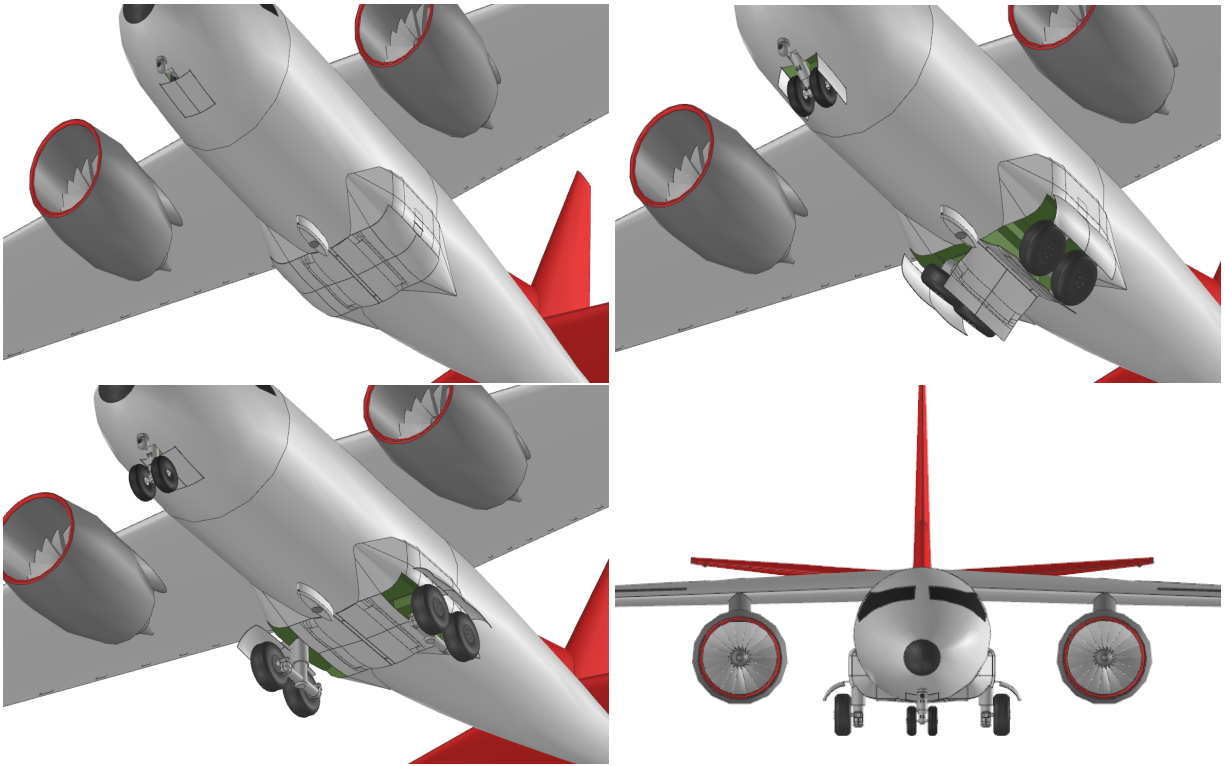


Fig. 62 Landing Gear Retraction.

B. Sizing

Upon determining configuration, the location as well as sizing of the tires and shock absorption system could be determined. The first step was to determine the lengthwise spacing between the main gear and nose gear. It was determined from guidelines mentioned in Chapter 11 of Raymer [2] that the main gear should bear 90% of the total aircraft weight and the nose should experience at maximum 10% and a minimum of 5% of the aircraft weight under static conditions. The reasoning for the minimum loading on the nose wheel is to ensure there is enough traction to allow for steering. Assuming the maximum static load of the aircraft to be 176,000 lbs, the forward CG was determined to be 331 inches from the nose and as a result, the main gear tires have been placed 35 inches behind the forward CG. The spacing of the gear struts was also determined by assuming 90% of the static load would rest on the main gear and the span between the two gear would be 350 inches. This is assuming the CG is the furthest backwards, under standard loading conditions. According to Raymer ([2], it was recommended that $\frac{M_a}{B}$ be greater than 0.05 and the $\frac{M_f}{B}$ is less than 0.2, which is satisfied by the dimensions visualized in Figure 63 and tabulated in Table 44.

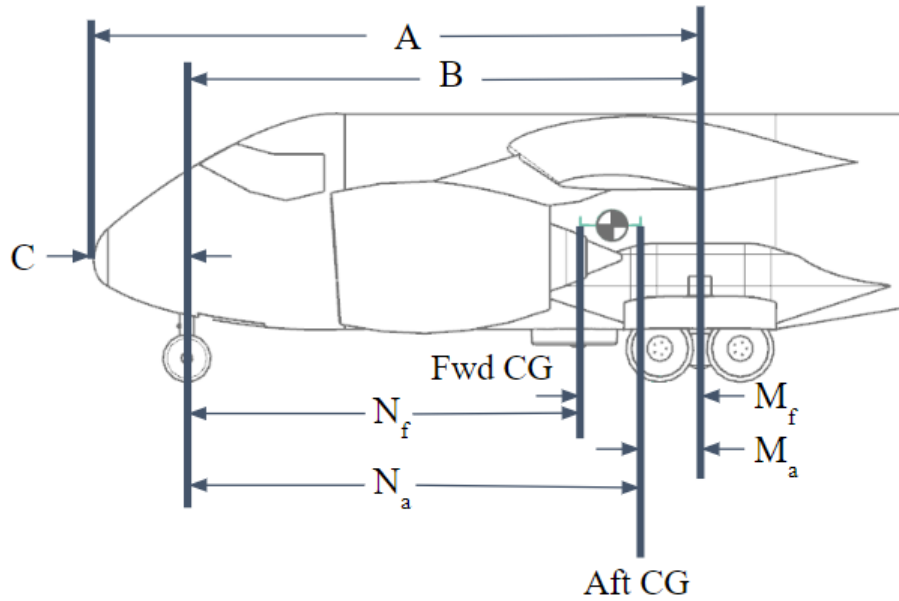


Fig. 63 Landing Gear Distances.

Table 44 Landing Gear Distances

Parameter	Distance (in)	Meaning
N_f	296	Distance from nose gear to max forward CG
N_a	315	Distance from nose gear to max aft CG
M_f	54	Distance from main gear to max forward CG
M_a	35	Distance from the main gear to max aft CG
B	350	Distance between middle of nose gear and main gear struts

The tire sizing process was completed using steps outlined in Chapter 11 of Raymer [2]. Assuming a maximum ramp weight, the minimum requirements for the size of the aircraft tires are outlined in Table 45 when assuming two tires per bogey of the main gear as well as two tires on the nose gear.

Table 45 Minimum Tire Size Requirements

Parameter	Nose Gear	Main Gear
Minimum Diameter (in)	28.49	45.75
Minimum Width (in)	8.16	16.79
Maximum Static Loading per Tire (lb)	7,900	35,500

The tires were selected from these dimensions and used to compute the rest of the details of the landing gear system. As each type tire is different there are certain characteristics that make each tire unique. The specific dimensions of the tire are listed below from Raymer chapter 11 or through calculations provided by Raymer [2].

Table 46 Selected Tire Characteristics

Parameter	Nose Gear	Main Gear
Tire Type	Type VII	Three Part
Tire Name	9.5-16	47x18-18
Tire Width (in)	9.7	17.9
Tire Diameter (in)	33.35	46.9
Rolling Radius, R_r (in)	13.9	19.2
Foot Print Area, A_p (in)	115	283
Air Pressure, P (psi)	90	175
Wheel Diameter (in)	16	18
Tire Stroke, S_T	2.775	4.25
Shock Absorber Efficiency η	0.47	0.47
Max Loading (lb)	9,250	43,700

With the tires selected and the understanding of their performance under Maximum loading conditions verified, it is possible to calculate the size and diameter of the stroke of oleopneumatic shock absorber. At this point in the design, the main gear are the ones designed to absorb the impact of landing as the aircraft will flare as it touches down, meaning the main gear will contact the ground first. It is assumed that the main gear will absorb 100% of the kinetic energy on landing. Using equations provided in Chapter 11 of Raymer [2], the stroke of the oleo shock absorber was determined to be 12 inches. As mentioned in Raymer a slightly larger stroke is recommended to be slightly larger for the nose gear, and at this point in the design has been arbitrarily set to 14 inches. Further calculations are required to verify the exact size of the nose gear shock absorber. The external diameter of the oleo absorber was also determined based on the loading each oleo would endure and as such was determined for both the nose and main gear of 10" and 15.7" respectively.

C. Braking System

Carbon brakes will be used on the aircraft as opposed to the conventional steel brakes. Conducting a brief trade study yielded that despite being more expensive upfront, the benefits that carbon brakes are outweigh the benefits of less expensive steel brakes. For example utilizing carbon brakes will provide roughly a 700 lb saving in empty weight which directly translates to reduced fuel requirements, improving the performance and fuel efficiency of the aircraft. Carbon brakes also have an average lifespan of about 2,200 landings per overhaul whereas steel brakes require an overhaul about twice as often. Carbon brakes also have about a 20% higher energy absorption rating which improves the balanced field length and ground operations. [62]

XIV. Repair and Maintenance

A. Maintenance Approach

The maintenance approach for the aircraft will be primarily centered around protecting the aircraft from its mission and surroundings. The aircraft will be flying through smoke and dropping retardant, mainly in the form of water, therefore the aircraft must have additional corrosion resistance. The solution to deal with water on and inside the aircraft is to apply a layer of corrosion protection to the outside as well as within the aircraft's retardant tank section. The primary choice of corrosion protection will be strontium chromate as it is currently the most prominent form of corrosion protection for aluminum. [63]

Additionally, there will be drain plugs on the bottom of the fuselage forward and aft of the retardant tanks to prevent water buildup inside the fuselage. Outside of preventative maintenance approaches, there will be scheduled A and B checks for the aircraft that depend on the aircraft operations. A checks should be scheduled for roughly every month assuming the aircraft is flying regularly, and will ground the aircraft for one day. B checks are more intensive airworthiness checks that will ground the aircraft for up to three days. B checks should be scheduled for in between fire seasons which will be typically twice per year assuming the aircraft transfers between the northern and southern hemisphere for each fire season. C and D checks will be scheduled in advance and be completed every two years and D checks every ten years.

B. Repair Approach

As the aircraft design is rather large, repairs and maintenance will be more time-consuming meaning that doors and access panels will need to be made in the complete design of the aircraft. Access panels allow for easier repair of hydraulic pumps, actuators, electrical generators, and overall inspections [2]. The aircraft is designed to carry spare equipment in the tail section of the aircraft aft of the fire retardant tanks. The aircraft will be certified to carry at least 5,000 pounds of spare equipment including spare tires, actuators, pumps, oil, and hydraulic fluid. The ability to carry spare equipment decreases the waiting time on the ground because components most likely to be replaced will be carried with the aircraft.

Although the aircraft has a high wing configuration, the engine overhaul procedure will be similar to existing commercial aircraft as the short landing gear keep the engine close to the ground. The engine can be connected to winch points next to the pylon to lower onto an engine cart just as in typical procedures. One of the major design decisions for the engine was finding a turbofan that is relatively common in order to source parts in the future. The CFM LEAP engines will be used as mentioned in the propulsion section of the report, however, the maintenance procedures for the engine should take less time in comparison with turboprops of comparable size due to the scarcity of large turboprop engines. It is anticipated that the time between overhaul will be around 10 years for each engine which will be comparable to a commercial transport jet. The reasoning for a similar time between overhaul is due to the fact that the

flight conditions will offset the flight hours required in between overhauls. This means that soot buildup in the engine may occur at shorter intervals than most aircraft although the flight hours will be less than a commercial transport.

Other considerations involve standardized parts such as actuators and fasteners which will work on both sides of the aircraft and for multiple components. Making the aircraft components as simple as possible will allow for reduced repair times, availability of spare parts, and keep the aircraft in the air.

C. Future Work

Future work will consist of detailing maintenance procedures and discovering possible issues. Identifying additional checks for a firefighting aircraft will be important and the repair and maintenance process will be refined by collaborating with flight crews. There is the possibility that specific checks for the engine will need to be conducted in order to work around soot buildup and loss of efficiency stemming from the firefighting missions.

XV. Cost Analysis

A. Business Case Analysis

Per the RFP provided by the AIAA [1], the estimates for the cost of the program as well as operational costs should be based on the production of roughly 4–10 aircraft per year. The RFP also mentioned to assume 1,200 flight hours per year in a combination of training, ferry and operational flights. At this point in the design, it is estimated that 75 aircraft will be produced for the entirety of the program, which includes two test aircraft. All in all, this translates to 7.5 planes being produced every year for ten years.

B. Production and Unit Cost

The model used to estimate the production cost of the entire program is a model developed by the RAND Corporation known as the Development and Procurement Costs of Aircraft or the DAPCA IV model. This model estimates the amount of time needed for research, development, testing and evaluation (RDT&E) for the aircraft and assigns a multiplier to convert hours into cost. The DAPCA IV model used in the design process is taken from Chapter 18 of Raymer [2]. Table 47 highlights the different parameters used in the DAPCA IV model and indicates the appropriate multiplier used to find the final cost of the entire program. It should be noted that this model was produced in 2012, and the final cost listed in Table 47 has been converted into the value of the dollar in 2022.

Table 47 DAPCA IV Model Breakdown

Parameter	Value	Multiplier	Final Cost (2012 \$)	Final Cost (2022 \$)
Engineering Hours	9,571,000	\$115/hour	\$1,100,665,000	\$1,347,677,000
Tooling Hours	5,872,000	\$118/hour	\$650,404,016	\$848,396,000
Manufacturing Hours	7,225,000	\$98/hour	\$708,050,000	\$866,951,000
Quality Control Hours	549,000	\$108/hour	\$59,292,000	\$72,598,000
Development Support Cost	\$174,120,000	-	\$174,120,000	\$213,196,000
Flight Test Cost	\$28,093,000	-	\$28,093,000	\$34,398,000
Manufacturing Materials Cost	\$682,892,000	-	\$682,892,000	\$836,147,000
Engine Costs (2022 \$)	\$14,500,000	150 Engines	\$2,175,000,000	\$2,175,000,000
Avionics Costs	\$6000	75,000 lbs	\$450,000,000	\$520,189,000
RDT&E + Flyaway costs	-	-	\$5,621,008,000	\$6,844,363,000

As shown in Table 47, the total program cost is roughly \$4.6 Billion, and for a program of 75 aircraft means the unit cost of each aircraft is roughly \$91.3 million. This is the cost to the manufacturer however, and to assume the 15% profit required by the RFP, the list price of the aircraft is \$105 million. The comparison of producing a different number of aircraft is tabulated in Table 48. It is seen that as increasing the number of aircraft produced over the lifetime of the program, the cost of each aircraft goes down. However, due to a rudimentary business case analysis, the demand for an aircraft this size would not justify producing that many aircraft.

Table 48 Comparison of Production Numbers

Production Number	Unit Cost
50	\$133,887,000
75	\$91,258,000
100	\$69,944,000

C. Operational Cost

Using the operational model provided by Zijp, which was written in 2012, the operational cost is mainly estimated as a function of the cost of each flight, cost of maintenance, and the cost of depreciation [64]. There is also an additional cost of the lead aircraft that is required for an aircraft of this weight class. The lead aircraft is assumed to be flying alongside the *Firehawk* during 50% of its flights, either in a training flight or for an active mission. Thus the operational cost assumes the lead aircraft will have 600 hours of flight time every year. The original cost per flight hour is \$1,500, but as the aircraft will only fly 50% of the time, \$750 is allotted for the flight hour cost of the *Firehawk*. Using the equation 3.26 from Zijp, the cost of each crew member is roughly \$60,000 which adjusted for inflation is roughly \$73,800 in 2022. The cost of A-1 jet fuel as published by the Secretary of Defense in 2022 [65] is \$3.77 per gallon. As this estimation assumes an even mix of training, operational and ferry flights, and under the assumption that not every mission will use the entire fuel tank, the average fuel consumed on a flight was assumed to be roughly 23,000 gallons. The average flight time is roughly 5.5 hours. Fuel costs in 2022 dollars and other associated costs of flying the plane are listed in Table 49 and visualized in Figure 64.

Table 49 Operating Cost Breakdown

Parameter	Value
Cost of Crew per Flight Hour	\$100
Cost of Fuel per Flight Hour	\$2,350
Material Cost per Flight Hour	\$2,300
Cost of Aircraft Insurance per Flight Hour	\$2,300
Cost of Lead Aircraft per Flight Hour	\$750
Total Expected Cost per Flight Hour	\$7800
Total Annual Operating Cost	\$9,360,000

There are many ways to reduce cost, especially in the operational sense of the aircraft. First and foremost, a more efficient engine and flying practices will return instant savings as less fuel will need to be burned. As can be seen, the estimated fuel burn of the aircraft is roughly 30% of the total operating cost every year. Reducing fuel burn will save a lot of money. Another design consideration that could reduce costs are that in the manufacturing and maintenance areas. Fewer moving parts or materials often lead to simpler designs and less cost to the engineers designing the aircraft. With that, it means fewer parts are required to stay in inventory and thus provide an additional savings to the airplane operators.

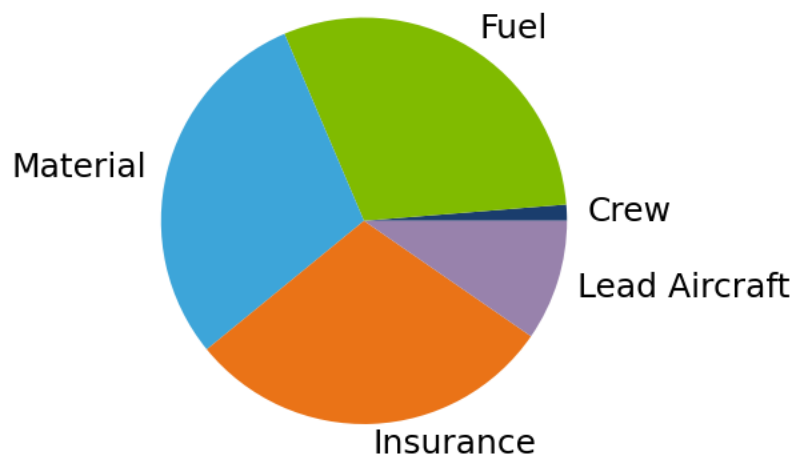


Fig. 64 Operational Cost Breakdown.

Additive manufacturing (AM) is a new field in aerospace engineering and using AM to simplify manufacturing and repair will also save a lot of money. A third way to reduce cost for the manufacturer is to increase the number of aircraft produced. 75 aircraft is a relatively small number compared to the thousands of commercial models that are produced. Through economies of scale, the aircraft unit, and subsequently list price decrease. If an operator came with a MOU for more than 75 aircraft, it would be beneficial to agree such that each aircraft is cheaper.

D. Future Work

As this is a first order estimate of the price of the aircraft and the entire program, more work is needed to find a more accurate cost. Uncertainties lie in the cost of specialized avionics and any other specialized systems that may cost more than the anticipated allotment in the DAPCA IV model. Other considerations would need to include airport landing fees, ground crew costs, as well as creating an accurate estimate for the exact number of planes that will need to be produced over the life of the program.

XVI. Conclusion

Firehawk, with max ferry range of 3,051 nmi, 8,000 gallon payload capacity, 6,100 ft BFL, and 72,275 lb empty weight, has all the tools to become an incredible fire fighting tool. Team Albatross believes that by meeting an extended amount of the design objectives laid out in the AIAA RFP, *Firehawk* will clearly set itself apart for other aircraft in a similar class. The team is confident in many specific differentiating factors of this aircraft, specifically its ability to perform a wide variety of mission profiles and the drop system's inclusion of four tanks. Team Albatross has begun to focus more on these factors, and continues to improve and add items to the design which set it apart from existing aircraft on the market. Placing the focus on improving these factors in order to set this design apart from existing aircraft, along with continued iteration of the design and improved calculation methods will allow this design to become an invaluable resource to fight increasingly severe and volatile forest fires.

References

- [1] “Responsive Aerial Fire Fighting Aircraft,” AIAA, 2021. <https://www.aiaa.org/get-involved/students-educators/Design-Competitions>, Accessed 10 Feb 2022.
- [2] Raymer, D. P., *Aircraft Design: A Conceptual Approach*, 6th ed., American Institute of Aeronautics and Astronautics, 2018.
- [3] Roskam, J., *Airplane Design Part V: Component Weight Estimation*, Roskam Aviation and Engineering Corporation, Ottawa, Kansas, 1985.
- [4] “C-130 Hercules Fact Sheet,” 2018. <https://www.af.mil/About-Us/Fact-Sheets/Display/Article/1555054/c-130-hercules/>, Accessed 28 Apr 2022.
- [5] “Modular Airborne Fire Fighting Systems (MAFFS),” 2022. <https://www.fs.usda.gov/managing-land/fire/planes/maffs>, Accessed 28 Apr 2022.
- [6] “737-classic-passenger,” Boeing, 2007. https://www.boeing.com/resources/boeingdotcom/company/about_bca/startup/pdf/historical/737-classic-passenger.pdf, Accessed 5 Mar 2022.
- [7] “MD-80 Airplane Characteristics for Airport Planning,” Boeing, 1990. <https://www.boeing.com/resources/boeingdotcom/commercial/airports/acaps/md80.pdf>, Accessed 28 Apr 2022.
- [8] “DC/MD-10 Airplane Characteristics for Airport Planning,” Boeing, Apr 2004. <https://www.boeing.com/resources/boeingdotcom/commercial/airports/acaps/dc10.pdf>, Accessed 28 Apr 2022.
- [9] “Coulson to convert 737’s into air tankers,” *Fire Aviation*, 2017. <https://fireaviation.com/2017/05/21/coulson-to-convert-737s-into-air-tankers/>, Accessed 28 Apr 2022.
- [10] “Classic MD-87s Still Earning a Living as Aerial Firefighting Tankers,” *Avgeekery*, 2018. <https://avgeekery.com/classic-md-87s-still-earning-a-living-as-aerial-firefighting-tankers/>, Accessed 28 Apr 2022.
- [11] “DC-10 - SBC Fire Department,” *sbcfire*, 2022. <https://www.sbcfire.com/links/2414-types-of-fixed-wing-aircraft-and-helicopters/resources/8933-dc-10>, Accessed 28 Apr 2022.
- [12] “Type Certificate Data Sheet No. A6WE,” FAA, 1 Nov 2001. https://rgl.faa.gov/Regulatory_and_Guidance_Library/rgMakeModel.nsf/0/c1817d49c964876886256b1400759d25/%24FILE/A6WE.pdf, Accessed 28 Apr 2022.
- [13] “Type Certificate Data Sheet E23EA,” FAA, 13 June 2010. https://rgl.faa.gov/Regulatory_and_Guidance_Library/rgMakeModel.nsf/0/2c339dd53360180c86257b9b004942ca/\protect\T1\textdollarFILE/E23EA_Rev_21.pdf, Accessed 28 Apr 2022.
- [14] Scholz, D., “Aircraft Design,” *Hamburg University of Applied Sciences*, 2017. <https://www.fzt.haw-hamburg.de/pers/Scholz/H00U/enhanced/index.html>, Accessed 6 Mar 2022.
- [15] “Anthropometry and Biomechanics,” NASA: MAN-SYSTEMS INTEGRATION STANDARDS, 2020. <https://msis.jsc.nasa.gov/sections/section03.htm>, Accessed 1 Apr 2022.
- [16] Sadraey, M., *Aircraft Design: A Systems Engineering Approach*, John Wiley & Sons, Ltd, Daniel Webster College, New Hampshire, USA, 2013.
- [17] Al Ahmari, S. A. S., “Design & fabrication of two seated aircraft with an advanced rotating leading edge wing,” Ph.D. thesis, King Fahd University of Petroleum and Minerals (Saudi Arabia), 2011.
- [18] Jin, Z., Zhang, Y., Liu, H., and Dong, D., “Design Methodology for Flight Deck Layout of Civil Transport Aircraft,” *International Conference on Intelligent Human Systems Integration*, Springer, 2019, pp. 98–104.
- [19] “eCFR :: 14 CFR Part 25 – Airworthiness Standards: Transport Category Airplanes,” *Code of Federal Regulations*, 19 Apr 2022. <https://www.ecfr.gov/current/title-14/chapter-I/subchapter-C/part-25>, Accessed 22 Apr 2022.
- [20] “TP400-D6,” *MTU Aero Engines*, 2022. <https://www.mtu.de/engines/military-aircraft-engines/transport-aircraft/tp400-d6/>, Accessed 4 Mar 2022.
- [21] McIntire, W.L., “A New Generation T56 Turboprop Engine,” *The American Society of American Engineers*, 1984. <http://asmedigitalcollection.asme.org/GT/proceedings-pdf/GT1984/79474/V002T02A007/2395358/v002t02a007-84-gt-210.pdf>, Accessed 4 Mar 2022.

- [22] Meier, N., “Jet Engine Specification Database,” *jet-engine.net*, 2021. <https://jet-engine.net/>, Accessed 8 Feb 2022.
- [23] Jewell, J., Soret, C., and Bradley, P., “LEAP-1B achieves major milestone,” *CFM International*, 2 May 2013. <https://www.cfmaeroengines.com/press-articles/leap-1b-achieves-major-milestone/>, Accessed 9 Feb 2022.
- [24] “PD-14 New Generation Engine for MC-21,” *Take-off*, December 2011, pp. 20–21. <https://issuu.com/aviationlive/docs/to22/22>, Accessed 4 Mar 2022.
- [25] “Type-Certificate Data Sheet,” *European Union Aviation Safety Agency*, 12 Dec 2019. <https://www.easa.europa.eu/sites/default/files/dfu/TCDS%20E.003%20issue%2005.pdf>, Accessed 4 Mar 2022.
- [26] “Type-Certificate Data Sheet,” *European Union Aviation Safety Agency*, 30 May 2018. <https://web.archive.org/web/20181013014334/https://www.easa.europa.eu/sites/default/files/dfu/EASA%20E110%20TCDS%20Issue%207%20LEAP-1A-1C.pdf>, Accessed 4 Mar 2022.
- [27] “Type-Certificate Data Sheet,” *European Union Aviation Safety Agency*, 9 Dec 2019. <https://www.easa.europa.eu/downloads/20016/en>, Accessed 4 Mar 2022.
- [28] “Corrosion Cuts Life Limit of A220 and E2 Compressor Hubs,” *FlightGlobal*, 4 June 2019. <https://www.flightglobal.com/mro/corrosion-cuts-life-limit-of-a220-and-e2-compressor-hubs/132978.article>, Accessed 4 Mar 2022.
- [29] Sinha, S., “Change all Neo Engines by Jan 31, IndiGo told,” *The Times of India*, 2 Nov 2019. <https://timesofindia.indiatimes.com/business/india-business/need-desperate-measures-to-put-things-in-order-dgca-tells-indigo-as-pratt-engine-snags-spiral/articleshow/71851883.cms>, Accessed 4 Mar 2022.
- [30] Daidzic, N. E., “Estimation of Performance Airspeeds for High-Bypass Turbofans Equipped Transport-Category Airplanes,” *Journal of Aviation Technology and Engineering*, 2016. <https://docs.lib.purdue.edu/cgi/viewcontent.cgi?article=1122&context=jate>, Accessed 4 Mar 2022.
- [31] “AIRBUS A320 AIRCRAFT CHARACTERISTICS - AIRPORT AND MAINTENANCE PLANNING Rev. 39,” *Airbus S.A.S.*, 1 Dec 2020. <https://www.airbus.com/sites/g/files/jlcbta136/files/2021-11/Airbus-Commercial-Aircraft-AC-A320.pdf>, Accessed 7 Apr 2022.
- [32] Torenbeek, E., *Synthesis of Subsonic Airplane Design*, Delft University Press, Delft, 1988.
- [33] “XFLR5,” *XFLR5*, 2021. <http://www.xflr5.tech/xflr5.htm>, Accessed 1 Feb 2022.
- [34] Hepperle, M., “JavaFoil – Analysis of Airfoils,” See <http://www.mh-aerotoools.de/airfoils/javafoil.html>, 2008.
- [35] Abbot, I., and Von Doenhoff, A., *Theory of Wing Sections*, Dover, 1959.
- [36] “Airfoil Tools,” *Airfoil Tools*, 2022. <http://airfoiltools.com/index>, Accessed 8 Feb 2022.
- [37] “Solidworks Flow Simulation,” , Dec 2021. <https://www.solidworks.com/product/solidworks-flow-simulation>.
- [38] “eCFR :: 14 CFR Part 23.933 – Ground clearance Standard,” *Code of Federal Regulations*, 19 Apr 2022. <https://www.ecfr.gov/current/title-14/chapter-I/subchapter-C/part-25>, Accessed 22 Apr 2022.
- [39] Talay, T. A., “Introduction to the Aerodynamics of Flight. NASA SP-367,” Scientific and Technical Information Office, Washington, D.C., 1975.
- [40] “AVL Overview: Extended Vortex-Lattice Model,” , 2022. <https://web.mit.edu/drela/Public/web/avl/>.
- [41] Nicolai, L. M., and Carichner, G. E., *Fundamentals of Aircraft and Airship Design*, volume 1 ed., American Institute of Aeronautics and Astronautics, Reston, Va., 1986. <https://doi.org/10.2514/4.867538>.
- [42] “OpenVSP,” *OpenVSP*, 6 Jan 2021. <http://openvsp.org/>, Accessed 1 Feb 2022.
- [43] Whitcomb, R. T., and Kelly, T. C., *A Study of the Flow Over a 45 Sweptback Wing-Fuselage Combination at Transonic Mach Numbers*, NACA, 1952.
- [44] Cipolla, V., Abu Salem, K., Palaia, G., Binante, V., and Zanetti, D., “Prediction of Maximum Lift Coefficient of Box-Wing Aircraft through the Combination of an Analytical Adaptation of the DATCOM Method and Vortex-Lattice Simulations,” *Journal of Aerospace Engineering*, Vol. 35, No. 3, 2022, p. 04022026.

- [45] Etkin, L., Bernard Reid, *Dynamics of Flight: Stability and Control, Third Edition*, John Wiley and Sons, 1995.
- [46] Roskam, J., *Airplane Design Part I: Airplane Flight Dynamics and Automated Controls*, Roskam Aviation and Engineering Corporation, Ottawa, Kansas, 1985.
- [47] Sforza, P., *Commercial Airplane Design Principles*, Butterworth-Heinemann, 2014.
- [48] Niu, M. C.-Y., *Airframe Structural Design*, Conmilit Press Ltd., Hong Kong, 1988.
- [49] Center, M. S. F., *NASA TM X-73306 Structures Manual Volume II*, 1975.
- [50] Vartabedian, T., *Design of an Aircraft Main Wing Spar*, 2018.
- [51] Gudmundsson, S., *General Aviation Aircraft Design*, Butterworth-Heinemann, 2014.
- [52] Brady, C., *The Boeing 737 Technical Guide*, Tech Pilot Services Ltd, 3 Mansefield Road, Kingsley, Frodsham, Cheshire, WA6 8BZ, 2021.
- [53] Moore, A., "Reliable Robotics Announces New Cargo Airline Led by Industry Veterans," *Businesswire*, 11 Jan 2022. <https://www.businesswire.com/news/home/20220106005356/en/Reliable-Robotics-Announces-New-Cargo-Airline-Led-by-Industry-Veterans>, Accessed 22 Apr 2022.
- [54] "Airbus A320," *Airframer*, 2022. https://www.airframer.com/aircraft_detail.html?model=A320, Accessed 5 Mar 2022.
- [55] "Boeing 787," *Airframer*, 2022. https://www.airframer.com/aircraft_detail.html?model=B787, Accessed 10 Apr 2022.
- [56] "Boeing 737," *Airframer*, 2022. https://www.airframer.com/aircraft_detail.html?model=B737, Accessed 5 Mar 2022.
- [57] Gabbert, B., "Using the 747 Supertanker to drop on fires at night," *Fire Aviation*, 4 Dec 2016. <https://fireaviation.com/2016/12/04/using-the-747-supertanker-to-drop-on-fires-at-night/>, Accessed 14 Apr 2022.
- [58] "AT-802F GENERATION III FIRE Response DISPERSAL SYSTEM," *Air Tractor*, 2022. <https://airtractor.com/firefighting/802f-fire-retardant-dispersal-system/>, Accessed 15 Apr 2022.
- [59] "Elbit Systems Successfully Demonstrates High-Altitude High-Precision Aerial Firefighting Solution," *Elbit Systems*, 21 Jan 2020. <https://elbitsystems.com/pr-new/elbit-systems-successfully-demonstrates-high-altitude-high-precision-aerial-firefighting-solution/>, Accessed 14 Apr 2022.
- [60] Richardson, M., "Multi-Link Drop Computer for Aerial Firefighting," *Canaan Avionics*, 15 July 2012. https://www.canaanavionics.com/MULTI-LINK%20DROP%20COMUPTER_REVC.pdf, Accessed 15 Apr 2022.
- [61] "List of Air Cylinder Parameters," *Catalina Cylinders*, 2022. <https://www.catalinacylinders.com/markets/specialtyindustrial/>, Accessed 24 Apr 2022.
- [62] ming SU, J., chao XIAO, Z., qiong LIU, Y., cai MENG, F., gang PENG, Z., min GU, L., feng LI, G., and peng XING, R., "Preparation and characterization of carbon/carbon aircraft brake materials with long service life and good frictional properties," *New Carbon Materials*, Vol. 25, No. 5, 2010, pp. 329–334. [https://doi.org/https://doi.org/10.1016/S1872-5805\(09\)60037-8](https://doi.org/https://doi.org/10.1016/S1872-5805(09)60037-8), Accessed 22 Apr 2022.
- [63] "What is Strontium Chromate?" *Corrosionpedia*, 2015. <https://www.corrosionpedia.com/definition/2468/strontium-chromate>, Accessed 8 Feb 2022.
- [64] Zijp, S., "Development of a Life Cycle Cost Model for Conventional and Unconventional Aircraft," 2014. Accessed 03/05/22.
- [65] "Current Cost Plus Rate for DLA Energy Petroleum Products," *US Department of Defense*, Dec 2021. https://www.dla.mil/Portals/104/Documents/Energy/Standard%20Prices/Petroleum%20Prices/E_2021Oct1PetroleumStandardPrices_210930.pdf.